# Efimov physics for non-separable finite-range interactions

Mestrom, Paul M.A.

*Award date:*
2017

# Efimov physics for non-separable finite-range interactions

P.M.A. Mestrom

June 2017
CQT 2017-09

## Master thesis

Supervisor:
dr.ir. S.J.J.M.F. Kokkelmans

Department of Applied Physics
Coherence and Quantum Technology

Eindhoven University of Technology

**Abstract**

The Efimov effect is a universal three-body phenomenon occuring in many different physical systems. Atoms interacting via van der Waals potentials exhibit an additional type of universality associated with the Efimov spectrum, namely the universality of the three-body parameter. This type of finite-range interaction has been studied extensively during the last decade. These studies have shown that the range of the potential is a very important model parameter in the context of Efimov physics.

In this work we study Efimov physics for three-body systems involving identical bosons interacting via a pairwise square well potential. This potential has a well-defined range and the off-shell two-body $T$-matrix is analytically known. So far only approximate results exist for the Efimov spectra corresponding to the potential resonances of the square well potential. We show that these results are not accurate enough by considering the full non-separable off-shell two-body $T$-matrix which is present in the three-body Faddeev equations. In order to calculate the Efimov spectrum, we solve these Faddeev equations by expanding the $T$-matrix in separable terms. We analyze different methods to obtain such a separable expansion. This momentum space treatment allows us to show that strong $d$-wave interactions lower the energy of the second Efimov state making it possible to prevent this Efimov state from merging with the atom-dimer threshold. In case of the shallow square well potential as two-body interaction the second Efimov state never crosses this threshold even when $d$-wave interactions are absent or when a separable approximation for the square well potential is used. We also show that separable approximations of the two-body $T$-matrix are insufficient to accurately compute the trimer states at large negative energies even when the off-shell two-body $T$-matrix is highly separable in this energy regime. In case of deep square well potentials, these separable approximations cannot even be used to determine the three-body parameter. Since we consider the full non-separable off-shell $T$-matrix, we can determine the three-body parameter accurately. Further research should point out how good the separable approximation of the two-body $T$-matrix is for more realistic interatomic potentials supporting at least one two-body bound state.

# Contents


**1 Introduction** **1**

1.1 The Efimov effect . . . 3

1.2 Finite-range corrections . . . 6

1.3 Feshbach resonance . . . 8

1.4 The square well potential . . . 10

1.4.1 Previous work on the square well potential . . . 10

1.5 Outline . . . 12

**2 Scattering theory** **13**

2.1 Two-body scattering theory . . . 13

2.1.1 The scattering operator . . . 14

2.1.2 The scattering matrix . . . 16

2.1.3 The transition operator . . . 16

2.1.4 The stationary scattering states . . . 17

2.1.5 The two-body $T$-matrix . . . 18

2.1.6 Properties of the two-body $T$-matrix . . . 20

2.2 Multichannel scattering theory . . . 21

**3 Three-body scattering theory** **23**

3.1 The Faddeev equations for three-body bound states . . . 23

3.2 The Faddeev equations for atom-dimer scattering states . . . 26

**4 Two-body scattering off a finite square well potential** **29**

4.1 Scattering length . . . 29

4.2 The off-shell two-body $T$-matrix . . . 30

**5 Separable expansions and approximations of the off-shell two-body $T$-matrix** **33**

5.1 Separable approximation of the $T$-matrix near a singular point . . . . . 33
5.2 Method I: the spectral representation . . . . . 34
5.3 Method II: the Weinberg series . . . . . 38
5.3.1 Method IIb: The unitary pole expansion . . . . . 41
5.4 Method III: the EST method . . . . . 46
5.5 Comparison of the separable expansions . . . . . 51
5.6 Comparison with van der Waals potentials . . . . . 54
5.7 Applicability for studying Efimov physics . . . . . 57

**6 Numerical model** **59**
6.1 Three-body bound state calculations . . . . . 59
6.2 Analysis of the kernel using the Weinberg series . . . . . 61
6.2.1 The diagonal of the kernel . . . . . 63
6.2.2 The eigenvalues of the kernel . . . . . 64
6.3 Calculation of the three-body resonances . . . . . 69
6.4 Elastic atom-dimer scattering calculations . . . . . 69

**7 Results and discussion** **73**
7.1 Results for the shallow square well . . . . . 73
7.2 Results for the deep square well . . . . . 80

**8 Conclusions and outlook** **85**
8.1 Conclusions . . . . . 85
8.2 Outlook . . . . . 87

**Technology Assessment** **89**

**Bibliography** **91**

**A Experimental observables to determine the three-body parameters** **95**
A.1 Three-body recombination rate . . . . . 95
A.2 Atom-dimer relaxation rate . . . . . 97

**B Mathematics** **99**
B.1 Some properties of the spherical harmonics . . . . . 99
B.2 Spherical Bessel functions . . . . . 99
B.3 Riccati-Bessel functions . . . . . 100

**C Multichannel scattering theory** **101**
C.1 Identical particles . . . . . 104

**D Exchange and permutation operators** **107**

**E Free-particle states and the momentum-space representation of operators** **109**
E.1 Free two-particle states . . . . . 109
E.2 Momentum-space representation of the potential . . . . . 110
E.3 Momentum-space representation of the wave function . . . . . 111
E.4 Three-particle momentum states . . . . . 112
E.5 Momentum-space representation of three-body operators . . . . . 113

**F Partial wave expansion of the three-body equations** **115**
F.1 Three-body bound states . . . . . 115
F.2 Atom-dimer scattering states . . . . . 119
F.2.1 The scattering amplitude . . . . . 123

**G Hilbert-Schmidt theory** **127**
G.1 Real symmetric matrices . . . . . 128

**H Additional figures** **129**
H.1 Method I . . . . . 129
H.2 Method II . . . . . 130
H.3 Method III . . . . . 131

# 1. Introduction

The work of this thesis is part of a bottom-up approach to study strongly interacting quantum systems. Via the unifying concepts of few-body physics we eventually want to describe such many-body systems. The approach of starting with few-body physics including finite-range interactions differs from the usual mean-field approach in many-body physics in which one starts immediately from a large number of particles together with a set of approximations to solve the problem. One of these approximations which is often used is neglecting the range of the two-body interaction potential and considering only contact interactions, which works well for dilute systems. Furthermore, these mean-field theories often contain only one- and two-body correlations which is only a valid description for weakly interacting many-body systems [1].

Many different strongly interacting quantum systems exist such as nuclear, atomic and condensed matter systems. We focus on ultracold atomic gases which are particularly useful for studying strongly interacting quantum systems. The experimental techniques such as laser cooling and trapping are highly advanced, making it possible to trap millions of atoms at sub-microkelvin temperatures. Furthermore, ultracold atoms can be precisely manipulated by lasers and external fields. For example, the two-body interactions can be accurately modulated using a magnetic-field controlled Feshbach resonance [2–4]. In this way, the collective many-body interaction can be made both attractive and repulsive. Moreover, a wide variety of different spin states, fermionic or bosonic isotopes and species can be used in experiments turning systems of ultracold atomic gases into a particularly rich research field.

The tunability of the interparticle interaction is a key feature of ultracold atomic gases and allows physicists to study strongly interacting systems in a controlled way. The two-body scattering length $a$ is the length scale which characterizes the interaction strength of a two-particle system. This length scale is related to the two-body elastic scattering cross section $\sigma$ at zero energy by $\sigma = 4\pi a^2$ [5]. If the magnitude of the scattering length is much larger than the characteristic range $r_0$ of the two-body interaction potential, the system is strongly interacting. This regime of large scattering lengths is also called the unitary regime. In the unitary limit, the scattering length diverges and the two-body interaction becomes resonant. In this case, the scattering length is much larger than the typical interparticle distance $d$ of the many-body system. Atomic quantum gases are very dilute, so that the inequality $r_0 \ll d \ll |a|$ holds in the strongly interacting regime [6].

Interesting physics happens in the unitary limit. For example, a Fermi gas consisting of fermions with two spin states shows a spectacular crossover between two different regimes of superfluidity which is known as the BCS-BEC crossover [6]. At positive scattering lengths, two-body molecular states can form a Bose-Einstein condensate, whereas at negative scat-

tering lengths the atoms form a BCS state in which fermions of opposite spin join to make Cooper pairs. Bosonic systems also exhibit remarkable effects in the unitary limit. One example is the Efimov effect [7, 8] which is discussed in detail in this thesis. The Efimov effect is not present in the two-component Fermi gas, so that the corresponding interactions are scale invariant when the scattering length $a$ is infinitely large [9]. The scale invariance is broken in the unitary Bose gas by the Efimov effect which introduces an additional length scale which is called the three-body parameter [9].

Ultracold atomic gases are not only important on a fundamental level, but they also have many applications such as atomic clocks [10] and interferometers [11]. Moreover, these quantum systems offer a highly controllable setting for quantum simulation of interacting many-body systems [12] and could even serve as a platform for quantum computation. Good theoretical models of quantum many-body systems are needed for the development of such applications. These models should contain the information about the few-body systems correctly. The existing many-body theories are not valid for particular many-body systems such as a strongly interacting homogeneous Bose-Einstein condensate [13], so that improved many-body models are needed. The first step in the development of a good theoretical model of strongly interacting quantum gases is understanding the important few-body interactions such as the Efimov effect which is a universal three-body phenomenon [7, 8, 14–16] and occurs when three particles interact via short-range attractive interactions that are nearly resonant. Such a three-particle system exhibits an infinite sequence of three-body bound states in the unitary limit, which is known as the Efimov effect. The three-body bound states are called Efimov states or Efimov trimers. The universality of the Efimov effect makes it possible to occur in many different physical systems such as nucleons [17, 18], atoms [19] and magnons [20].

The Efimov effect had been predicted by Vitaly Efimov in 1970. From then on, physicists focussed mainly on the observation of the Efimov effect in nuclear systems, but it could not be proven that certain nuclear three-body bound states originate from the Efimov effect. The breakthrough came from the field of ultracold atoms due to the high controllability of the two-body interactions provided by Feshbach resonances. The search for Efimov states in ultracold atomic systems started with the proposal of Ref. [21] in 1999 to observe the signatures of Efimov states in ultracold atomic systems by measuring the three-body recombination rate as a function of the two-body scattering length. This signature was first measured in an ultracold gas of cesium atoms ($^{133}$Cs) by a research group at the University of Innsbruck in 2006 [22], which is the first experimental evidence for Efimov states. Since then, Efimov states have also been observed in ultracold gases of lithium ($^{7}$Li, $^{6}$Li) [23–35], potassium ($^{39}$K) [36], rubidium ($^{85}$Rb) [37] and mixtures of atomic species [38]. It has even become possible to measure the triatomic Efimov resonance corresponding to the first excited Efimov state [39], which fully confirms the Efimov effect. A few years ago, the Efimov effect has also been observed in helium ($^{4}$He) without artificial tuning of the two-body interaction via Feshbach resonances [40]. Another recent achievement is the successful measurement of the lifetime of the Efimov states by studying the decay dynamics of a molecular gas [41].

## 1.1 The Efimov effect

In 1935 —a long time before the Efimov effect was predicted— Thomas [42] studied three-particle systems interacting via short-range attractive two-body potentials. He showed that no lower limit exists on the three-body ground state energy when the depth of the two-body interaction approaches $-\infty$, while its range approaches 0. This finding is known as the Thomas collapse. The interpretation of this collapse was given by Vitaly Efimov [7, 8] in the early seventies, who —in contrast to Thomas' approach— fixed the range $r_0$, but varied the two-body scattering length $a$ which is a parameter related to the underlying two-body interactions. Efimov [7] studied systems consisting of three identical bosons in which $|a| \gg r_0$ and showed that in the unitary limit a geometric series of infinitely many three-body bound states exists with an accumulation point at zero energy. This is called the Efimov effect. He also recognized that short-range physics would introduce a cut-off to the three-body spectrum which produces a well-defined ground state energy, avoiding the Thomas collapse. However, Efimov himself did not consider scattering lengths which are on the order of the range $r_0$ of the potential.

Fig. 1.1 shows the energy spectrum of the three-body system as a function of the inverse scattering length in the zero-range theory. The scattering length $a$ describes the $s$-wave two-body interactions near zero energy. At negative scattering lengths ($a < 0$), the potential does not support a two-body bound state and a 'virtual' state lies in the two-body continuum ($E > 0$). At positive scattering lengths ($a > 0$), the potential supports a two-body bound state with zero angular momentum. The binding energy of this so-called 'dimer state' can be approximated for large $a$ by

$$E_{2b} = -\frac{\hbar^2}{ma^2} \tag{1.1}$$

where $m$ is the mass of each boson. This equation is exact in the zero-range theory at all nonzero values of $a$ because the condition $|a| \gg r_0$ is always satisfied in case of zero-range potentials. The black curve in Fig. 1.1 indicates the two-body bound state energy given by Eq. (1.1). In this figure, the energy $E$ of the three-particle system is represented by the wave number $\kappa$ which is defined by

$$\kappa = \text{sign}(E)\sqrt{\frac{m|E|}{\hbar^2}}. \tag{1.2}$$

Thus the dimer energy is represented by a straight line in the $(1/a, \kappa)-$plane.

The Efimov states are indicated by the red solid lines in Fig. 1.1. The universality of the Efimov spectrum is reflected in the geometric scaling of the energies and lengths scales. The trimer energies at diverging scattering length ($a \to \pm\infty$) are given by

$$E^*_{3b,n+1} = e^{-2\pi/s_0} E^*_{3b,n} \tag{1.3}$$

where $s_0 = 1.00624$ for three identical bosons [15], so that $e^{2\pi/s_0} \approx (22.7)^2 \approx 515$. The index $n$ labels the Efimov state. In the zero-range limit, $n$ is an integer in the range $(-\infty, \infty)$. The size of the Efimov states goes to infinity as $n$ goes to infinity. Since the scaling of the trimer states is universal, one only needs to know one characteristic point to fix the full Efimov spectrum. There are many possibilities to choose this so-called 'three-body parameter'. One

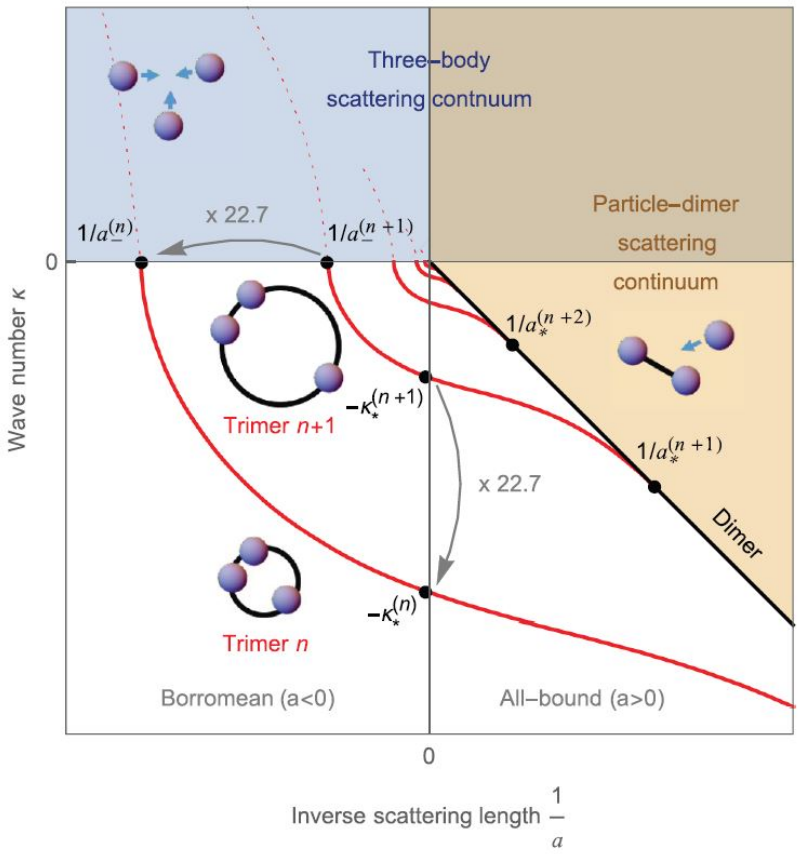


Figure 1.1: Schematic representation of the Efimov spectrum for three identical bosons of mass $m$ in the zero-range theory (figure taken from Ref. [16]). The wave number $\kappa$, defined by Eq. (1.2), is plotted as a function of the inverse scattering length $1/a$. The red curves indicate the three-body bound states, which become trimer resonances in the three-body continuum (dashed lines). The two-body $s$-wave binding energy is indicated by the black curve.

possibility is to specify the wave number $\kappa_n^*$ corresponding to the energy of the $n$th trimer state at diverging scattering length. One could also choose to specify the scattering length $a_{-,n}$ at which the $n$th trimer state emerges from the three-body continuum. This choice is experimentally more interesting because $a_{-,n}$ can be determined from the maxima in the three-body recombination rate $K_3$ in an ultracold gas of trapped atoms [21]. At positive scattering lengths, the recombination rate $K_3$ shows minima at particular values of the scattering length [21], indicated by $a_{+,n}$, which also scales universally and can thus be used as a three-body parameter. Finally, the scattering length $a_{*,n}$ at which an Efimov state disappears at the atom-dimer threshold could also be chosen as the three-body parameter. This special value can also be experimentally observed by measuring the atom-dimer relaxation rate in an ultracold mixture of atoms and weakly bound dimers in a trap and determining the maxima in the loss rate. More information about these experimental observables is given in Appendix A. The scaling of the three-body parameters in the zero-range theory is given by

$$\begin{aligned} \kappa_{n+1}^* &= e^{-\pi/s_0}\kappa_n^*, \\ a_{\alpha,n+1} &= e^{\pi/s_0}a_{\alpha,n}, \end{aligned} \tag{1.4}$$

where $\alpha = -, +$ or $*$. This geometric scaling is also indicated in Fig. 1.1. The various three-body parameters are also related to each other. For example, Gogolin *et al.* [43] have found that

$$a_{-,n}\kappa_n^* = -1.50763, \tag{1.5}$$

whereas Braaten and Hammer [15] have shown that

$$a_{*,n}\kappa_n^* = 0.0707645. \tag{1.6}$$

It is important to realize that zero-range theory does not predict a value for the three-body parameter.

The Efimov states emerge from the three-body threshold ($E = 0$) at negative scattering lengths. This makes the Efimov effect counterintuitive. It implies that three-body bound states exists even when a pair of bosons cannot form a bound state. This situation is analogous to the one of the Borromean rings where all three of them are bound even though each individual pair is unbound. Therefore, the part of the Efimov spectrum for which $a < 0$ is also called the Borromean region.

The Efimov effect is universal in the sense that it happens for all bosonic systems interacting via short-range attractive interactions that are nearly resonant regardless of the type of particles (e.g., atoms, nucleons or molecules) which are considered. It can even happen for fermionic systems if at least two particles are distinguishable [15]. To be more precise, with short-range interactions we mean that the two-body potential should decay faster than $1/r^3$ where $r$ is the interparticle distance [16]. If this requirement is fulfilled, one can introduce a characteristic length $r_0$ of the two-body interaction, which is called the range of the potential. The term 'nearly resonant interactions' refers to potentials which can almost or just barely support a weakly two-body bound state, in which case the magnitude of the scattering length is much larger than the range. Only when the scattering length $a$ diverges, the number of Efimov states is infinite. This effect arises from an effective three-body long-range force whose

potential is proportional to $-1/R^2$ in the range $r_0 \ll R \ll |a|$ where the hyperradius $R$ is defined by $R = \sqrt{\frac{2}{3}\left(r_{12}^2 + r_{23}^2 + r_{31}^2\right)}$ and describes the size of the three-body system[1].

## 1.2 Finite-range corrections

In case of zero-range potentials the condition $|a| \gg r_0$ is always satisfied for nonzero $a$, so that Efimov's results describe exactly what happens for contact interactions. As recognized by Efimov, finite-range potentials will always have a three-body ground state. Consequently, the index $n$ which labels the Efimov state becomes an integer in the range $[0, \infty)$. The ground Efimov state is labeled by $n = 0$.

The universal Efimov spectrum shown by Fig. 1.1 changes as a result of the nonzero interaction range. First of all, local finite-range potentials which are attractive may support deeper two-body bound states which allows the Efimov trimers to decay. A zero-range two-body potential can support at most one two-body bound state, so that only one potential resonance is associated with this potential. When a finite-range two-body interaction supports more than one $s$-wave two-body bound state, many potential resonances at which the scattering length diverges, are associated with this potential and infinitely many Efimov states show up at each potential resonance. These Efimov states are not true bound states when a deeper dimer state is present. In those cases, the Efimov states are called resonant states. The lifetime of these states is finite because they are embedded in the atom-dimer scattering continuum as shown in Fig. 1.2. This figure shows the Efimov spectra corresponding to the first three potential resonances of the finite-range potential $gV(r)$. The interaction strength $g$ is used to tune $s$-wave scattering length.

Fig. 1.2 also shows that near each potential resonance a regime can be defined in which the universal scaling of the three-body parameters given by Eq. (1.4) is approximately valid. Note that this is the universal regime studied by Efimov. Inside this regime, Eq. (1.4) is still valid because $|a_{\alpha,n}| \gg r_0$ and $\kappa_n^* r_0 \ll 1$. Outside this universal regime, the discrete scale invariance of the Efimov states is broken due to the finite-range interactions. The three-body parameters corresponding to the lowest Efimov state are strongly affected. This Efimov state may not even cross the two-body threshold. There exists even a variational principle [45] which constrains the ground-state energy of three identical bosons, interacting via spherically symmetric pair potentials, to always lie below the ground-state energy of two of such bosons, more precisely $E_{3b,0} \leq 3E_{2b,0}$. For such systems, the three-body parameter $a_{*,0}$ is absent near the first potential resonance.

The three-body parameter was thought to strongly depend on the short-range details of the two-body interaction potential. This concept has changed over the past decade in which many experiments in ultracold quantum gases have been successfully performed with different atomic species to measure the three-body parameter $a_-$ [22–30, 36–39, 46, 47], resulting in $a_{-,0} \approx 9\, r_{vdW}$ within $\pm 20\%$ deviation [16], where $r_{vdW}$ is the van der Waals length defined by $r_{vdW} \equiv \frac{1}{2}\left(\frac{mC_6}{\hbar^2}\right)^{1/4}$. The origin of this universality is the result of a strongly repulsive universal barrier in the effective three-body potential at a hyperradius $R \approx 2\, r_{vdW}$ which prevents the three particles from simultaneously getting close together, so that the short-range details are

[1] Other definitions of the hyperradius also exist. The hyperradius defined by Ref. [15] is a factor $\sqrt{2}$ smaller, whereas the definition of Ref [44] is a factor $\frac{2^{1/2}}{3^{1/4}} \approx 1.07$ smaller.

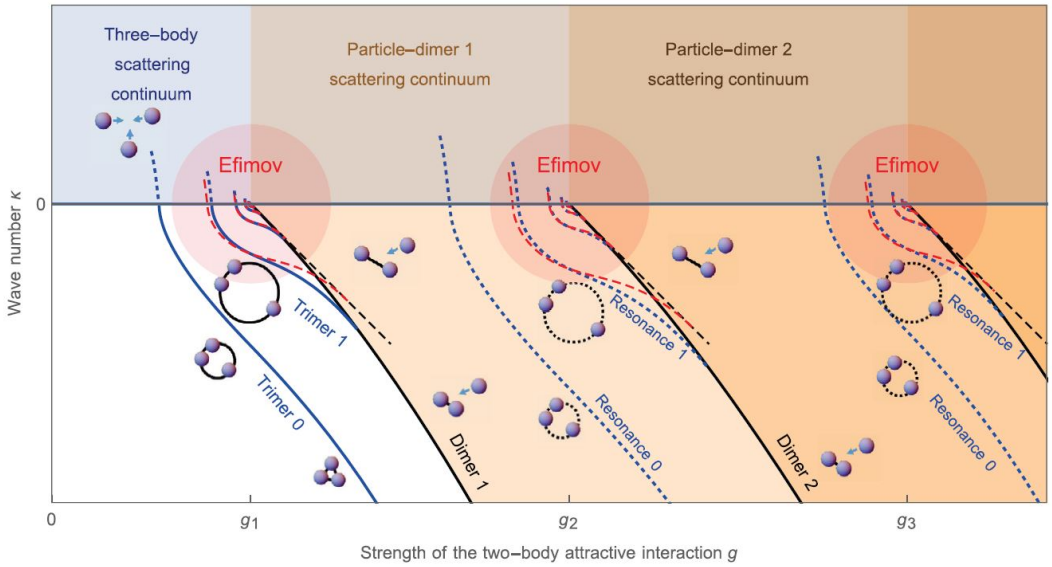


Figure 1.2: Schematic representation of the Efimov spectra for three identical bosons of mass $m$ interacting via a short-range attractive two-body potential $gV(r)$ (figure taken from Ref. [16]). The black solid curves indicate the $s$-wave two-body bound states. The three-body bound states are indicated by the solid blue curves, whereas the dashed blue curves indicate three-body resonant states. The red discs indicate the Efimov windows of universality [16] in which good agreement with the zero-range theory is found (red dashed curves). Note that this figure only shows states with zero angular momentum.

less important than one would naïvely expect [48, 49]. The three-body repulsive barrier is caused by the increase of the kinetic energy corresponding to the hyperangular motion which originates from an abrupt change of the geometry of the three-particle system. This change is caused by the small probability density to find two particles close together.

The universal shape of the Efimov spectrum implies that universal negative three-body parameters $a_-$ should lead to universality for positive scattering lengths. Therefore one would expect that the values of the scattering length at which the three-body recombination minima and the atom-dimer resonances occur, indicated by $a_+$ and $a_*$ respectively, should also be universal. The universality of these parameters has not been observed experimentally [19, 22–27, 31–36, 46, 50, 51] (see also Ref. [52] for a careful analysis of the experimental data). Theoretical models which are more sophisticated than the contact interaction model, are needed to describe these experimental results. For instance, Ref. [31] measured the energy of the first excited Efimov state at positive scattering lengths by performing radio-frequency association measurements and found that the universal model based on contact interactions is insufficient to predict the correct value of $a_*$.

The necessity to go beyond zero-range universal theories has also been shown by a recent numerical study on the first three potential resonances of the Lennard-Jones potential [52] revealing that the first excited Efimov trimer does not intersect the atom-dimer threshold (just like the ground Efimov state). However, this Efimov state approaches the threshold close enough to produce a resonance in the atom-dimer loss rate near $a = 3.3\ r_{vdW}$. The authors of Ref. [52] attributed this non-crossing of the second Efimov resonance to strong $d$-wave interactions near $a = 1\ r_{vdW}$ [53]. The adiabatic hyperspherical representation used by Ref. [52] did not allow to exclude the $d$-wave interactions in order to confirm their hypothesis. Other theoretical studies [54, 55] which considered separable approximations for van der Waals potentials, considering only $s$-wave interactions, showed that the second Efimov state does unbind into a dimer and a free particle at some positive value of the scattering length.

## 1.3 Feshbach resonance

The schematic representation of the Efimov spectra in Fig. 1.2 describes how the bound and resonant states are affected when one varies the strength $g$ of the single-channel interaction. The scattering length $a$ diverges for specific values of $g$ (indicated in Fig. 1.2 by $g_1$, $g_2$ and $g_3$) at which an $s$-wave two-body bound state becomes bound. This phenomenon is called a potential resonance. However, in most physical systems it is not possible to tune the single-channel interaction strength $g$ experimentally, so that a potential resonance is not typically accessible in experiments. Although the scattering length in a potential resonance is not experimentally tunable, it can be used theoretically to study the Efimov effect. Experimentally, it is possible to tune the scattering length of ultracold atomic systems by means of a Feshbach resonance [56], named after Herman Feshbach who described such resonances in the context of nuclear physics [2, 3]. Fano [4] approached the problem on the background of atomic physics, so that this resonance is also known as the Fano-Feshbach resonance.

In a Feshbach resonance a closed channel supports a two-body bound state whose energy equals the collision threshold of the open channel. This situation is sketched in Fig. 1.3. The open and closed channels correspond to different hyperfine state configurations of the two interacting atoms. This means that the magnetic moments corresponding to the open

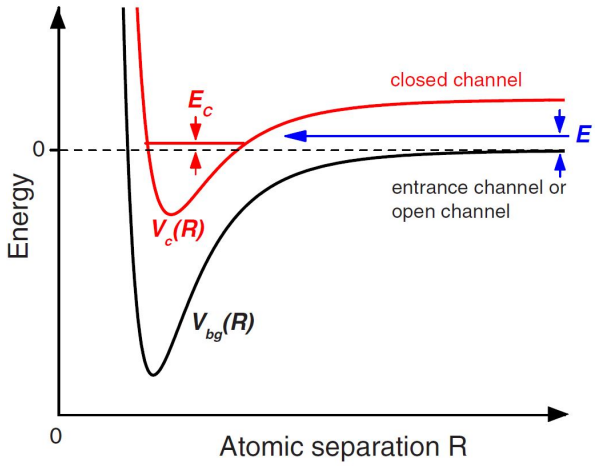


Figure 1.3: Schematic representation of the two-channel model for a Feshach resonance (figure adapted from [56]). Two atoms collide at energy $E$ in the entrance channel (indicated by the blue arrow) which is coupled to the closed channel potential $V_c$ supporting a bound state with energy $E_c$.

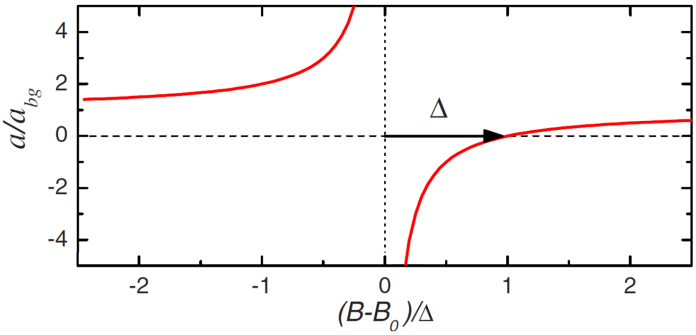


Figure 1.4: Scattering length $a$ as function of the magnetic field $B$ for a Feshbach (figure adapted from [56]). Here $a_{bg}$ denotes the background scattering length due to scattering in the open channel, $B_0$ is the resonance position and $\Delta$ the width of the resonance.

and closed channels are different. Application of an external magnetic field can therefore be used to detune the energy difference between the bound state of the closed channel and the scattering threshold of the incoming channel. At resonance, this energy difference is zero and the scattering of the atoms in the open channel is enhanced [15]. Mathematically, this means that the scattering length $a$ diverges when a particular magnetic field $B_0$ is applied. Near a Feshbach resonance without inelastic two-body channels, the scattering length $a$ is given by

$$a = a_{bg}\left(1 - \frac{\Delta}{B - B_0}\right), \tag{1.7}$$

where $a_{bg}$ is the background scattering length which results from the background collision in the open channel potential $V_{bg}$ and $\Delta$ controls the width of the resonance [57, 58] as sketched in Fig. 1.4. So modification of the strength of an external magnetic field is equivalent to modifying the two-body scattering length $a$.

## 1.4 The square well potential

In order to get a full understanding of the experimental results, theoretical models should include the effects of finite-range interatomic potentials, the multichannel nature of atomic systems and the corresponding finite-width effects related to the Feshbach resonances which are used to tune the scattering length experimentally by variation of an applied magnetic field. One method to study finite-range effects on the Efimov spectrum is to model broad Feshbach resonances by the potential resonances of some finite-range interaction potential. Such analyses have been performed for many different kinds of potentials [48, 49, 55, 59]. In particular, Ref. [59] considered both potentials with a power-law decaying tail, $-C_n r^{-n}$, and potentials which decay faster than any power law. However, the square well potential given by

$$V_{SW}(r) = \begin{cases} -V_0 & 0 \leq r < R \\ 0 & r \geq R, \end{cases} \tag{1.8}$$

is not fully understood yet in the context of Efimov physics. This is a very simple model for atomic interactions whose long-range behaviour is in fact described by the van der Waals tail $-\frac{C_6}{r^6}$ where the dispersion coefficient $C_6$ depends on the atomic species. The advantage of the square-well potential is the fact that it is one of the simplest extensions of zero-range interaction models, in which finite-range effects are incorporated in a pure way (i.e., the range is extremely well defined). Furthermore, many two-body properties relevant for three-body physics, such as the off-shell two-body $T$-matrix, are known analytically, which eases the three-body calculations and thus makes it easier to go beyond the usual separable approximation for the $s$-wave component of the off-shell two-body $T$-matrix when computing the Efimov states in the momentum-space treatment.

### 1.4.1 Previous work on the square well potential

The Efimov physics associated with the square well model has been considered before in Ref. [60–63]. Jensen *et al.* (1997) [60] solved the Faddeev equations in coordinate space and showed that an infinite number of Efimov states exists when the three particles interact via a pairwise square well potential. Their methods were mainly analytical, and they did not calculate the Efimov spectrum.

In Ref. [61–63], the Efimov trimers corresponding to the square well potential were calculated by substituting the off-shell two-body $T$-matrix into the Skorniakov-Ter-Martirosian equation, which applies to separable two-body interactions. The square well potential is non-separable in the momentum-space representation just like all local finite-range potentials, so that the validity of these calculations needs to be tested. Mestrom [61] focused on a shallow square well potential, whereas Debets [62] considered an infinitely deep square well potential and found that the corresponding three-body parameter ($a_{-,0} = -14.6\ R$) is five times larger than for the shallow square well ($a_{-,0} = -3\ R$). Kroeze [63] generalized the Feshbach formalism to an off-shell theory and calculated the off-shell $T$-matrix describing scattering off an infinitely deep square well including a Feshbach resonance. For very broad Feshbach resonances this model resulted in a three-body parameter which matches the value found in experiments. One problem of this model is the huge impact of the background scattering

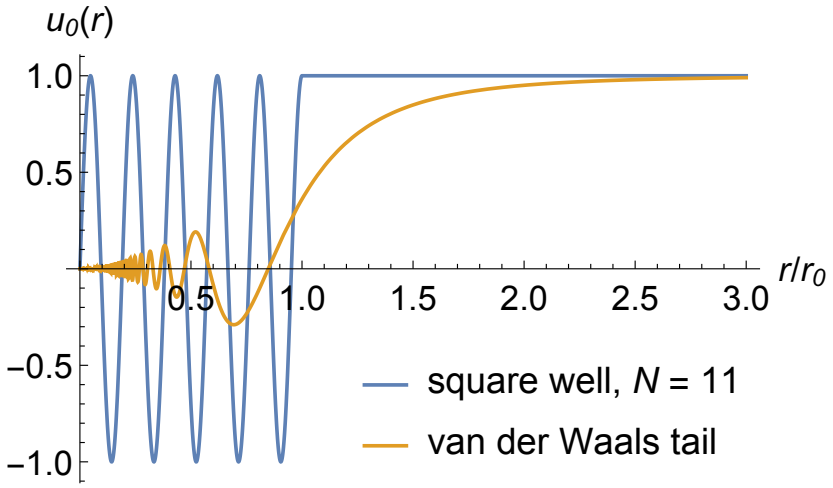


Figure 1.5: The $s$-wave radial wave functions $u_0(r)$ of the square well potential and the van der Waals tail $-C_6/r^6$ at zero energy (normalized asymptotically to unity) as a function of the interparticle distance $r$ expressed in the range $r_0$ ($r_0 = R$ in case of the square well and $r_0 = r_{vdW}$ in case of the van der Waals tail). The considered square well potential supports 11 $s$-wave two-body bound states, whereas the van der Waals tail supports infinitely many bound states. In both cases, the magnitude of the $s$-wave scattering length is infinite, so that $u_0(r) \to 1$ for $r \to \infty$.

length on the three-body parameter which is not expected. The studies of Ref. [60–63] involved only $s$-wave interactions which dominate in the ultracold regime. However, the effects of $d$-wave interactions could be important when the scattering length is comparable to the range of the potential [52, 53].

Ref. [61–63] have only considered a shallow and infinitely deep square well potential, but did not analyze the intermediate regime. Naidon *et al.* [59] formulated a hypothesis for the behavior of the three-body parameter of the square well potential: they expect that the square well potential does not reveal any universality of the three-body parameter. As discussed above, the universality of the three-body parameter originates from a three-body repulsive barrier in the effective hyperradial potential which is caused by the reduced probability to find particles inside the attractive two-body potential well [48, 49]. Such a reduction of the probability density is not the case for the square well potential as can be seen from Fig. 1.5. This figure compares the zero-energy two-body $s$-wave radial wave functions of the square well potential and the van der Waals potential $-C_6/r^6$ at diverging scattering length. The analytical form of these wave functions can be found in Ref. [61] and Ref. [49] respectively. Ref. [59] considered both potentials with a power-law decaying tail, $-C_n r^{-n}$, and potentials which decay faster than any power law. In both cases the two-body probability density drops significantly inside the well. This suggests that the square well potential is an exception and may not reveal any universality [59]. This hypothesis should be tested in order to gain more insight into the universality of the three-body parameter in general.

## 1.5 Outline

In this work we study Efimov physics associated with the potential resonances of the square well potential. We solve the three-body Fadddeev equations which apply to three identical spinless bosons. This momentum space representation allows us to exclude and include $d$-wave interactions and to study their effects. Previous calculations in Efimov physics using this momentum-space treatment involved only $s$-wave interactions for which non-local separable interaction potentials were used as a model for local potentials. Since the Faddeev equations reduce to a set of one-dimensional integral equations when the off-shell two-body $T$-matrix is approximated by a separable expansion, it is important to understand the different existing expansion methods and to judge their accuracy and usefulness in calculations of the energies of the Efimov states. A systematic analysis of these different expansion methods by simply calculating the energies of the Efimov states using these different methods has not been performed before and is therefore also presented in this work. Elastic atom-dimer scattering processes are also considered to investigate the crossing of the Efimov states with the atom-dimer threshold.

This thesis is organized as follows. In Chapter 2 we will review some important concepts of two-body scattering theory. This Chapter introduces the off-shell two-body $T$-matrix which is very important when performing three-body calculations. The three-body Faddeev equations are presented in Chapter 3. We focus on the equations corresponding to three-body bound states and to the scattering process between a two-body bound state and a free particle. Chapter 4 summarizes and expands the on-shell and off-shell two-body scattering results presented in Ref. [63] for a square well potential as two-body interaction. In Chapter 5 we present different methods to perform a separable expansion of the off-shell two-body $T$-matrix which we use to solve the Faddeev equations. The numerical approach to solve these equations is presented in Chapter 6. The resulting Efimov spectra corresponding to the square well potential are analyzed in Chapter 7. We mainly focus on the shallow and very deep potentials. Finally, Chapter 8 summarizes the main conclusions of our work, followed by an outlook to possible future research.

# 2. Scattering theory

In this Chapter we will treat the quantum theory of nonrelativistic scattering. We will assume that the particles are spinless. The most important concepts which we will introduce here are the scattering length and the off-shell two-body $T$-matrix. This Chapter is based on the textbooks written by Taylor (1972) [64] and Sitenko (1991) [5].

## 2.1 Two-body scattering theory

The Hamiltonian of a two-particle system is given by

$$H = \frac{\mathbf{p}_1^2}{2m_1} + \frac{\mathbf{p}_2^2}{2m_2} + V(\mathbf{r}_1, \mathbf{r}_2, t) \tag{2.1}$$

where $\mathbf{p} = -i\hbar\nabla$ is the momentum operator. When the interaction potential $V(\mathbf{r}_1, \mathbf{r}_2, t)$ is time-independent, the general solution of the Schrödinger equation, $i\hbar\frac{\partial}{\partial t}|\Psi\rangle = H|\Psi\rangle$, is given by

$$|\Psi\rangle = e^{-iHt/\hbar}|\psi\rangle \tag{2.2}$$

where $|\psi\rangle$ is the time-independent wave function. It should satisfy the time-independent Schrödinger equation, $H|\psi\rangle = E|\psi\rangle$. If $V(\mathbf{r}_1, \mathbf{r}_2, t)$ depends only on the relative distance $\mathbf{r} = \mathbf{r}_1 - \mathbf{r}_2$, the eigenfunctions of the Hamiltonian can be chosen to be separable in the center-of-mass coordinate $\mathbf{R} = \frac{m_1\mathbf{r}_1 + m_2\mathbf{r}_2}{m_1+m_2}$ and the relative coordinate $\mathbf{r}$, i.e. $|\psi\rangle = |\psi_{\mathbf{R}}\rangle|\psi_{\mathbf{r}}\rangle$. The wave function $|\psi_{\mathbf{R}}\rangle$ satisfies the Schrödinger equation for a free particle with mass $M = m_1 + m_2$, whereas the wave function $|\psi_{\mathbf{r}}\rangle$ satisfies the one-particle Schrödinger equation with reduced mass $\mu = \frac{m_1 m_2}{m_1+m_2}$ subject to the potential $V$. So we have

$$-\frac{\hbar^2}{2M}\nabla_{\mathbf{R}}^2|\psi_{\mathbf{R}}\rangle = E_{\mathbf{R}}|\psi_{\mathbf{R}}\rangle, \tag{2.3}$$

$$\left[-\frac{\hbar^2}{2\mu}\nabla_{\mathbf{r}}^2 + V(\mathbf{r})\right]|\psi_{\mathbf{r}}\rangle = E_{\mathbf{r}}|\psi_{\mathbf{r}}\rangle. \tag{2.4}$$

Therefore two-body scattering theory is equivalent to solving two one-particle Schrödinger equations. The corresponding Hamiltonians are $H_{cm} = -\frac{\hbar^2}{2M}\nabla_{\mathbf{R}}^2$ and $H_{rel} = \left[-\frac{\hbar^2}{2\mu}\nabla_{\mathbf{r}}^2 + V(\mathbf{r})\right]$.

### 2.1.1 The scattering operator

The general solution of Eq. (2.2) contains the so-called evolution operator $U(t)$ which is defined by

$$U(t) \equiv e^{-iHt/\hbar} = e^{-i(H_{cm}+H_{rel})t/\hbar} \quad = e^{-iH_{cm}t/\hbar} \otimes e^{-iH_{rel}t/\hbar} \tag{2.5}$$

where we have made use of the fact that $H_{cm}$ and $H_{rel}$ commute. Similarly, we define the free evolution operator $U^0(t)$ as

$$\begin{aligned} U^0(t) &\equiv e^{-iH^0t/\hbar} = e^{-i(H_{cm}+H^0_{rel})t/\hbar} \\ &= e^{-iH_{cm}t/\hbar} \otimes e^{-iH^0_{rel}t/\hbar} \end{aligned} \tag{2.6}$$

where $H^0_{rel} = -\frac{\hbar^2}{2\mu}\nabla^2_{\mathbf{r}}$ is the kinetic energy operator of the relative motion. This free evolution operator $U^0(t)$ describes the system of two noninteracting particles.

For every scattering state $|\psi\rangle$ the orbit is given by $U(t)|\psi\rangle$. This time-dependent wave function is expected to behave as

$$\begin{aligned} \lim_{t\to-\infty} U(t)|\psi\rangle &= U^0(t)|\psi_{in}\rangle, \text{ and} \\ \lim_{t\to\infty} U(t)|\psi\rangle &= U^0(t)|\psi_{out}\rangle \end{aligned} \tag{2.7}$$

which are called the in- and out-asymptotes respectively. This expectation is based on the assumption that the potential $V(\mathbf{r})$ falls off sufficiently fast as $\mathbf{r} \to \infty$. For a spherically symmetric potential $V(r)$ this means that it should fall off quicker than $r^{-3}$ at infinity [64]. This is only one of the conditions to which the scattering theory presented in this Section applies. In the rest of this Section we will always assume that the particles interact via a spherically symmetric potential which satisfy the following conditions [64]:

1. $V(r) = O(r^{-3-\epsilon})$ as $r \to \infty$ (some $\epsilon > 0$)
2. $V(r) = O(r^{-\frac{3}{2}+\epsilon})$ as $r \to 0$ (some $\epsilon > 0$)
3. $V(r)$ is continuous for $0 < r < \infty$, except perhaps at a finite number of finite discontinuities.

So a wide class of potentials including the atomic interaction potentials considered in this thesis fulfill these conditions. Note that the Coulomb potential does not fulfill the above conditions.

If the above conditions are satisfied, it can be proven that every state $|\psi_{in}\rangle$ in the two-particle Hilbert space $\mathcal{H}$ is the in-asymptote of some actual orbit $U(t)|\psi\rangle$ [64], which is known as the asymptotic condition. So we can define the two-particle Møller operator $\mathbf{\Omega}_+$ as

$$\mathbf{\Omega}_+ = \lim_{t\to-\infty} U(t)^\dagger U^0(t), \tag{2.8}$$

so that

$$|\psi\rangle = \mathbf{\Omega}_+|\psi_{in}\rangle. \tag{2.9}$$

From Eq. (2.8) it can be easily derived that

$$\begin{aligned}\mathbf{\Omega}_+ = \lim_{t\to-\infty} U(t)^\dagger U^0(t) &= 1_{cm} \otimes \left(\lim_{t\to-\infty} e^{iH_{rel}t/\hbar} e^{-iH^0_{rel}t/\hbar}\right) \\ &\equiv (1_{cm} \otimes \Omega_+)\end{aligned} \tag{2.10}$$

Here we have defined the operator $\Omega_+$ which acts on $\mathcal{H}_{rel}$. The unit operator $1_{cm}$ acts on the subspace $\mathcal{H}_{cm}$ and reflects the fact that the center of mass moves as a free particle. Similarly, we can define the two-particle Møller operator $\mathbf{\Omega}_-$ as

$$\begin{aligned}\mathbf{\Omega}_- \equiv \lim_{t\to\infty} U(t)^\dagger U^0(t) &= 1_{cm} \otimes \left(\lim_{t\to\infty} e^{iH_{rel}t/\hbar} e^{-iH^0_{rel}t/\hbar}\right) \\ &\equiv (1_{cm} \otimes \Omega_-)\,,\end{aligned} \tag{2.11}$$

so that

$$|\psi\rangle = \mathbf{\Omega}_-|\psi_{out}\rangle. \tag{2.12}$$

The scattering theory presented in this Section does not only satisfy the asymptotic condition, but it is also asymptotically complete [64]. This means that the subspace which contains all states with in-asymptotes is the same as the subspace which contains all states with out-asymptotes and that this subspace of the Hilbert space $\mathcal{H}$ is just the subspace of all states orthogonal to the bound states [64]. We call this subspace $\mathcal{R}$. This theorem allows us to write

$$|\psi\rangle = \mathbf{\Omega}_+|\psi_{in}\rangle = \mathbf{\Omega}_-|\psi_{out}\rangle. \tag{2.13}$$

The Møller operators are isometric operators on $\mathcal{H}$ which means that they are linear operators which preserve the norm. This property allows us to define the scattering operator $\mathbf{S}$ as

$$\mathbf{S} \equiv \mathbf{\Omega}_-^\dagger \mathbf{\Omega}_+ = 1_{cm} \otimes \Omega_-^\dagger \Omega_+ \equiv 1_{cm} \otimes S, \tag{2.14}$$

so that

$$|\psi_{out}\rangle = \mathbf{S}|\psi_{in}\rangle. \tag{2.15}$$

So the scattering operator $\mathbf{S}$ relates the in-asymptote directly to the out-asymptote. Therefore it contains all information which is of experimental interest. From the fact that the Møller wave operators are isometric it follows that scattering operator $\mathbf{S}$ is linear and norm preserving, so that it is also isometric. Moreover, from the asymptotic completeness it follows that $\mathbf{S}$ is a mapping from the subspace $\mathcal{R}$ onto $\mathcal{R}$, so that is unitary. So

$$\mathbf{S}^\dagger\mathbf{S} = \mathbf{S}\mathbf{S}^\dagger = 1. \tag{2.16}$$

In the rest of the Section we will consider operators such as the scattering operator $S$ which acts on the subspace $\mathcal{H}_{rel}$. We will write the time-independent wave function $|\psi_{\mathbf{r}}\rangle$ corresponding to the relative motion of the two particles as $|\psi\rangle$. So we drop the index for convenience. We will also write the Hamiltonian $H_{rel}$ simply as $H$.

### 2.1.2 The scattering matrix

The scattering operator $S$ commutes with $H^0$, and also with the angular momentum operators $\mathbf{L}^2$ and $L_z$ if the interaction potential is spherically symmetric. Therefore, the $S$-matrix is diagonal in the spherical wave basis $\{|E, l, m\rangle\}$ (defined in Appendix E.1), i.e.,

$$\langle E', l', m'|S|E, l, m\rangle = S_l(E)\delta_{l'l}\delta_{m'm}\delta(E - E'). \tag{2.17}$$

This is also called the energy normalized $S$-matrix, whereas the momentum normalized scattering matrix is defined as $\langle \mathbf{p}'|S|\mathbf{p}\rangle$. The scattering operator $S$ is unitary, so that $S_l(E)$ can be written as

$$S_l(E) = e^{2i\delta_l(E)}. \tag{2.18}$$

The phase shift $\delta_l(E)$ is real. It defines the partial-wave scattering length $a_l$ and effective range $R_l$ by the so-called effective range expansion:

$$k^{2l+1}\cot(\delta_l(k)) = -\frac{1}{a_l} + \frac{1}{2}R_l k^2 + O(k^4). \tag{2.19}$$

The wave number $k$ is related to the energy $E$ by $E = \frac{\hbar^2 k^2}{2\mu}$ as usual. The coefficient $R_0$ is usually related to the range of the potential. Note that only the $s$-wave scattering length $a_0$ has the dimension of length. Eq. (2.19) holds for exponentially bound potentials. The effective range expansion in powers of $k^2$ is usually not possible for other types of potentials.

### 2.1.3 The transition operator

So far we have described collisions in terms of the scattering operator $S$. However, the transition operator $T(z)$ and the Green's operator $G(z)$ are also very useful in scattering theory. The transition operator $T$ is defined as

$$T(z) = V + VG(z)V \tag{2.20}$$

where $G(z) = (z - H)^{-1}$ is the so-called Green's operator or resolvent [64]. The variable $z$ is a complex variable which represents the energy of the two-particle system in the center-of-mass frame when it is real. Clearly, $T(z)$ is analytic for all $z$ not in the spectrum of $H$ just like the operator $G(z)$. The transition operator $T(z)$ has a pole for the values of $z$ corresponding to a bound state of $H$ and it has a branch cut on the real positive axis [64].

We can also define the free Green's operator $G^0(z) = (z - H^0)^{-1}$ where $H^0$ is the kinetic energy operator in the center-of-mass frame. The operators $G(z)$ and $G^0(z)$ are related by

$$\begin{aligned} &G(z) = G^0(z) + G^0(z)VG(z) \text{ or} \\ &G(z) = G^0(z) + G(z)VG^0(z) \end{aligned} \tag{2.21}$$

which are both called the Lippmann-Schwinger equation for $G(z)$. By combining this equation with Eq. (2.20) it can be easily derived that

$$\begin{aligned} &G^0(z)T(z) = G(z)V \text{ and} \\ &T(z)G^0(z) = VG(z). \end{aligned} \tag{2.22}$$

These important identities can be substituted in Eq. (2.20) in order to obtain the Lippmann-Schwinger equation for $T(z)$:

$$\begin{aligned} &T(z) = V + VG^0(z)T(z) \text{ or} \\ &T(z) = V + T(z)G^0(z)V. \end{aligned} \tag{2.23}$$

When the potential $V$ is not strong enough to support any bound states, it is possibile to obtain a solution of Eq. (2.23) by iteration:

$$T(z) = V + VG^0(z)V + VG^0(z)VG^0(z)V + ... \tag{2.24}$$

This series is known as the Born series. This series does not converge for $z$ near the bound state energies [65]. After all, the series in Eq. (2.24) does not have any poles in $z$. Therefore the Born series is not useful for our purposes. However, Weinberg [65] has introduced a method which can be used when the Born series does not converge. The idea is to modify the Hamiltonian by introducing quasiparticles, so that the original interaction weakens and the Born series can be used.

### 2.1.4 The stationary scattering states

The in-asymptote $|\psi_{in}\rangle$ is an eigenstate of the kinetic energy operator $H^0$ because the potential $V(r)$ is assumed to go sufficiently fast to zero for $r \to \infty$. So $|\psi_{in}\rangle$ is just a wave packet composed of plane wave states $|\mathbf{p}\rangle$ which are improper eigenvectors of the Hamiltonian $H^0$. More information about these plane wave states is given in Appendix E.1.

We can also introduce the momentum states $|\mathbf{p}+\rangle$ and $|\mathbf{p}-\rangle$ by

$$|\mathbf{p}\pm\rangle \equiv \Omega_\pm|\mathbf{p}\rangle. \tag{2.25}$$

The states $|\mathbf{p}\pm\rangle$ are improper eigenvectors of the Hamiltonian $H = H^0 + V$ with outgoing and ingoing spherical wave boundary conditions respectively, i.e., $H|\mathbf{p}\pm\rangle = E_p|\mathbf{p}\pm\rangle$ where $E_p = \frac{p^2}{2\mu}$. As a result of the definition of Eq. (2.25), the state $|\psi+\rangle = \Omega_+|\psi_{in}\rangle$ representing the actual state of the system at $t = 0$ has the same expansion in terms of $|\mathbf{p}+\rangle$ as does its in-asymptote $|\psi_{in}\rangle$ in terms of $|\mathbf{p}\rangle$. Similarly, the state $|\psi-\rangle = \Omega_-|\psi_{out}\rangle$ has the same expansion in terms of $|\mathbf{p}-\rangle$ as does its out-asymptote $|\psi_{out}\rangle$ in terms of $|\mathbf{p}\rangle$. However, the states $|\mathbf{p}+\rangle$ and $|\mathbf{p}-\rangle$ should not be interpreted as the actual state at $t = 0$ that has evolved from the initial state $|\mathbf{p}\rangle$ or that would evolve into the final state $|\mathbf{p}\rangle$ respectively [64]. Even though Eq. (2.7) holds, similar equalities do not hold for the states $|\mathbf{p}\pm\rangle$ and $|\mathbf{p}\rangle$, i.e.,

$$\begin{aligned} &\lim_{t\to-\infty} U(t)|\mathbf{p}+\rangle \neq U^0(t)|\mathbf{p}\rangle, \text{ and} \\ &\lim_{t\to\infty} U(t)|\mathbf{p}-\rangle \neq U^0(t)||\mathbf{p}\rangle\rangle. \end{aligned} \tag{2.26}$$

It can be proven [64] that the states $|\mathbf{p}\pm\rangle$ are related to $|\mathbf{p}\rangle$ by

$$|\mathbf{p}\pm\rangle = |\mathbf{p}\rangle + G(E_p \pm i0)V|\mathbf{p}\rangle. \tag{2.27}$$

and

$$|\mathbf{p}\pm\rangle = |\mathbf{p}\rangle + G^0(E_p \pm i0)V|\mathbf{p}\pm\rangle. \tag{2.28}$$

where the operator $G^0(E_p \pm i0) = \lim_{\epsilon\to 0} G^0(E_p \pm i\epsilon)$ and $G(E_p \pm i0) = \lim_{\epsilon\to 0} G(E_p \pm i\epsilon)$. From those Lippmann-Schwinger equations for the scattering states $|\mathbf{p}\pm\rangle$ and the definition of the transition operator, Eq. (2.20), the following important property of the transition operator can be proven [64]:

$$T(E_p \pm i0)|\mathbf{p}\rangle = V|\mathbf{p}\pm\rangle. \tag{2.29}$$

### 2.1.5 The two-body $T$-matrix

The two-body $T$-matrix can be calculated from the two-body transition operator $T$ defined by Eq. (2.20). In the momentum-space representation, it is given by

$$\langle \mathbf{p}'|T(z)|\mathbf{p}\rangle = \langle \mathbf{p}'|V|\mathbf{p}\rangle + \int \langle \mathbf{p}'|V|\mathbf{p}''\rangle \frac{1}{z - \frac{p''^2}{2\mu}} \langle \mathbf{p}''|T(z)|\mathbf{p}\rangle \, d\mathbf{p}''. \tag{2.30}$$

Two-particle interactions are specified by the on-shell two-body $T$-matrix in which all energies are equal, i.e. $z = \frac{p^2}{2\mu} = \frac{p'^2}{2\mu}$. However, the incoming kinetic energy of the two-particle system need not to be equal to the outgoing kinetic energy of the two-particle system when a third particle is involved. Therefore the full off-shell two-body $T$-matrix in which $z \neq \frac{p^2}{2\mu} \neq \frac{p'^2}{2\mu}$ is important for the description of three-particle interactions. Just like the $S$-matrix, the $T$-matrix possesses singularities in the plane of complex energy which correspond to the two-body continuum and bound states.

For spherically symmetric interactions we can expand the potential and the $T$-matrix in terms of the Legendre polynomials $P_l(\hat{\mathbf{p}} \cdot \hat{\mathbf{p}}')$ as

$$\langle \mathbf{p}'|T(z)|\mathbf{p}\rangle = \sum_{l=0}^{\infty} (2l+1) P_l(\hat{\mathbf{p}}' \cdot \hat{\mathbf{p}}) t_l(p, p', z) = 4\pi \sum_{l=0}^{\infty} \sum_{m=-l}^{l} Y_l^m(\hat{\mathbf{p}}) \bar{Y}_l^m(\hat{\mathbf{p}}') t_l(p, p', z), \tag{2.31}$$

$$\langle \mathbf{p}'|V|\mathbf{p}\rangle = \sum_{l=0}^{\infty} (2l+1) P_l(\hat{\mathbf{p}}' \cdot \hat{\mathbf{p}}) V_l(p, p') = 4\pi \sum_{l=0}^{\infty} \sum_{m=-l}^{l} Y_l^m(\hat{\mathbf{p}}) \bar{Y}_l^m(\hat{\mathbf{p}}') V_l(p, p'). \tag{2.32}$$

The functions $Y_l^m(\hat{\mathbf{p}})$ are the spherical harmonics (see Appendix B). So from Eq. (2.30) one can easily derive the Lippmann-Schwinger equation for the off-shell partial-wave components $t_l(p, p', z)$ which is given by

$$t_l(p, p', z) = V_l(p, p') + 4\pi \int_0^{\infty} V_l(p', p'') \frac{1}{z - \frac{p''^2}{2\mu}} t_l(p, p'', z) p''^2 \, dp''. \tag{2.33}$$

The on-shell $T$-matrix can simply be calculated from Eq. (2.29) if one first calculates the scattering state $|\mathbf{p}+\rangle$ from the Schrödinger equation. The on-shell $T$-matrix satisfies

$$\langle \mathbf{p}'|T(E_p + i0)|\mathbf{p}\rangle = \langle \mathbf{p}'|V|\mathbf{p}+\rangle. \tag{2.34}$$

Here all energies are equal, i.e., $E_p = \frac{p^2}{2\mu} = \frac{p'^2}{2\mu}$. It can be proven [64] that the on-shell $T$-matrix is related to the $S$-matrix by

$$\langle \mathbf{p}'|S|\mathbf{p}\rangle = \delta(\mathbf{p}' - \mathbf{p}) - 2\pi i \delta(E_{p'} - E_p) \langle \mathbf{p}'|T(E_p + i0)|\mathbf{p}\rangle. \tag{2.35}$$

This shows that the $S$-matrix is zero for $E_{p'} \neq E_p$, so that the scattering operator conserves energy.

The calculation of the off-shell $T$-matrix is not as straightforward as the calculation of the on-shell $T$-matrix. The simplest way is to define a new operator $\Omega(z)$ which extends the definition of the Møller operators $\Omega_\pm$. We define this operator as [66]

$$(z - H)\Omega(z) = (z - H^0), \tag{2.36}$$

so that it satisfies

$$|\mathbf{p}+\rangle = \Omega(E_p + i0)|\mathbf{p}\rangle. \tag{2.37}$$

So we see that $\Omega(E_p + i0) = \Omega_+$. From Eq. (2.22) we find that

$$T(z) = VG(z)(z - H^0) = V\Omega(z). \tag{2.38}$$

The next step is to define the off-shell wave function $|\psi_{\mathbf{p},z}\rangle$, where $z$ need not to be equal to $\frac{p^2}{2\mu}$, as [67]

$$|\psi_{\mathbf{p},z}\rangle = \Omega(z)|\mathbf{p}\rangle. \tag{2.39}$$

So we see that

$$\begin{aligned} T(z)|\mathbf{p}\rangle &= V\Omega(z)|\mathbf{p}\rangle \\ &= V|\psi_{\mathbf{p},z}\rangle. \end{aligned} \tag{2.40}$$

So the off-shell $T$-matrix can simply be calculated if the off-shell wave function $|\psi_{\mathbf{p},z}\rangle$ is known. In order to calculate this wave function we multiply Eq. (2.36) from the right by $|\mathbf{p}\rangle$, so that we obtain the off-shell Schrödinger equation [67]

$$(z - H)|\psi_{\mathbf{p},z}\rangle = \left(z - \frac{p^2}{2\mu}\right)|\mathbf{p}\rangle \tag{2.41}$$

whose position-space representation is given by

$$\begin{aligned} \langle\mathbf{x}|(z - H)|\psi_{\mathbf{p},z}\rangle &= \left(z - \frac{p^2}{2\mu}\right)\langle\mathbf{x}|\mathbf{p}\rangle \\ \left(z + \frac{\hbar^2}{2\mu}\nabla^2 - V(\mathbf{x})\right)\langle\mathbf{x}|\psi_{\mathbf{p},z}\rangle &= \left(z - \frac{p^2}{2\mu}\right)\langle\mathbf{x}|\mathbf{p}\rangle \\ \left(z + \frac{\hbar^2}{2\mu}\nabla^2 - V(\mathbf{x})\right)\langle\mathbf{x}|\psi_{\mathbf{p},z}\rangle &= \frac{1}{(2\pi\hbar)^{3/2}}\left(z - \frac{p^2}{2\mu}\right)e^{i\mathbf{p}\cdot\mathbf{x}/\hbar}. \end{aligned} \tag{2.42}$$

This off-shell Schrödinger equation reduces to the on-shell Schrödinger equation for $z = E_p \pm i0$, for which the state $|\psi_{\mathbf{p},z}\rangle$ is just the scattering state $|\mathbf{p}\pm\rangle$. The boundary conditions for the wave function $\langle\mathbf{x}|\psi_{\mathbf{p},z}\rangle$ ought to be chosen consistently with the three-body equations which one wants to solve. The off-shell two-body $T$-matrix can be calculated from Eq. (2.40) as

$$\begin{aligned} \langle\mathbf{p}'|T(z)|\mathbf{p}\rangle &= \langle\mathbf{p}'|V|\psi_{\mathbf{p},z}\rangle \\ &= \iint \langle\mathbf{p}'|\mathbf{x}\rangle\langle\mathbf{x}|V|\mathbf{x}'\rangle\langle\mathbf{x}'|\psi_{\mathbf{p},z}\rangle\, d\mathbf{x}\, d\mathbf{x}' \\ &= \int \langle\mathbf{p}'|\mathbf{x}\rangle V(\mathbf{x})\langle\mathbf{x}|\psi_{\mathbf{p},z}\rangle\, d\mathbf{x}. \end{aligned} \tag{2.43}$$

Note that we have assumed in Eqs. (2.42) and (2.43) that the pairwise interaction potential $V$ is local, so that [68]

$$\langle \mathbf{x}|V|\mathbf{x}'\rangle = V(\mathbf{x})\delta\left(\mathbf{x}' - \mathbf{x}'\right). \tag{2.44}$$

In order to obtain an expression for the partial-wave off-shell $T$-matrix elements (defined by Eq. (2.31)) we first expand the off-shell wave function $\langle \mathbf{x}|\psi_{\mathbf{p},z}\rangle$ into legendre polynomials as

$$\langle \mathbf{x}|\psi_{\mathbf{p},z}\rangle = (2\pi)^{-3/2}\frac{1}{pr}\sum_{l=0}^{\infty}(2l+1)i^l\omega_l(r,p,z)P_l(\hat{\mathbf{x}}\cdot\hat{\mathbf{p}}). \tag{2.45}$$

Substitution of this equation and Eq. (E.2) into the off-shell Schrödinger equation, Eq. (2.42), results in

$$\left[\frac{\hbar^2}{2\mu}\left(\frac{d^2}{dr^2} - \frac{l(l+1)}{r^2}\right) + z - V(r)\right]\omega_l(r,p,z) = \left(z - \frac{p^2}{2\mu}\right)\frac{1}{\sqrt{\hbar}}\hat{j}_l\left(\frac{pr}{\hbar}\right), \tag{2.46}$$

from which the partial-wave components $\omega_l(r,p,z)$ of the off-shell wave function can be calculated. The function $\hat{j}_l$ is the Riccati-Bessel function (see Appendix B.3). Similarly, a partial-wave expansion of Eq. (2.43) results in

$$t_l(p,p',z) = \frac{1}{2\pi^2\hbar^{1/2}}\frac{1}{pp'}\int_0^{\infty}\hat{j}_l\left(\frac{p'r}{\hbar}\right)V(r)\omega_l(r,p,z)\,dr. \tag{2.47}$$

### 2.1.6 Properties of the two-body $T$-matrix

The two-body $T$-matrix evaluated at small momenta is related to the partial-wave scattering length $a_l$. The behaviour of the momentum-normalized on-shell $T$-matrix at small values of the momentum $p = \hbar k$ is given by

$$t_l(k) \simeq \frac{1}{4\pi^2\mu\hbar k}\frac{a_l k^{(2l+1)}}{1 + ia_l k^{(2l+1)}}. \tag{2.48}$$

Taking the limit $k \to 0$, we have

$$t_0(0) = \frac{a_0}{4\pi^2\mu\hbar} \tag{2.49}$$

or

$$a_0 = 4\pi^2\mu\hbar \lim_{p,p',z\to 0} t_0(p,p',z). \tag{2.50}$$

Those results can be easily derived from the definition of the scattering length (see Eq. (2.19)), the definition of the phase shift (Eq. (2.18)) and the relation between the $S$-matrix and the $T$-matrix (Eq. (2.35)).

Another important property of the off-shell two-body $T$-matrix is the symmetry under exchange of $\mathbf{p}$ and $\mathbf{p}'$, which can immediately be seen from the definition of the transition

operator in Eq. (2.20). Therefore the partial-wave components of the off-shell two-body $T$-matrix satisfy

$$t_l(p, p', z) = t_l(p', p, z). \tag{2.51}$$

Finally, we should comment that the functions $t_l(p, p', z)$ are not separable in the momenta $p$ and $p'$ if the potential $V$ is local (except for a zero-range interaction). Here the word 'separable' means that $t_l(p, p', z)$ can be written as $g_l(p, z)g_l(p', z)$ where the function $g_l(p, z)$ is called the form factor. The two-body $T$-matrix can only be separable if the potential $V$ is separable. This means that the potential has the operator form

$$V = |g\rangle\lambda\langle g|, \tag{2.52}$$

where $|g\rangle$ defines the form factor and $\lambda$ determines the strength of the interaction.

Realistic physical potentials are local and the corresponding partial-wave components $V_l(p, p')$ are not separable which makes the three-body problem more difficult to solve. Short-range square-integrable potentials can be approximated well by a separable expression for the partial-wave components $V_l(p, p')$ [5] from which a separable approximation of the partial-wave components $t_l(p, p', z)$ follows. Therefore the approach to approximate $t_l(p, p', z)$ by the best separable expression is often used to study three-particle physics. Furthermore, the two-body $T$-matrix becomes separable at energies close to the binding energy of a dimer state [69]. Since the Efimov states lie very close to a weakly bound $s$-wave dimer state, it is usual to assume that the partial-wave off-shell $T$-matrix elements $t_l(p, p', z)$ are separable. However, the three-body equations which include a non-separable two-body $T$-matrix can still be simplified if the partial-wave components $t_l(p, p', z)$ are approximated by a sum of terms which are separable in $p$ and $p'$. This approach has not been explored yet in Efimov physics. Therefore we will also consider this approach to determine how good the separable approximation of the off-shell two-body $T$-matrix really is for the calculation of the Efimov states.

## 2.2 Multichannel scattering theory

So far we have discussed two-body collisions in which only one open channel is present. Therefore these scattering processes are always elastic, i.e., the incoming channel is the same as the outgoing channel. Therefore the theory presented in Section 2.1 has to be extended to describe inelastic scattering processes in which the outgoing channel is different from the incoming channel. Multichannel scattering theory plays an important role in Efimov physics. For example, this theory is necessary for the understanding of scattering processes such as three-body recombination and atom-dimer relaxation which can be studied to measure the three-body parameters of the Efimov spectrum experimentally or to calculate those parameters. In Appendix C we summarize the important concepts of multichannel scattering theory such as the scattering amplitude and the scattering length for two composite particles with multiple internal degrees of freedom.

# 3. Three-body scattering theory

In this Chapter we present the Faddeev equations for three-body bound states and for the scattering process between a two-body bound state and a free particle. We assume that all particles are identical zero-spin bosons with mass $m$ and interact only by pairwise forces. A nice overview of three-particle scattering theory can be found in Ref. [5].

## 3.1 The Faddeev equations for three-body bound states

The three-body bound states can be found by solving the three-body Schrödinger equation:

$$(H_0 + V)\Psi = E\Psi. \tag{3.1}$$

Here $H_0$ is the sum of the three kinetic energy operators and $V = V_{12} + V_{23} + V_{31}$ is the sum of the two-body interactions. Following Faddeev [69], one can construct a solution $\Psi$ of the three-body Schrödinger equation as follows:

$$\Psi = -\sum_{\alpha=1}^{3} G_0 \Phi_\alpha, \tag{3.2}$$

where the Green's function $G_0(z) = (z - H_0)^{-1}$ contains the kinetic energy operators for all three particles. The state $\Phi_\alpha$ can be calculated from the following set of coupled equations:

$$\Phi_\alpha = T_\alpha(z) G_0(z) \left(\Phi_\beta + \Phi_\gamma\right), \; \alpha\beta\gamma = 123, 231, 312. \tag{3.3}$$

The operator $T_\alpha(z)$ is the two-body $T$-operator for scattering between particles $\beta$ and $\gamma$ in the presence of particle $\alpha$. So this operator is given by $T_\alpha(z) = V_\alpha + V_\alpha G_0(z) T_\alpha(z)$ where $V_\alpha \equiv V_{\beta\gamma}$ describes the interaction between particles $\beta$ and $\gamma$. It is very similar to the two-body transition operator $T(z)$ which satisfies Eq. (2.23). The only difference is that the Green's function $G^0$ in Eq. (2.23) contains two kinetic energy operators, whereas the Green's function $G_0$ contains three kinetic energy operators.

In order to proof that Eq. (3.2) is a solution of the three-particle Schrödinger equation, we multiply Eq. (3.3) with $1 - V_\alpha G_0$ which gives

$$(1 - V_\alpha G_0)\Phi_\alpha = V_\alpha(z) G_0(z) \sum_{\gamma \neq \alpha} \Phi_\gamma, \tag{3.4}$$

so that

$$\Phi_\alpha = V_\alpha G_0 \sum_{\gamma} \Phi_\gamma \tag{3.5}$$

$$= -V_\alpha \Psi. \tag{3.6}$$

Summing this equation over $\alpha$ and multiplying by $-G_0$ gives

$$\Psi = G_0(V_\alpha + V_\beta + V_\gamma)\Psi \tag{3.7}$$

which reduces to the three-body Schrödinger equation after multiplying by $(z - H_0)$. It can be proven that this three-body wave function $\Psi$ constructed by Eq. (3.2) is square integrable [69].

Furthermore, the set of equations (3.3) reduces to a single operator equation when the three particles are identical bosons in which case the bound state $\Psi$ must be symmetric. The first step in deriving this equation is to define the permutation operators $P_+ = P_{\alpha\gamma}P_{\beta\gamma}$ and $P_- = P_{\alpha\beta}P_{\beta\gamma}$ (see Appendix D), so that the $T_\alpha = P_+T_\beta P_- = P_-T_\gamma P_+$. Therefore after multiplying the set of equations (3.3) with $P_+$ and $P_-$, two equivalent sets of equations can be derived, namely

$$\begin{aligned} P_+\Phi_\alpha &= P_+T_\alpha(z)(P_-P_+)G_0(z)\sum_{\gamma\neq\alpha}\Phi_\gamma \\ &= T_\gamma(z)G_0(z)(P_+\Phi_\beta + P_+\Phi_\gamma) \end{aligned} \tag{3.8}$$

and

$$\begin{aligned} P_-\Phi_\alpha &= P_-T_\alpha(z)(P_+P_-)G_0(z)\sum_{\gamma\neq\alpha}\Phi_\gamma \\ &= T_\beta(z)G_0(z)(P_-\Phi_\beta + P_-\Phi_\gamma). \end{aligned} \tag{3.9}$$

Eqs. (3.3), (3.8) and (3.9) are equivalent, so that the symmetric solutions satisfy $\Phi_\gamma = P_+\Phi_\alpha = P_-\Phi_\beta$, or equivalently $\Phi_\beta = P_+\Phi_\gamma = P_-\Phi_\alpha$ and $\Phi_\alpha = P_+\Phi_\beta = P_-\Phi_\gamma$. Therefore, Eq. (3.3) can be formulated as

$$\Phi_\alpha = T_\alpha(z)G_0(z)P\Phi_\alpha, \tag{3.10}$$

where $P = P_+ + P_-$.

The Faddeev equations for three-body bound states, Eq. (3.10), can be written in the momentum-space representation. Appendix E.4 defines the three-particle momentum states $|\mathbf{q},\mathbf{p}\rangle$ [70] which describe the system of three free noninteracting particles. The momentum $2\mathbf{q}$ is defined as the relative momentum of particle $\alpha$ with respect to the center-of-mass of the two-particle system $(\beta\gamma)$ and $2\mathbf{p}$ is defined as the relative momentum between particles $\beta$ and $\gamma$. As derived in Appendix E.5, we can transform Eq. (3.10) into

$$\langle\mathbf{p},\mathbf{q}|\Phi_\alpha(E)\rangle = \int d\mathbf{q}'\frac{t_s\left(\mathbf{p},\frac{1}{2}\mathbf{q}+\mathbf{q}',E-\frac{3}{4m}q^2\right)}{E-\frac{1}{m}\left(q^2+\mathbf{q}\cdot\mathbf{q}'+q'^2\right)}\langle\mathbf{q}+\frac{1}{2}\mathbf{q}',\mathbf{q}'|\Phi_\alpha(E)\rangle. \tag{3.11}$$

The function $t_s\left(\mathbf{p},\mathbf{p}',E\right)$ is the symmetrized two-body $T$-matrix defined by Eq. (E.31). Note that $t_s\left(\mathbf{p},\mathbf{p}',E\right)$ is just $2\sum_{l=0,\text{even}}^{\infty}(2l+1)P_l(\hat{\mathbf{p}}'\cdot\hat{\mathbf{p}})t_l(p,p',E)$. This means that the partial-wave contributions with odd $l$ are not present in the three-body equations, which is expected for identical bosons.

Eq. (3.11) tells us how the projection of $|\Phi_\alpha(E)\rangle$ on the three-particle momentum states should look. In this derivation no restrictions have been made on the energy of the momentum

state $|\mathbf{p},\mathbf{q}\rangle$. This energy is always positive, so that it is not equal to the energy $E$ of the three-particle system in the state $|\Psi\rangle$ which is always negative for bound states.

We will look for solutions with total angular momentum $L$ equal to zero. So the next step is to apply a partial-wave expansion [5, 71] on Eq. (3.11) for $L = 0$. The details of this expansion is given in Appendix F. Here we will summarize the important steps and assumptions of this derivation. For simplicity, we drop the index $\alpha$ in Eq. (3.11) and expand the function $\langle \mathbf{p},\mathbf{q}|\Phi(E)\rangle$ as

$$\langle \mathbf{p},\mathbf{q}|\Phi(E)\rangle = \sum_{l=0}^{\infty}\sum_{m_l=-l}^{l}(-1)^l Y_l^{m_l}(\hat{\mathbf{p}})\bar{Y}_l^{m_l}(\hat{\mathbf{q}})\tilde{\Phi}_l(p,q,E). \tag{3.12}$$

Now Eq. (3.11) reduces to

$$\begin{aligned}\tilde{\Phi}_l(p,q,E) = \int d\mathbf{q}' \frac{1}{E-\frac{1}{m}\left(q^2+\mathbf{q}\cdot\mathbf{q}'+q'^2\right)}\left(2\Delta_l P_l(\hat{\mathbf{q}}\cdot\widehat{\tfrac{1}{2}\mathbf{q}+\mathbf{q}'})t_l(p,|\frac{1}{2}\mathbf{q}+\mathbf{q}'|,E-\frac{3}{4m}q^2)\right)\\ \sum_{l'=0}^{\infty}(2l'+1)\Delta_{l'}P_{l'}(\widehat{\mathbf{q}+\tfrac{1}{2}\mathbf{q}'}\cdot\widehat{\mathbf{q}'})\tilde{\Phi}_{l'}(|\mathbf{q}+\frac{1}{2}\mathbf{q}'|,q',E)\end{aligned} \tag{3.13}$$

where $\Delta_l = \frac{1}{2}\left(1+(-1)^l\right)$. Therefore all components $\tilde{\Phi}_l(p,q,E)$ with odd $l$ are equal to zero. This set of equations is an infinite set of coupled two-dimensional integral equations. The Efimov states are located close to the $s$-wave dimer state, so that the $s$-wave component $\tilde{\Phi}_0(p,q,E)$ of the three-body wave function dominates and all other components can be neglected in which case only one integral equation needs to be considered. We want to reduce Eq. (3.13) to an infinite set of one-dimensional integral equations because two-dimensional integral equations are much harder to solve than one-dimensional integral equations. Therefore, we expand the partial-wave components $t_l(p,p',z)$ as

$$t_l(p,p',z) = -\sum_{n=1}^{\infty}\tau_{nl}(z)g_{nl}(p,z)g_{nl}(p',z). \tag{3.14}$$

Each term is separable in $p$ and $p'$. There exists many ways in which this separable expansion can be done and we will discuss some methods in Chapter 5.

Now we reduce Eq. (3.13) to an infinite set of one-dimensional integral equations by substituting the separable expansion given by Eq. (3.14) into Eq. (3.13). If we also define the quantities $\tilde{\phi}_{ln}(q,E)$ as the expansion coefficients of $\tilde{\Phi}_l(p,q,E)$ with respect to the orthonormal basis $\left\{g_{nl}(p,E-\frac{3}{4m}q^2)\right\}$, i.e. $\tilde{\Phi}_l(p,q,E) = \sum_{n=1}^{\infty} g_{nl}(p,E-\frac{3}{4m}q^2)\tilde{\phi}_{ln}(q,E)$, it can be derived that the resulting three-body equation is

$$\begin{aligned}\tilde{\phi}_{ln}(q,E) = -\int d\mathbf{q}'\frac{2\Delta_l P_l(\hat{\mathbf{q}}\cdot\widehat{\tfrac{1}{2}\mathbf{q}+\mathbf{q}'})}{E-\frac{1}{m}\left(q^2+\mathbf{q}\cdot\mathbf{q}'+q'^2\right)}\tau_{nl}(Z_q)g_{nl}(|\frac{1}{2}\mathbf{q}+\mathbf{q}'|,Z_q)\\ \sum_{l'=0}^{\infty}\sum_{n'=1}^{\infty}(2l'+1)\Delta_{l'}P_{l'}(\widehat{\mathbf{q}+\tfrac{1}{2}\mathbf{q}'}\cdot\widehat{\mathbf{q}'})g_{n'l'}(|\mathbf{q}+\frac{1}{2}\mathbf{q}'|,Z_{q'})\tilde{\phi}_{l'n'}(q',E),\end{aligned} \tag{3.15}$$

where $Z_q = E-\frac{3}{4m}q^2$. Here we have also assumed that an orthonormalization condition for the form factors $g_{nl}(p,z)$ exists which is the case for the considered separable expansions

considered in Chapter 5. This infinite set of coupled one-dimensional integral equations reduces to a finite set of equations when only a finite number of terms is used to expand the off-shell components $t_l(p, p', z)$.

## 3.2 The Faddeev equations for atom-dimer scattering states

When a free particle impinges on a two-body bound state, there are three kinds of processes possible. The first process is elastic atom-dimer scattering

$$i + (j, k) \to i + (j, k). \tag{3.16}$$

The second process is rearrangement for which two possibilities exist, namely

$$i + (j, k) \to j + (k, i), \tag{3.17}$$
$$i + (j, k) \to k + (i, j). \tag{3.18}$$

These processes are elastic for identical particles. The final process is the breakup process

$$i + (j, k) \to i + j + k. \tag{3.19}$$

which is only possible for positive energies.

If deeper two-body bound states, $(j, k)^*$, $(k, i)^*$ and $(i, j)^*$, exist, relaxation to these deeper bound states is also possible. In this case, the atom-dimer scattering and rearrangement processes are inelastic. In these inelastic processes, the final kinetic energy of the particles is larger than the initial kinetic energy.

The Faddeev equations for atom-dimer scattering are similar to the Faddeev equations for three-body bound states. However, just as is the case for two-particle scattering states (see Eq. (2.28)), we need an extra term representing the asymptotic wave function. So if particle $\alpha$ is scattered by a bound state of particles $\beta$ and $\gamma$, then the atom-dimer scattering wave function $\Psi_\alpha$ is given by [5]

$$\begin{aligned}
\Psi_\alpha &= \Psi_\alpha^{(\alpha)} + \Psi_\alpha^{(\beta)} + \Psi_\alpha^{(\gamma)} \\
\Psi_\alpha^{(\alpha)} &= \Phi_\alpha + G_0(z) T_\alpha(z) \left( \Psi_\alpha^{(\beta)} + \Psi_\alpha^{(\gamma)} \right) \\
\Psi_\alpha^{(\beta)} &= G_0(z) T_\beta(z) \left( \Psi_\alpha^{(\gamma)} + \Psi_\alpha^{(\alpha)} \right) \\
\Psi_\alpha^{(\gamma)} &= G_0(z) T_\gamma(z) \left( \Psi_\alpha^{(\alpha)} + \Psi_\alpha^{(\beta)} \right) \\
\text{in which } z &= \lim_{\epsilon \to 0} E + i\epsilon.
\end{aligned} \tag{3.20}$$

The functions $\Psi_\beta$ and $\Psi_\gamma$ satisfy a similar set of equations. The state $\Phi_\alpha$ is here defined as the asymptotic wave function which is just $|\mathbf{q}_0, \varphi\rangle$ consisting of the two-body bound state $|\varphi\rangle$ formed by particles $\beta$ and $\gamma$ and a free particle $\alpha$ in a momentum eigenstate. The momentum $\mathbf{q}_0$ is the relative momentum between the free particle and the center-of-mass of the dimer.

When the three particles are identical and spinless, the total wave function $\Psi$ must be symmetric with respect to permutations of any pairs of particles [5]. Consequently, we have

$$\begin{aligned}\Psi &= \Psi_\alpha + \Psi_\beta + \Psi_\gamma \\ &= \sum_{\alpha,\beta} \Psi_\alpha^{(\beta)} \\ &= \sum_\alpha \tilde{\Psi}_\alpha,\end{aligned} \tag{3.21}$$

where we have defined the functions $\tilde{\Psi}_\alpha$ as

$$\tilde{\Psi}_\alpha \equiv \Psi_\alpha^{(\alpha)} + \Psi_\beta^{(\alpha)} + \Psi_\gamma^{(\alpha)}. \tag{3.22}$$

From this defintion and Eq. (3.20) it can be shown that

$$\tilde{\Psi}_\alpha = \Phi_\alpha + G_0(z)T_\alpha(z)\left(\tilde{\Psi}_\beta + \tilde{\Psi}_\gamma\right). \tag{3.23}$$

Similarly,

$$\tilde{\Psi}_\beta = \Phi_\beta + G_0(z)T_\beta(z)\left(\tilde{\Psi}_\gamma + \tilde{\Psi}_\alpha\right) \tag{3.24}$$

$$\tilde{\Psi}_\gamma = \Phi_\gamma + G_0(z)T_\gamma(z)\left(\tilde{\Psi}_\alpha + \tilde{\Psi}_\beta\right). \tag{3.25}$$

These equations are just the anticyclic permutation and the cyclic permutation of Eq. (3.23). Therefore we find that $\tilde{\Psi}_\beta = P_-\tilde{\Psi}_\alpha$ and $\tilde{\Psi}_\gamma = P_+\tilde{\Psi}_\alpha$. The system of three integral equations, Eq. (3.20), can thus be reduced to the following single integral equation for the function $\tilde{\Psi}_\alpha$:

$$\tilde{\Psi}_\alpha = \Phi_\alpha + G_0(z)T_\alpha(z)P\tilde{\Psi}_\alpha. \tag{3.26}$$

In the momentum-space representation this equation is given by

$$\begin{aligned}\langle \mathbf{p},\mathbf{q}|\tilde{\Psi}(\mathbf{q}_0,E)\rangle = \delta(\mathbf{q}-\mathbf{q}_0)\langle \mathbf{p}|\varphi\rangle + \\ \left(E - \frac{p^2}{m} - \frac{3}{4m}q^2\right)^{-1} \int d\mathbf{q}' t_s\left(\mathbf{p}, \frac{1}{2}\mathbf{q}+\mathbf{q}', E - \frac{3}{4m}q^2\right)\langle \mathbf{q}+\frac{1}{2}\mathbf{q}', \mathbf{q}'|\tilde{\Psi}(\mathbf{q}_0,E)\rangle\end{aligned} \tag{3.27}$$

in which the index $\alpha$ is removed for convenience. The three-body energy $E$ is equal to $E_{2b} + \frac{3}{4m}q_0^2$ in which $E_{2b}$ is the binding energy of the dimer state $|\varphi\rangle$. For ultracold collisions between the atom and the dimer, the value of $q_0$ is very small. In this limit all scattering amplitudes with nonzero total angular momenta vanish [5]. Therefore we will perform a partial wave expansion on Eq. (3.27) for zero total angular momentum.

The steps from the previous Section in which three-body bound states have been treated can also be applied to Eq. (3.27). The details of these steps can be found in Appendix F.2 or in Ref. [5, 71]. The resulting set of coupled integral equations which describes the elastic scattering of an atom with a ground-state dimer at zero total angular momentum is given by

$$A_{nl}(q,q_0) = 2U_{nl,1,0}(q,q_0,E) + 8\pi\sum_{n',l'}\int_0^\infty \tau_{n'l'}\left(Z_{q'}\right)U_{nl,n'l'}(q,q',E)A_{n'l'}(q',q_0)q'^2\,dq', \tag{3.28}$$

where the amplitudes $A_{nl}(q,q_0)$ describe the scattering process. The functions $U_{nl,n'l'}(q,q',E)$ are defined by

$$U_{nl,n'l'}(q,q',E) = \frac{1}{4\pi}\Delta_l\Delta_{l'}\sqrt{2l+1}\sqrt{2l'+1} \int \frac{P_l(\hat{\mathbf{q}}\cdot\widehat{\tfrac{1}{2}\mathbf{q}+\mathbf{q}'})P_{l'}(\hat{\mathbf{q}}'\cdot\widehat{\tfrac{1}{2}\mathbf{q}'+\mathbf{q}})}{\frac{1}{m}\left(q^2+\mathbf{q}'\cdot\mathbf{q}+q'^2\right)-E} g_{nl}\left(|\frac{1}{2}\mathbf{q}+\mathbf{q}'|,Z_q\right) g_{n'l'}\left(|\frac{1}{2}\mathbf{q}'+\mathbf{q}|,Z_{q'}\right) d\hat{\mathbf{q}}'. \tag{3.29}$$

The $s$-wave atom-dimer scattering length can be calculated from the amplitudes $A_{nl}(q,q_0)$ by

$$a_{ad} = -\frac{2}{3}\pi m\hbar X_{1,0}^2 \lim_{q_0\to 0} A_{1,0}(q_0,q_0). \tag{3.30}$$

The constant $X_{nl}$ relates the form factors of the expansion of $t_l(p,p',z)$ to the two-body bound state wave function in the momentum-space representation, $\langle\mathbf{p}|\varphi\rangle = \varphi_{nl}(p)Y_l^m(\hat{\mathbf{p}})$, according to

$$\varphi_{nl}(p) = X_{nl}\frac{g_{nl}(p,E_{2b,nl})}{E_{2b,nl}-\frac{p^2}{2\mu}}, \tag{3.31}$$

where $E_{2b,nl}$ is the binding energy of the $n$th dimer state with angular momentum quantum number $l$.

# 4. Two-body scattering off a finite square well potential

This Chapter summarizes and expands the on-shell and off-shell two-body scattering results presented in Ref. [63] for a square well potential as two-body interaction. The square well potential is given by Eq. (1.8). We will use it as a simple model for atomic interactions whose long-range behaviour is in fact described by the van der Waals tail $-\frac{C_6}{r^6}$. The big advantage of the square well potential over more realistic models is that the two-body properties can be calculated analytically. Throughout this thesis we will use dimensionless units when considering the square well potential. We will use a bar on top of a variable to indicate that it has been made dimensionless by using the parameters $R$, $\hbar$ and $m$. So lengths, momenta and energies will be expressed in units of $R$, $\hbar/R$ and $\hbar^2/(mR^2)$ respectively.

## 4.1 Scattering length

In this Section we analyze the two-body scattering length $a_l$ of the square well potential for $l = 0$ and $l = 2$ in order to illustrate the corresponding resonances and to compare the $d$-wave effects with van der Waals potentials. We do not consider $l = 1$ because in the case of identical bosons, the quantum number $l$ must be even to ensure that the symmetrization requirement of the wave function, $\psi(\mathbf{r}_1, \mathbf{r}_2) = \psi(\mathbf{r}_2, \mathbf{r}_1)$, is fulfilled. More properties of the $p$-wave scattering length and bound states of the square well potential can be found in Ref. [63].

The partial-wave two-body scattering length of the square well potential is given by [63]

$$a_l = -\frac{R^{2l+1}}{(2l+1)!!(2l-1)!!}\frac{\hat{j}_{l+1}(\bar{q}_0)}{\hat{j}_{l-1}(\bar{q}_0)}. \tag{4.1}$$

It only depends on the range $R$ and the depth $V_0$ of the potential and on the mass $m$ of the particles. We define the dimensionless scattering length $\bar{a}_l$ as $\bar{a}_l \equiv a_l R^{-(2l+1)}$. In particular, the $s$-wave two-body scattering length $\bar{a}_0$ is given by

$$\bar{a}_0 = 1 - \frac{\tan(\bar{q}_0)}{\bar{q}_0} \tag{4.2}$$

where $\bar{q}_0 = \frac{\sqrt{2\mu V_0}R}{\hbar}$. So the scattering length is just the sum of a non-resonant part and a resonant part which diverges when $\bar{q}_0 = (2N-1)\pi/2$ where $N$ is any positive integer. The $s$-wave and $d$-wave scattering lengths are shown in 4.1. The $d$-wave scattering length diverges when $\tan(\bar{q}_0) = \bar{q}_0$. This means that a two-body bound state with $l = 2$ is formed exactly at $\bar{a}_0 = 0$.

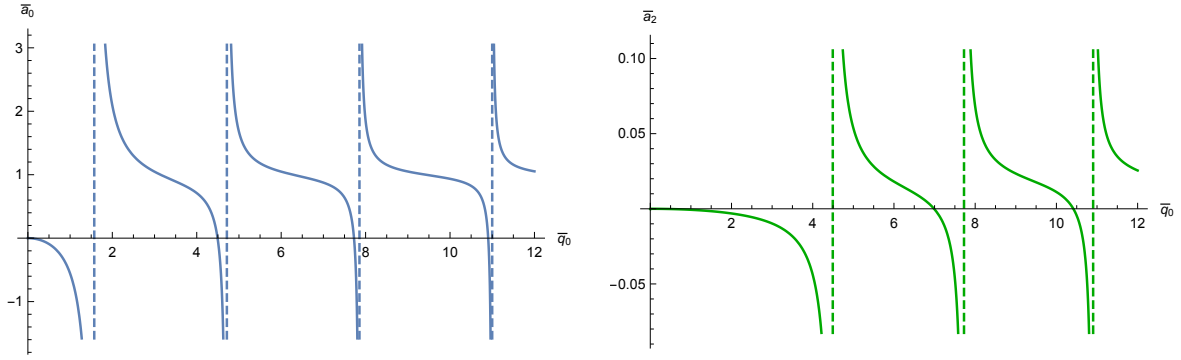


(a) $s$-wave scattering length

(b) $d$-wave scattering length

Figure 4.1: The $s$-wave and $d$-wave two-body scattering lengths as a function the strength $\bar{q}_0$ of the square well potential. The dashed lines indicate the resonances.

The formation of the $d$-wave dimer at $\bar{a}_0 = 0$ is a typical feature of the square well potential. For single-channel interactions with a van der Waals tail, $-C_6 r^{-6}$, the $d$-wave dimer always becomes bound at a scattering $a_0 = 4\pi/[\Gamma(1/4)]^2 \approx 0.956\ r_{vdW}$ as predicted by Gao [72]. This prediction has been confirmed by Wang *et al.* [53] using the Lennard-Jones potential as two-body interaction. For the first ten $d$-wave resonances they calculated the scattering length $a_0$ when the $d$-wave dimer becomes bound and their results agree well with Gao's prediction. The agreement is better when the number of bound states increases. The first three $d$-wave states of the Lennard-Jones potential become bound at $a_0/r_{vdW} = 1.03, 1.00$ and 0.98 respectively [73].

Since the $d$-wave dimer of the square well potential always becomes bound when $\bar{a}_0 = 0$, we expect that $d$-wave effects on the positive side ($a_0 > 0$) of the Efimov spectrum are much smaller for the potential resonances of the square well potential than for the potential resonances of a van der Waals potential which better describes the interatomic interactions.

## 4.2 The off-shell two-body $T$-matrix

Now we consider the off-shell two-body $T$-matrix. The off-shell partial-wave components $t_l(p, p', z)$ of the square well potential are given by [63]

$$t_l(p, p', z) = \frac{R}{4\pi^2 \mu \bar{p}\bar{p}'\hbar} \frac{\bar{q}^2 - \bar{p}_z^2}{\bar{q}^2 - \bar{p}^2} \left[\sigma(\bar{q}; \bar{p}, \bar{p}', \bar{p}_z) - \sigma(\bar{p}; \bar{p}, \bar{p}', \bar{p}_z)\right], \tag{4.3}$$

where

$$\begin{aligned}\sigma(x; \bar{p}, \bar{p}', \bar{p}_z) = \left(\bar{p}_z^2 - x^2\right) &\frac{\bar{p}\hat{j}_{l+1}(\bar{p})\hat{h}_l^{(1)}(\bar{p}_z) - \bar{p}_z \hat{j}_l(\bar{p})\hat{h}_{l+1}^{(1)}(\bar{p}_z)}{x\hat{j}_{l+1}(x)\hat{h}_l^{(1)}(\bar{p}_z) - \bar{p}_z \hat{j}_l(x)\hat{h}_{l+1}^{(1)}(\bar{p}_z)} \\ &\cdot \frac{\bar{p}'\hat{j}_{l+1}(\bar{p}')\hat{j}_l(x) - x\hat{j}_l(\bar{p}')\hat{j}_{l+1}(x)}{\bar{p}'^2 - x^2}.\end{aligned} \tag{4.4}$$

Here we have introduced the dimensionless momenta $\bar{p} = \frac{pR}{\hbar}$, $\bar{p}' = \frac{p'R}{\hbar}$, $\bar{q} = \sqrt{\bar{q}_0^2 + \bar{p}_z^2}$ and $\bar{p}_z = \frac{\sqrt{2\mu z}R}{\hbar}$. The $T$-matrix elements given by Eq. (4.3) are not suitable to solve the three-body

equations. These elements have to be approximated by a sum of terms which are separable in $p$ and $p'$. In Chapter 5 we will present some approaches by which such a separable expansion can be obtained.

The partial-wave components $t_l(p,p',z)$ have poles at energies $z$ for which a two-body bound state exist with angular momentum quantum number $l$. This result is simply a consequence of the definition of the $T$-operator given by Eq. (2.20). Therefore the bound state energies can be obtained from the following transcendental equation:

$$\bar{q}\hat{j}_{l+1}(\bar{q})\hat{h}_l^{(1)}(\bar{p}_z) - \bar{p}_z\hat{j}_l(\bar{q})\hat{h}_{l+1}^{(1)}(\bar{p}_z) = 0. \tag{4.5}$$

For $l = 0$, this equation simplifies to

$$\sqrt{\bar{q}_0^2 + \bar{p}_z^2}\cot\sqrt{\bar{q}_0^2 + \bar{p}_z^2} = \bar{p}_z i. \tag{4.6}$$

A peculiar property of the function $t_0(p,p',z)$ of the square well potential is that it also contains the off-shell $d$-wave component $t_2(p,p',z)$. The functions $t_0(p,p',z)$ and $t_2(p,p',z)$ are related by

$$t_2(p,p',z) = t_0(p,p',z) - \tilde{t}_0(p,p',z) \tag{4.7}$$

where we have defined $\tilde{t}_0(p,p',z)$ as

$$\tilde{t}_0(p,p',z) = \frac{\left[\lim_{p\to 0} t_0(p,p',z)\right]\left[\lim_{p'\to 0} t_0(p,p',z)\right]}{\lim_{p,p'\to 0} t_0(p,p',z)}. \tag{4.8}$$

So knowledge of the off-shell $s$-wave $T$-matrix implies knowledge of the off-shell $d$-wave $T$-matrix. This surprising result is a special property of the square well potential and does not hold for realistic interatomic potentials. It is also important to note that Eq. (4.7) applies to the off-shell $T$-matrix. The on-shell $d$-wave $T$-matrix cannot be determined from the on-shell $s$-wave $T$-matrix.

The function $\tilde{t}_0(p,p',z)$ is separable in $p$ and $p'$ and it contains many singularities for negative values of $z$ when the potential supports many bound states. Since $t_0(p,p',z)$ and $t_2(p,p',z)$ have poles at the energies $z$ for which there exist an $s$-wave and $d$-wave two-body bound state respectively, the function $\tilde{t}_0(p,p',z)$ must have poles corresponding to both the $s$-wave and $d$-wave two-body bound states.

The partial-wave components $V_l(p,p')$ of the square well potential (see Appendix E.2) satisfy a similar relation as Eq. (4.7), namely

$$V_2(p,p') = V_0(p,p') - \frac{\left[\lim_{p\to 0} V_0(p,p')\right]\left[\lim_{p'\to 0} V_0(p,p')\right]}{\lim_{p,p'\to 0} V_0(p,p')}. \tag{4.9}$$

This equation is a special case of the general formula

$$V_l(p,p') - V_{l+2}(p,p') = \frac{\left[\lim_{p\to 0} \frac{d^l V_l(p,p')}{dp^l}\right]\left[\lim_{p'\to 0} \frac{d^l V_l(p,p')}{dp'^l}\right]}{\lim_{p,p'\to 0} \frac{d^{2l} V_l(p,p')}{dp^l dp'^l}} \tag{4.10}$$

which applies to the square well potential. Eq. (4.7) cannot be generalized in the same way.

# 5. Separable expansions and approximations of the off-shell two-body $T$-matrix

In Chapter 3 we have seen that even for a non-separable two-body $T$-matrix the three-body equations can still be simplified if the off-shell partial-wave components $t_l(p, p', z)$ are approximated by a sum of terms which are separable in $p$ and $p'$. In this Chapter we present some useful methods to perform such a separable expansion and methods which provide a one-term separable approximation for $t_l(p, p', z)$.

## 5.1 Separable approximation of the $T$-matrix near a singular point

The two-body $T$-matrix contains singularities at the binding energies of the pair of particles. Near any singular point, the $T$-matrix can be written as [69]

$$\langle \mathbf{p}'|T(z)|\mathbf{p}\rangle \simeq \frac{\langle \mathbf{p}'|\tilde{g}_i\rangle\langle \tilde{g}_i|\mathbf{p}\rangle}{z - E_{2b,i}} \tag{5.1}$$

where the index $i$ numbers the singularity. The form factors $\langle \mathbf{p}|\tilde{g}_i\rangle$ are defined as

$$\langle \mathbf{p}|\tilde{g}_i\rangle = \int \langle \mathbf{p}|V|\mathbf{q}\rangle\langle \mathbf{q}|\varphi_i\rangle \, d\mathbf{q} \tag{5.2}$$

where $\langle \mathbf{q}|\varphi_i\rangle$ is the two-body bound state wave function in the momentum-space representation corresponding to the energy $E = E_{2b,i}$. This bound state wave function is normalized as $\langle \varphi_i|\varphi_i\rangle = 1$. The definition of the form factor $\langle \mathbf{p}'|\tilde{g}_i\rangle$ is almost the same as the definition of the half-off-shell $T$-matrix which is defined by Eq. (2.34) for $E_p = \frac{p^2}{2\mu} \neq \frac{p'^2}{2\mu}$. The difference is that the state $|\varphi_i\rangle$ is a bound state, whereas the state $|\mathbf{p}+\rangle$ is a scattering state.

Eq. (5.1) only holds very close to the specific singularity. Therefore, it is not useful for our purposes. However, the pole of this separable approximation of the two-body $T$-matrix has a simple form which makes this separable approximation useful for calculations in which one needs to integrate over this pole of the two-body $T$-matrix. For instance, when one considers elastic atom-dimer scattering, it is useful to use this separable approximation close to the singularity (see Appendix F.2).

## 5.2 Method I: the spectral representation

Now we present some approaches which can be used to expand the partial-wave components of the off-shell two-body $T$-matrix in a series of terms which are separable in the initial and final momenta. The first method which we describe can be used when the off-shell two-body $T$-matrix is known explicitly. In this case the form factors $g_{nl}(p,z)$ can be defined as the solutions of the following integral equation:

$$-\int_0^\infty t_l(p,p',z)g_{nl}(p',z)dp' = \tau_{nl}(z)g_{nl}(p,z). \tag{5.3}$$

The index $n$ labels the eigenvalues and corresponding eigenvectors. Since the kernel $t_l(p,p',z)$ is symmetric, the eigenvalues $\tau_{nl}(z)$ are real [74]. Furthermore, the eigenvectors $g_{nl}(p,z)$ corresponding to different eigenvalues are orthogonal and eigenvectors corresponding to the same eigenvalue can be orthogonalized [74]. The orthonormalization condition is given by

$$\int_0^\infty g_{n'l}(p,z)g_{nl}(p,z)dp = \delta_{n'n}. \tag{5.4}$$

Hilbert-Schmidt theory which deals with real symmetric kernels [74] makes it possible to approximate $t_l(p,p',z)$ with its spectral representation which is given by

$$t_l(p,p',z) = -\sum_{n=1}^{\infty} \tau_{nl}(z)g_{nl}(p,z)g_{nl}(p',z). \tag{5.5}$$

More details about the spectral representation can be found in Appendix G.

The form factors of the square well potential can be numerically calculated from Eq. (5.3). Fig. 5.1 shows the first three form factors for $l=0$ and $l=2$ evaluated at $z=0$, $z=-\frac{1}{4}V_0$ and $z=-4V_0$. The index $n$ is determined by sorting the form factors by the absolute magnitude of the eigenvalue $\tau_{n,l}(z)$ at large negative energies, i.e. $|z| \gg V_0$. As a result of this labeling, the function $\tau_{nl}(z)$ diverges at one particular negative value of the energy $z$ when the potential supports at least $n$ bound states with angular momentum quantum number $l$. When the energy of this bound state is $E_{2b,nl}$, $\tau_{nl}(z)$ diverges at $z=E_{2b,nl}$. This is illustrated in Fig. 5.2 for $n=2$ and $n=3$. The considered potential supports two $s$-wave bound states with energy $E_{2b}=-\frac{q_2^2}{2\mu}$ where $\bar{q}_2=7.333$ and $\bar{q}_2=5.585$, so that $\tau_{2,0}(z)$ diverges at $\bar{p}_z=5.585i$ as can be seen in the figure. The potential also supports two $d$-wave bound states with $\bar{q}_2=5.981$ and $\bar{q}_2=1.083$ and the corresponding form factors also diverge at those energies. The function $\tau_{3,0}(z)$ does not diverge at negative energies because the potential is not deep enough to support the third $s$-wave dimer state. Since this dimer state is almost bound, $\tau_{3,0}(z)$ is large at $z=0$.

Fig. 5.1 clearly shows that the energy dependence of the form factors is quite weak for most values of $p$. We have confirmed this by considering much more values of the energies than those considered in this figure. The energy dependence is expected to be weak for energies below the depth of the well, i.e. $|\bar{p}_z|>\bar{q}_0$, because the two-body $T$-matrix depends weakly on the energy in that regime. It may be surprising that the form factors for $z=0$ and $z=-4V_0$ look very similar, but this is not a coincidence. The reason for this effect can be understood by considering the Lippmann-Schwinger equation for $t_l(p,p',z)$ given by Eq. (2.33). If we fill

in $z = 0$, it is immediately clear that eigenfunctions of $V_l(p, p')$, which also satisfy Eq. (5.4), must also be eigenfunctions of $t_l(p, p', z)$. Furthermore, for $|z| \gg V_0$, $t_l(p, p', z) \simeq V_l(p, p')$, so that the corresponding eigenfunctions will again be similar. So for both $z = 0$ and $|z| \to \infty$ the eigenfunctions of $t_l(p, p', z)$ are the same as those of $V_l(p, p')$.

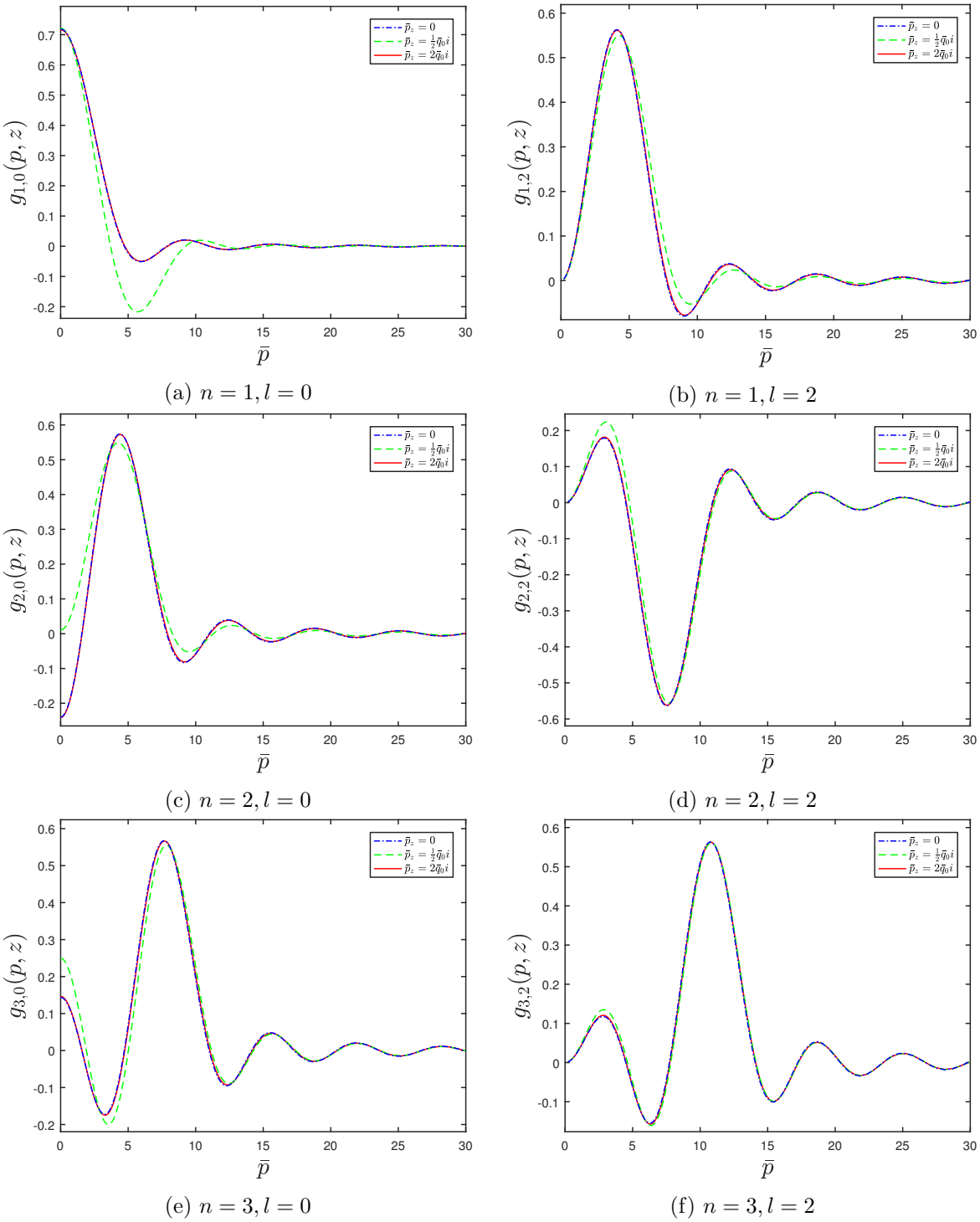


(a) $n = 1, l = 0$ (b) $n = 1, l = 2$

(c) $n = 2, l = 0$ (d) $n = 2, l = 2$

(e) $n = 3, l = 0$ (f) $n = 3, l = 2$

Figure 5.1: The $s$-wave and $d$-wave form factors $g_{n,l}(p, z)$ of method I as a function of $p$ for $\bar{a}_0 = -10$ near the third potential resonance of the square well potential ($\bar{q}_0 = 7.84239$). Different energies $z$ are chosen. The form factors and corresponding eigenvalues are sorted by the absolute magnitude of the eigenvalue $\tau_{n,l}(z)$ at large negative energies, i.e. $|z| \gg V_0$.

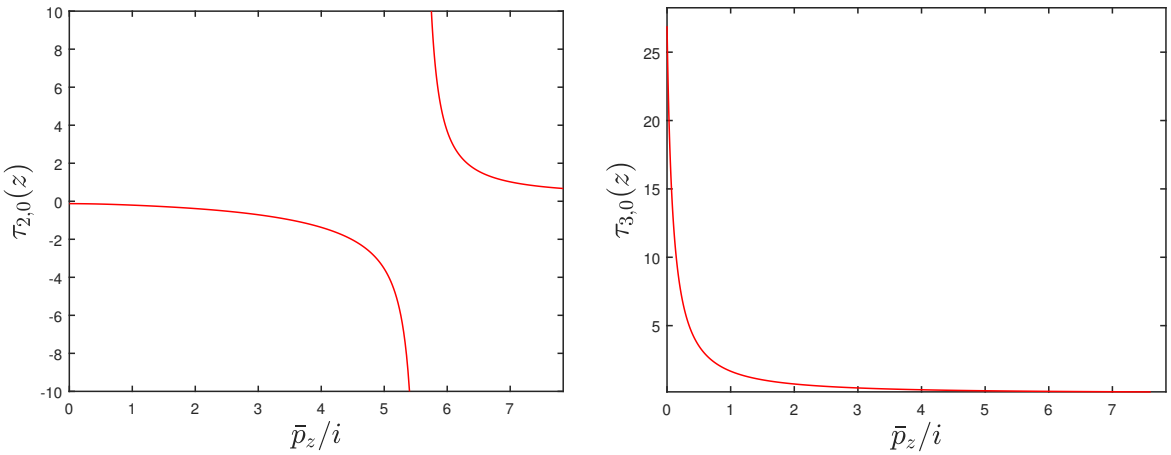


(a) $n = 2, l = 0$

(b) $n = 3, l = 0$

(c) $n = 2, l = 2$

(d) $n = 3, l = 2$

Figure 5.2: The functions $\tau_{nl}(z)$ of method I as a function of $z$ for $\bar{a}_0 = -10$ near the third potential resonance of the square well potential ($\bar{q}_0 = 7.84239$). The labeling is the same as in Fig. 5.1.

## 5.3 Method II: the Weinberg series

Here we discuss another approach which is based on the Hilbert-Schmidt theorem for symmetric integral equations (see Appendix G), to expand the partial-wave components of the off-shell two-body $T$-matrix in a series of separable terms. This approach has been used first by Weinberg [65] who showed that the divergence of the Born series could be eliminated by introducing quasiparticles in close correspondence with real bound states or resonances. Therefore this method is also called the quasiparticle method [75]. Another name for this method is the Weinberg series. More details about this approach can be found in [5, 71, 75].

In the quasiparticle method we define the functions $|g(z)\rangle$ as the eigenfunctions of the operator $VG_0(z)$ with eigenvalue $\eta(z)$, i.e.

$$VG_0(z)|g(z)\rangle = \eta(z)|g(z)\rangle. \tag{5.6}$$

$G_0(z)$ is the free two-body Green's operator $(z - H_0)^{-1}$ which we have encountered before in Chapter 2. For $z < 0$ the eigenfunctions of the operator $VG_0$ are related to the two-body bound state wave functions of the potential $\frac{V}{\eta(z)}$. In order to derive this relation, we first introduce the functions

$$|\phi(z)\rangle = G_0(z)|g(z)\rangle. \tag{5.7}$$

Since $|g(z)\rangle$ is an eigenfunction of the operator $VG_0$ with eigenvalue $\eta(z)$, the functions $|\phi(z)\rangle$ satisfy

$$G_0V|\phi(z)\rangle = \eta(z)|\phi(z)\rangle \tag{5.8}$$

which is just the Schrödinger equation with an energy-dependent potential $\frac{V}{\eta(z)}$. For real, negative energies this potential is Hermitian [5], so that $|\phi(z)\rangle$ represents the two-body bound states. We see that $\eta(z)$ is just a number by which the potential has to be divided in order to have a bound state at this particular energy $z$. So if we define the functions $\phi_{nl}(p, z)$ as

$$\langle \mathbf{p}|\phi_{nlm}(z)\rangle = Y_l^m(\hat{\mathbf{p}})\phi_{nl}(p, z) \tag{5.9}$$

where the states $|\phi_{nlm}(z)\rangle$ are eigenfunctions of the Hamiltonian $H_0 + \frac{V}{\eta_{nl}(z)}$, it follows from Eq. (5.7) that $\langle \mathbf{p}|g_{nlm}(z)\rangle = Y_l^m(\hat{\mathbf{p}})g_{nl}(p, z)$ and that the form factors $g_{nl}(p, z)$ are related to the wave functions $\phi_{nl}(p, z)$ by

$$\phi_{nl}(p, z) = N_{nl}\frac{g_{nl}(p, z)}{z - \frac{p^2}{2\mu}}, \tag{5.10}$$

where $N_{nl}$ is a normalization constant. Note that the index $n$ just labels the eigenfunctions for each value of $l$.

Now Eq. (5.6) can be rewritten in the momentum-space representation. By using the partial wave expansion of the potential, Eq. (2.32), we end up with

$$-4\pi \int_0^\infty V_l(p, p')\frac{1}{\frac{p'^2}{2\mu} - z}g_{nl}(p', z)p'^2\, dp' = \eta_{nl}(z)g_{nl}(p, z), \tag{5.11}$$

The eigenfunctions $g_{nl}(p,z)$ of Eq. (5.11) can be used as form factors in the separable expansion of the two-body $T$-matrix. We label the eigenvalues $\eta_{nl}(z)$ in decreasing order of their absolute values. The form factors $g_{nl}(p,z)$ are orthogonal. The orthonormalization condition is given by

$$\int_0^\infty g_{n'l}(p,z)g_{nl}(p,z)\frac{1}{\frac{p^2}{2\mu}-z}p^2dp=\delta_{n'n}. \tag{5.12}$$

The eigenvalues $\eta_{nl}(z)$ and form factors $g_{nl}(p,z)$ are real for real, negative energies, i.e. $z<0$ [5]. Although the form factors are not complete, the partial-wave components $t_l(p,p',z)$ can be approximated by the following separable representation [5, 71]:

$$t_l(p,p',z)=-\frac{1}{4\pi}\sum_{n=1}^{\infty}\frac{\eta_{nl}(z)}{1-\eta_{nl}(z)}g_{nl}(p,z)g_{nl}(p',z). \tag{5.13}$$

The energy-independent components $V_l(p,p')$ can be expanded as

$$V_l(p,p')=-\frac{1}{4\pi}\sum_{n=1}^{\infty}\eta_{nl}(z)g_{nl}(p,z)g_{nl}(p',z). \tag{5.14}$$

Eqs. (5.13) and (5.14) can be derived from the two-body Lippmann-Schwinger equation, Eq. (2.33), and the orthonormalization condition given by Eq. (5.12). Eq. (5.13) clearly shows that each term of the expansion contains a singularity when $\eta_{nl}(z)=1$. This singularity corresponds to the existence of the $n$th two-body bound state with angular momentum quantum number $l$ at energy $z$.

The form factors can always be calculated numerically from Eq. (5.11). Nevertheless, it is usually easier to calculate the form factors directly from the two-body bound state wave functions. Eq. (5.7) implies that

$$|g(z)\rangle=(z-H_0)|\phi(z)\rangle \tag{5.15}$$

$$=\frac{V}{\eta}|\phi(z)\rangle. \tag{5.16}$$

So the form factors can simply be obtained by applying the operator $\frac{V}{\eta}$ onto the two-body bound state wave functions corresponding to the scaled potential $\frac{V}{\eta}$.

In case of the square well potential the eigenfunctions $g_{nl}(p,z)$ and eigenvalues $\eta_{nl}(z)$ can be found analytically for negative energies [5, 76]. The form factors are given by Eq. (E.17) with $V_0$ replaced by $V_0/\eta_{nl}$. If we also orthonormalize them according to Eq. (5.12), the $s$-wave form factors are given by [5, 76]

$$g_{n,0}(p,z)=C_n(z)\frac{\bar{q}_0^2}{\eta_{n,0}(z)}\frac{\cos(\bar{p})-i\bar{p}_z/\bar{p}\sin(\bar{p})}{\frac{\bar{q}_0^2}{\eta_{n,0}(z)}+(\bar{p}_z^2-\bar{p}^2)}, \tag{5.17}$$

where

$$C_n^2(z)=\frac{2R}{\pi\mu\hbar}\frac{1+\bar{p}_z^2\frac{\eta_{n,0}(z)}{\bar{q}_0^2}}{\frac{\bar{q}_0^2}{\eta_{n,0}(z)}-i\bar{p}_z}. \tag{5.18}$$

The eigenvalues $\eta_{n,0}(z)$ can be calculated from the transcendental equation

$$\sqrt{\frac{\bar{q}_0^2}{\eta_{n,0}(z)} + \bar{p}_z^2}\cot\left(\sqrt{\frac{\bar{q}_0^2}{\eta_{n,0}(z)} + \bar{p}_z^2}\right) = i\bar{p}_z. \tag{5.19}$$

From these equations we see that the prefactors $\eta_{n,0}(z)$ only depend on the phase $\bar{q}_0$, whereas the form factors $g_{nl}(p,z)$ depend only on $R$. This can be understood from the definition of the form factors, Eq. (5.11). The form factors $g_{nl}(p,z)$ cannot depend on the depth $V_0$ of the well because it can be factored out and incorporated in the eigenvalues $\eta_{nl}$. So the form factors include only information about the range $R$, whereas the eigenvalues only depend on the phase $\bar{q}_0 = \frac{q_0 R}{\hbar}$.

For negative energies $z$, all eigenvalues $\eta_{nl}(z)$ of the square well potential will be positive, so that Mercer's theorem which is given in Appendix G applies after symmetrizing the kernel of Eq. (5.11). Consequently, it can be proven that the series in Eq. (5.14) converges absolutely and uniformly for any value of $z$ and so does the series of Eq. (5.13).

For large negative energies, i.e. $|z| \gg V_0$, the convergence of the Weinberg series is slow because the eigenvalues $\eta_{nl}(z)$ decrease with increasing $|z|$ [71]. This is caused by the fact that the depth of the potential must increase in order to form a bound state at large negative energies. At those energies, it is not valid to use a full separable approximation of the two-body $T$-matrix based on this method. We have confirmed this for the square well potential, but it is also the case for other local potentials [77]. The slow convergence for large negative $z$ is not a problem since this energy regime is less important for the calculation of the weakly bound Efimov trimers.

When the off-shell partial-wave component $t_0(p,p',z)$ is approximated by a finite number of separable terms, the scattering length corresponding to the approximated potential can be calculated from Eq. (2.49). Since the analytical expressions for $\tau_{n,0}(z)$ and $g_{n,0}(p,z)$ are known at $z=0$, it can be shown that

$$\bar{a}_0 = \sum_n \bar{a}_{n,0}, \tag{5.20}$$

where

$$\bar{a}_{n,0} = -\frac{32\bar{q}_0^2}{(2n-1)^2\pi^2\left((2n-1)^2\pi^2 - 4\bar{q}_0^2\right)}. \tag{5.21}$$

From this equation it is clear that the scattering length does not go to zero on the positive side of the $n$th potential resonance if the $(n+1)$th term (or higher order terms) is not present in the expansion. In this case the scattering length will converge to the background scattering length

$$\bar{a}_{bg} = \frac{8}{(2n-1)^2\pi^2}. \tag{5.22}$$

for an infinite value of $\bar{q}_0$.

In Section 5.2 we have seen that for $z=0$ the eigenfunctions of $t_l(p,p',z)$ are the same as those of $V_l(p,p')$. From Eq. (5.11) we see that the form factors of the Weinberg series at

$z = 0$ are exactly the same as the eigenfunctions of $V_l(p, p')$. This indicates that method I and II are exactly the same at $z = 0$ and are quite similar at small negative energies. This energy regime is also most important when calculating the three-body parameter $a_-$ of the Efimov spectrum. Therefore we will now analyze the Weinberg series of $t_0(p, p', z)$ at zero energy keeping in mind that this analysis also applies to method I.

Fig. 5.3 shows how the $s$-wave form factors $g_{n,0}(p, 0)$ of the square well potential behave. Clearly, the absolute maximum of $|g_{n,0}(p, 0)|$ shifts to larger momenta $p$ as $n$ increases. This maximum is located near $\bar{p} \simeq \frac{(2n-1)\pi}{2}$ (except for $n = 1$), which is the depth $\bar{q}_0$ at which the $n$th $s$-wave two-body bound state becomes bound at zero energy. The larger the value of $n$, the closer is the maximum to $\bar{p} = \frac{(2n-1)\pi}{2}$. This big peak indicates that the probability density for two particles — separated by $r < R$ — to have a relative momentum $\bar{q}_0$ is very large when the energy of the two-particle system is zero.

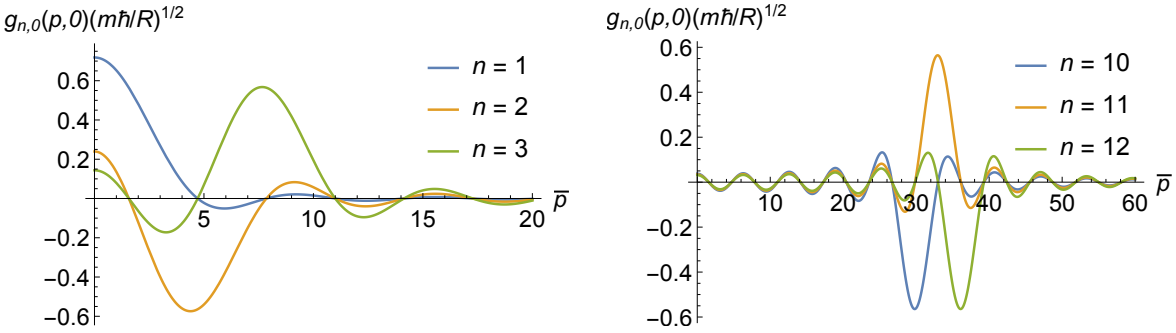


(a) $n = 1, 2, 3$ (b) $n = 10, 11, 12$

Figure 5.3: The $s$-wave form factors $g_{n,0}(p, z)$ of the Weinberg series for the square well potential at $z = 0$.

In Fig. 5.4 we show that at $z = 0$ a lot of terms are necessary to accurately represent the full two-body $T$-matrix whenever the scattering length is not very large. This figure shows that the single term approximation $-\tau_{4,0}(z)g_{4,0}(p)^2$ only works well at small momenta $p$ when the scattering length $\bar{a}_0$ is large. For small $\bar{a}_0$ this separable approximation fails at small values of $p$ and more terms are needed in the expansion. The one-term approximation always reproduces the big peak of $t_0(p, p, z)$ very well which occurs at $p = 0$ in case of the first potential resonance. Therefore the separable approximation is much better near the first potential resonance as can be seen from Fig. 5.5.

### 5.3.1 Method IIb: The unitary pole expansion

Another method to expand the off-shell partial-wave components $t_l(p, p', z)$ is the unitary pole expansion (UPE) which was first suggested by Harms [77] and which is just a special case of the Weinberg series discussed in Section 5.3. The energy-dependent form factors defined by the Weinberg series can be made energy-independent if one fixes the energy $z$ in Eq. (5.6) at some constant $E_b$. The UPE is therefore very closely related to the Weinberg series. Furthermore, when we choose $E_b = 0$, the unitary pole expansion is simply the spectral representation of the kernel $V_l(p, p')$ in which case the equations defining the form factors are similar to those of method I with $t_l(p, p', z)$ replaced by $V_l(p, p')$.

The form factors of the UPE are defined by Eq. (5.6) in which the energy $z$ is fixed at some constant $E_b$. The definition of the form factors is thus given by

$$VG_0(E_b)|g(E_b)\rangle = \eta(E_b)|g(E_b)\rangle. \tag{5.23}$$

For Efimov physics we are mainly interested at energies close to zero, so it is natural to choose $E_b = 0$. The one-term approximation of the UPE is called the unitary pole approximation (UPA) and had already been used before Harms [77] presented the UPE.

Since we set $E_b$ to zero, the energy-independent form factors $g_{nl}(p)$ of the UPE are defined as the solutions of following integral equation:

$$-\int_0^\infty V_l(p,p')g_{nl}(p')dp' = \nu_{nl}g_{nl}(p). \tag{5.24}$$

Note that we have defined $\nu_{nl} = \frac{\eta_{nl}}{8\pi\mu}$, so that Eq. (5.24) has the same form as Eq. (5.3). The index $n$ labels the eigenvalues $\nu_{nl}$ in decreasing order in case of attractive potentials. The kernel $V_l(p,p')$ is symmetric, so that the eigenvalues $\nu_{nl}$ are real and the eigenfunctions $g_{nl}(p)$ can be orthonormalized in the following way:

$$\int_0^\infty g_{n'l}(p)g_{nl}(p)dp = \delta_{n'n}. \tag{5.25}$$

The partial-wave components $V_l(p,p')$ can be well approximated by its spectral representation which is given by

$$V_l(p,p') = -\sum_{n=1}^{\infty} \nu_{nl}g_{nl}(p)g_{nl}(p'). \tag{5.26}$$

The off-shell partial-wave components $t_l(p,p',z)$ can then be approximated by

$$t_l(p,p',z) = -\sum_{n,n'=1}^{\infty} \tau_{nn'l}(z)g_{nl}(p)g_{n'l}(p'). \tag{5.27}$$

where the energy-dependent expansion coefficients $\tau_{nn'l}(z)$ are determined from the two-body Lippmann-Schwinger equation, Eq. (2.33), and the orthonormalization condition, Eq. (5.25).

The definition of the form factors in Eq. (5.24) is exactly the same as the definition in Eq. (5.11) at zero energy $z$. This means that the form factors defined in this Section are just proportional to the zero-energy two-body bound state wave functions in the momentum-space representation, so $g_{nl}(p) \propto p^2\phi_{nl}(p,0)$.

In case of the square well potential, the $s$-wave form factors $g_{n,0}(p)$ and eigenvalues $\nu_{n,0} = \frac{\eta_{n,0}}{8\pi\mu}$ can be calculated analytically as we have seen in Section 5.3. The expressions are given by

$$\eta_{n,0} = \left(\frac{2\bar{q}_0}{(2n-1)\pi}\right)^2, \tag{5.28}$$

$$g_{n,0}(p) = \sqrt{\frac{2R\bar{q}_0^2}{\pi\mu\hbar\eta_{n,0}}}\frac{\cos(\bar{p})}{\frac{\bar{q}_0^2}{\eta_{n,0}} - \bar{p}^2}. \tag{5.29}$$

The main advantage of the form factors defined by Eq. (5.24) is that they are independent of the energy $z$, which reduces the computation time for solving the three-body equation. Secondly, the normalized form factors do not depend on the depth of the well and therefore also not on the $s$-wave scattering length $a_0$ for fixed range $R$. So for the calculations of the Efimov states in the $(\bar{a}_0, E)$-plane one only needs to calculate the form factors once.

It is important to note that the three-body equation given by Eq. (3.15) changes when the expansion of the two-body $T$-matrix is given by Eq. (5.27) which contains terms which are not symmetric in $p$ and $p'$ [77]. In this work we will not perform any three-body calculations using the unitary pole expansion because the UPE is very similar to the Weinberg series. The form factors of both methods are very similar. Furthermore, the form factors of the Weinberg series for the square well potential are known analytically, so that the calculation of the form factors is not a problem.

Finally, we want to note that the eigenfunctions and eigenvalues of $V_l(p, p')$ are the same as the eigenfunctions and eigenvalues of $t_l(p, p', z)$ for $z \to -\infty$. This is a simple consequence of

$$\lim_{z \to -\infty} t_l(p, p', z) = V_l(p, p'). \tag{5.30}$$

Therefore, the eigenfunctions of $t_l(p, p', z)$ and $V_l(p, p')$ look quite similar for negative energies below the depth of the well because we have seen that the eigenfunctions of $t_l(p, p', z)$ are weakly dependent on the energy in this regime. Thus the functions $\tau_{nn'l}(z)$ with $n \neq n'$ are zero for $z \to -\infty$. They are also zero for $z = 0$ because in Section 5.2 we have seen that the eigenfunctions of $t_l(p, p', 0)$ and $V_l(p, p')$ are also the same.

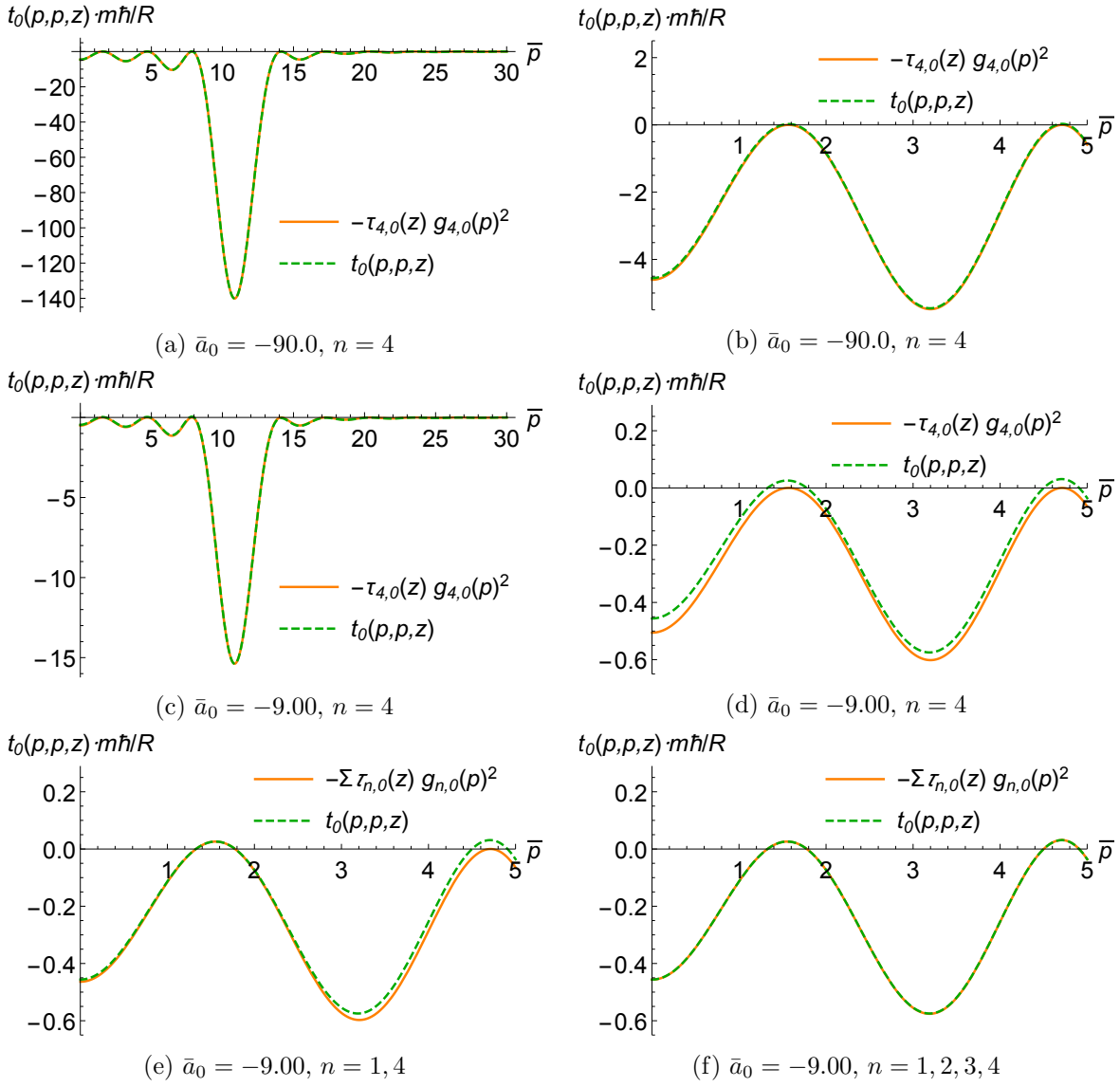


(a) $\bar{a}_0 = -90.0$, $n = 4$

(b) $\bar{a}_0 = -90.0$, $n = 4$

(c) $\bar{a}_0 = -9.00$, $n = 4$

(d) $\bar{a}_0 = -9.00$, $n = 4$

(e) $\bar{a}_0 = -9.00$, $n = 1, 4$

(f) $\bar{a}_0 = -9.00$, $n = 1, 2, 3, 4$

Figure 5.4: The diagonal of $t_0(p, p', z)$ (green) and the corresponding approximation (orange) using the functions $g_{n,0}(p, z)$ and $\tau_{n,0}(z)$ of the Weinberg series for the square well potential at zero energy ($z = 0$). The terms which are included in the expansion are written below each figure. In all cases the depth of the well is chosen such that the fourth $s$-wave dimer state is almost bound. The considered scattering lengths are $\bar{a}_0 = -90.0$ and $\bar{a}_0 = -9.00$.

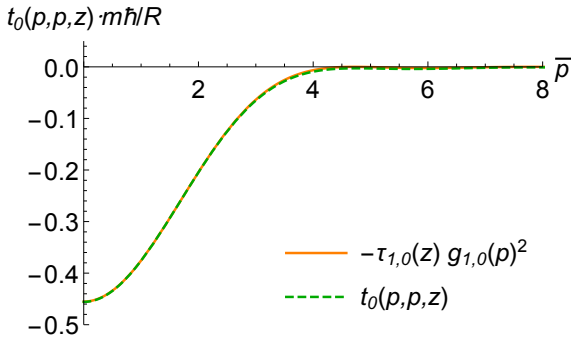


Figure 5.5: The diagonal of $t_0(p, p', z)$ (green) and the corresponding approximation (orange) using the functions $g_{n,0}(p, z)$ and $\tau_{n,0}(z)$ of the Weinberg series for the square well potential at zero energy. The depth of the well is chosen such that the first $s$-wave dimer state is almost bound and $\bar{a}_0 = -9.00$.

## 5.4 Method III: the EST method

The EST method [78] (named after the authors Ernst, Shakin and Taylor) can also be used to approximate the partial-wave components $t_l(p,p',z)$ by a separable expansion. Since one disadvantage of this method is that it is difficult to obtain the next separable term in the expansion of $t_l(p,p',z)$ [79], most three-body calculations involving the EST method take only the first separable term into account. This one-term approximation is a generalization of the unitary pole approximation. It has also been used to calculate the energies of Efimov states corresponding to the potential resonances of some van der Waals potentials [49, 55, 59].

The separable approximation of the EST method is exactly the same as the UPA for negative energies ($E = E_b < 0$). So this means that the separable potential is chosen such that the corresponding bound state wave function is the same as the one of the original Hamiltonian which involves the non-separable potential $V$. For energies $E \geq 0$ we can do something similar. This means that we want a separable potential for which the eigenfunction of the corresponding Hamiltonian is identical to the eigenfunction of the original Hamiltonian. The method to find such a separable potential is called the EST method [78] which is described below.

The EST approach is used to approximate the off-shell two-body $T$-matrix, so the eigenfunctions of the original Hamiltonian which we want to reproduce are the scattering states $|\mathbf{p}+\rangle$ which satisfy the Lippmann-Schwinger equation given by Eq. (2.28). If we define the separable potential $V_{sep}$ as

$$V_{sep} = |g\rangle\lambda\langle g|, \tag{5.31}$$

then Eq. (2.28) corresponding to this potential is given by

$$|\mathbf{p}\pm\rangle_{sep} = |\mathbf{p}\rangle + \lambda G_0^{(\pm)}(E_p)|g\rangle\langle g|\mathbf{p}\pm\rangle_{sep}. \tag{5.32}$$

The solution of this equation is given by

$$|\mathbf{p}\pm\rangle_{sep} = |\mathbf{p}\rangle + \frac{\lambda G_0^{(\pm)}(E_p)|g\rangle\langle g|\mathbf{p}\rangle}{1-\lambda\langle g|G_0^{(\pm)}(E_p)|g\rangle}. \tag{5.33}$$

Similarly, the scattering states $|\mathbf{p}\pm\rangle$ corresponding to the potential $V$ satisfy Eq. (2.28), so

$$|\mathbf{p}+\rangle = |\mathbf{p}\rangle + G_0^{(+)}(E_p)V|\mathbf{p}+\rangle. \tag{5.34}$$

From Eqs. (5.33) and (5.34) we see that the scattering states $|\mathbf{p}+\rangle$ and $|\mathbf{p}+\rangle_{sep}$ are exactly the same when the states $|g\rangle$ and coefficients $\lambda$ satisfy

$$G_0^{(+)}(E_p)V|\mathbf{p}+\rangle = G_0^{(+)}(E_p)|g\rangle \tag{5.35}$$

and

$$\frac{\lambda\langle g|\mathbf{p}\rangle}{1-\lambda\langle g|G_0^{(+)}(E_p)|g\rangle} = 1. \tag{5.36}$$

The equality of Eq. (5.35) is fulfilled if we define $|g\rangle$ as

$$|g\rangle = V|\mathbf{p}+\rangle, \tag{5.37}$$

so that the second condition, Eq. (5.36), can be written as

$$\frac{\lambda\langle \mathbf{p}+|V|\mathbf{p}\rangle}{1-\lambda\langle \mathbf{p}+|VG_0^{(+)}(E_p)V|\mathbf{p}+\rangle} = 1, \tag{5.38}$$

or equivalently

$$\frac{1}{\lambda} = \langle \mathbf{p}+|V|\mathbf{p}\rangle + \langle \mathbf{p}+|VG_0^{(+)}(E_p)V|\mathbf{p}+\rangle \tag{5.39}$$

$$= \langle \mathbf{p}+|V|\mathbf{p}+\rangle. \tag{5.40}$$

In the last step we have again used Eq. (5.34). So now we have constructed a separable potential $V_{sep}$ defined by Eqs. (5.31), (5.37) and (5.39) which reproduces the same scattering state $|\mathbf{p}+\rangle$ as the original Hamiltonian at a single energy $E_p \geq 0$.

The above procedure can be generalized to reproduce the wave function at a number of different energies in which case the potential is a sum of separable terms [78]. However, it may be difficult to determine which additional energies one should choose in order to approximate the off-shell components $t_l(p,p',z)$ in the best way [79].

In the context of Efimov physics the EST approach is useful when we are interested in properties occuring at small negative energies such as the three-body parameters $a_-$ or $\kappa^*$. In this case we choose $E_p = 0$, so that the separable potential reproduces the same $s$-wave scattering length as the original potential $V$. This suggests that this method is especially useful for calculations of the three-body parameter $a_-$. This is an important advantage of the EST approach over other separable approximations such as the single-term approximation of the Weinberg series. Whenever we use the one-term EST approximation in this thesis, we always choose $E_p = 0$, so that the zero-energy $s$-wave scattering state of the separable interaction is the same as the one of the considered non-separable potential.

Once we have calculated the form factors from Eq. (5.37), we can find the separable approximation to the two-body $T$-matrix. The separable approximation $V_{sep}(p,p') = \lambda g(p)g(p')$ and the ansatz $t_0(p,p',z) = \tau(z)g(p)g(p')$[2] can be substituted in the Lippmann-Schwinger equation for $t_0(p,p',z)$, Eq. (2.33), from which we can obtain a solution if $\tau(z)$ satisfies

$$\tau(z) = \left(\frac{1}{\lambda} - 4\pi\int_0^\infty \frac{1}{z-\frac{p^2}{2\mu}}|g(p)|^2p^2\,dp\right)^{-1}. \tag{5.41}$$

The value of $\lambda$ can be calculated from Eq. (5.39), but if we specify the $s$-wave scattering length, we can immediately obtain it from Eq. (5.41) in the limit $z \to 0$. Using Eq. (2.49), $a_0 = 4\pi^2\mu\hbar\tau(0)|g(0)|^2$, the resulting expression is

$$\lambda = \frac{1}{4\pi^2\mu}\left(\hbar\frac{|g(0)|^2}{a_0} - \frac{2}{\pi}\int_0^\infty |g(p)|^2\,dp\right)^{-1}. \tag{5.42}$$

In case of the square well potential the form factors can simply be calculated from Eq. (5.37). The radial components of the zero-energy scattering state for two particles interacting via square well potential are proportional to $\hat{j}_l(\bar{q}_0)$ for $0 \leq r \leq R$. The separable

[2]Note that the variable $p$ in $t_0(p,p',z)$ and $V_{sep}(p,p')$ is different from the fixed parameter $p$ in Eq. (5.37).

potential $V_{sep,l}$ whose the partial-wave component (labeled by the angular momentum quantum number $l$) of the zero-energy scattering state is exactly the same as the one for square well potential is therefore given by $V_{sep,l} = \lambda g_l(p) g_l(p')$ where

$$g_l(p) \propto -\frac{\hbar \bar{q}_0^2}{2\mu \bar{p}} \frac{\bar{q}_0 \hat{j}_{l+1}(\bar{q}_0)\, \hat{j}_l(\bar{p}) - \bar{p} \hat{j}_{l+1}(\bar{p})\, \hat{j}_l(\bar{q}_0)}{\bar{q}_0^2 - \bar{p}^2}. \tag{5.43}$$

A related derivation can be found in Appendix E.3. For Efimov physics we choose $l = 0$ as discussed above, so that we can define

$$g(p) = \frac{1}{\bar{p}} \frac{\bar{q}_0 \cos(\bar{q}_0) \sin(\bar{p}) - \bar{p} \cos(\bar{p}) \sin(\bar{q}_0)}{\bar{q}_0^2 - \bar{p}^2}. \tag{5.44}$$

The function $\tau(z)$ can then be calculated from Eqs. (5.41) and (5.42). The form factors $g(p)$ are very similar to those of the spectral representation (method I) and the Weinberg series (method II) at $z = 0$. At diverging scattering length these form factors are exactly the same. In Fig. 5.6 we show the form factors of Eq. (5.44) at $\bar{a}_0 = -10.00$ for different potential resonances and normalize them according to

$$2\mu \int_0^\infty g(p)^2\, dp = 1. \tag{5.45}$$

Fig. 5.6 shows that the form factors have a big peak at $\bar{p} \simeq \frac{(2n-1)\pi}{2}$ (except for $n = 1$) where $n$ labels the potential resonance. So these form factors are similar to the form factors of the Weinberg series which is not surprising because they correspond to the same potential.

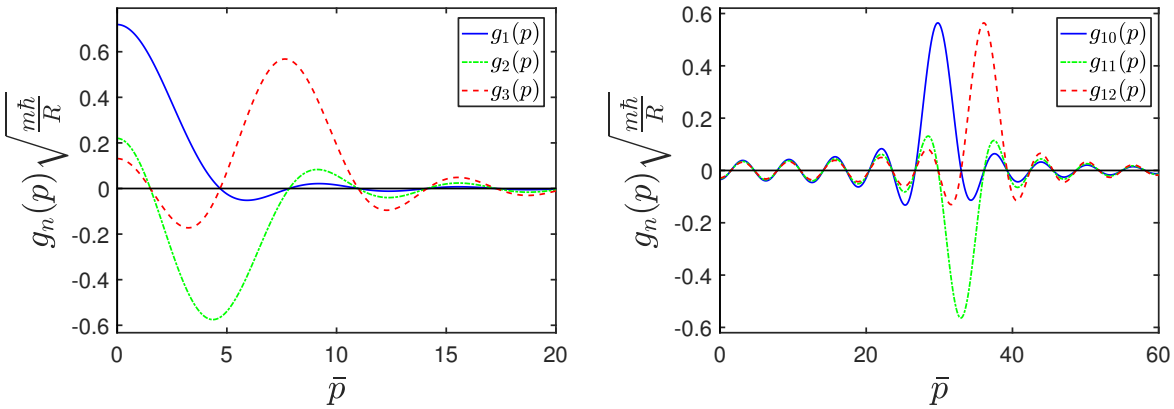


(a) $n = 1, 2, 3$ (b) $n = 10, 11, 12$

Figure 5.6: The form factors $g_n(p)$ of the EST method applied to the square well potential at $\bar{a}_0 = -10.00$. The index $n$ labels the potential resonance. The form factors are normalized according to Eq. (5.45).

Fig. 5.7 shows the diagonal of the off-shell partial-wave component $t_0(p, p', z)$ corresponding to the square well potential at $z = 0$ compared to the one-term approximation of the EST-method. From this figure it is clear that the approximation works quite well near the first potential resonance at $\bar{a}_0 = -9$, but it is less good for the higher order potential resonances. If we increase the absolute value of the scattering length, $t_0(p, p', z)$ becomes more separable and the EST approximation works better as can be seen from Fig. 5.7d.

The results of Fig. 5.7 can be explained by noting that Eq. (4.8) evaluated at zero energy is exactly the same as the one-term EST approximation of the square well potential evaluated at zero energy. Therefore the difference between the full function $t_0(p,p',0)$ and the EST approximation is just the off-shell $d$-wave component $t_2(p,p',0)$ which follows from Eq. (4.7). So whenever $|\frac{t_2(p,p',0)}{t_0(p,p',0)}|$ is not small, the EST approximation at $z=0$ is not working. We know that $t_2(p,p',0)$ diverges when a $d$-wave dimer state becomes bound which occurs at $\bar{a}_0 = 0$. This explains why the EST approximation works quite well at negative scattering lengths near the first potential resonance in which case there is no $d$-wave resonance close. However, the off-shell $d$-wave $T$-matrix is quite big at small negative scattering lengths ($|a| \approx 1$) near the higher order resonances, so that the EST approximation fails in this regime.

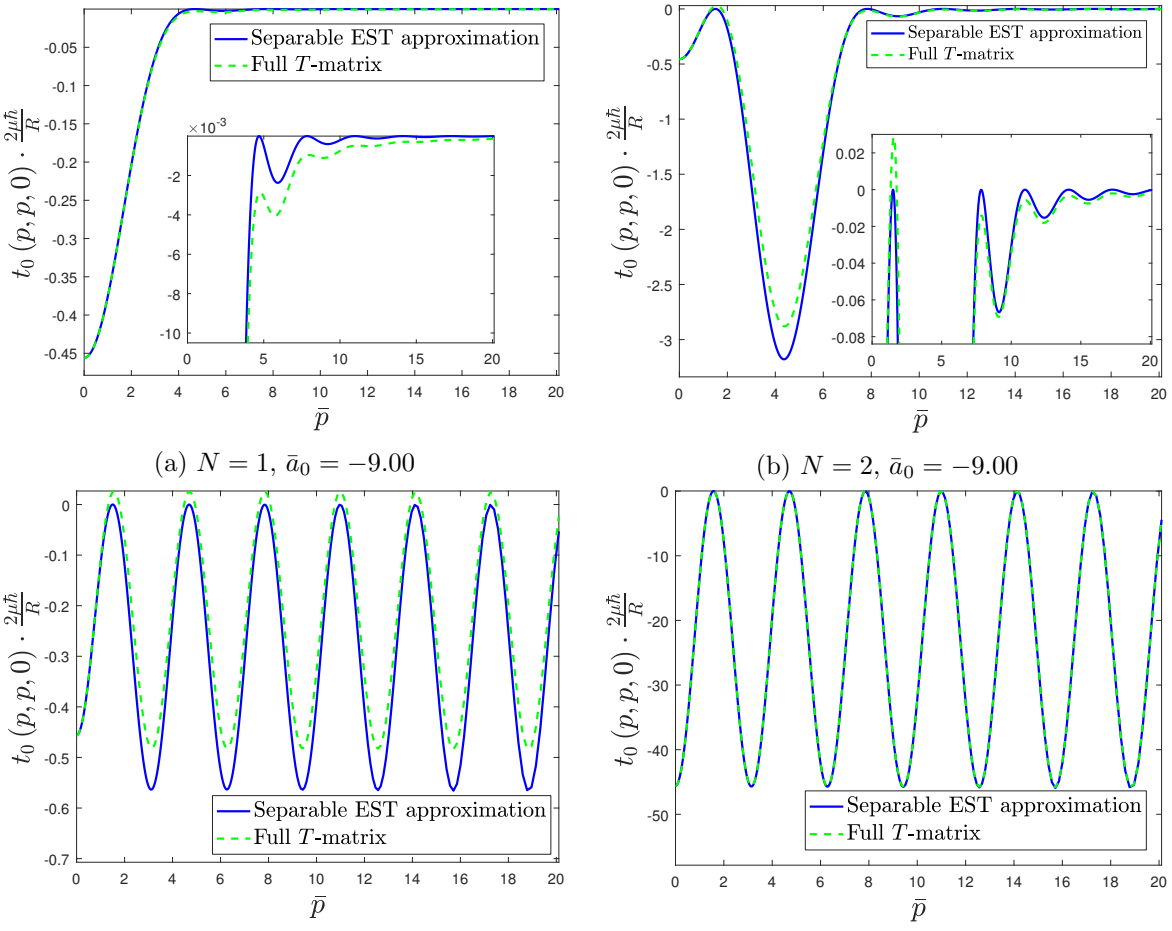


(a) $N = 1$, $\bar{a}_0 = -9.00$

(b) $N = 2$, $\bar{a}_0 = -9.00$

(c) $N = 100$, $\bar{a}_0 = -9.00$

(d) $N = 100$, $\bar{a}_0 = -900$

Figure 5.7: Comparison of the off-shell partial-wave component $t_0(p,p,0)$ corresponding to the square well potential with the one-term approximation of the EST method as a function of $p$. The depth of the square well is chosen such that the $N$th $s$-wave dimer state is almost bound.

At zero energy, $z = 0$, the EST method with $E_p = 0$ provides a good approximation of the partial-wave component $t_0(p,p',z)$ near small values of $\bar{p}$ and $\bar{p}'$. When we decrease the energy $z$, the one-term approximation at $\bar{p} = \bar{p}' = 0$ fails for $|\bar{p}_z| \gtrsim 0.5$ at $\bar{a}_0 = -9$

as can be seen from Fig. 5.8. Note that this is only the case when two-body bound states exist. In case of the first potential resonance the EST method works fine at $\bar{a}_0 = -9$ as can be seen from Fig. 5.8a. The reason is that $t_0(0,0,z)$ does not change sign in this case. If we would have considered a potential with a strong repulsive barrier, the function $t_0(0,0,z)$ would have changed sign, so that for these potentials the behaviour of $t_0(0,0,z)$ near the first potential resonance would be similar to the behaviour near the other resonances and the EST approximation would be worse. Furthermore, the failure of the EST approximation for $|\bar{p}_z| \gtrsim 0.5$ also prevails at larger negative values of the scattering length and for much deeper square well potentials as can be seen from Fig. 5.8c and Fig. 5.8d respectively.

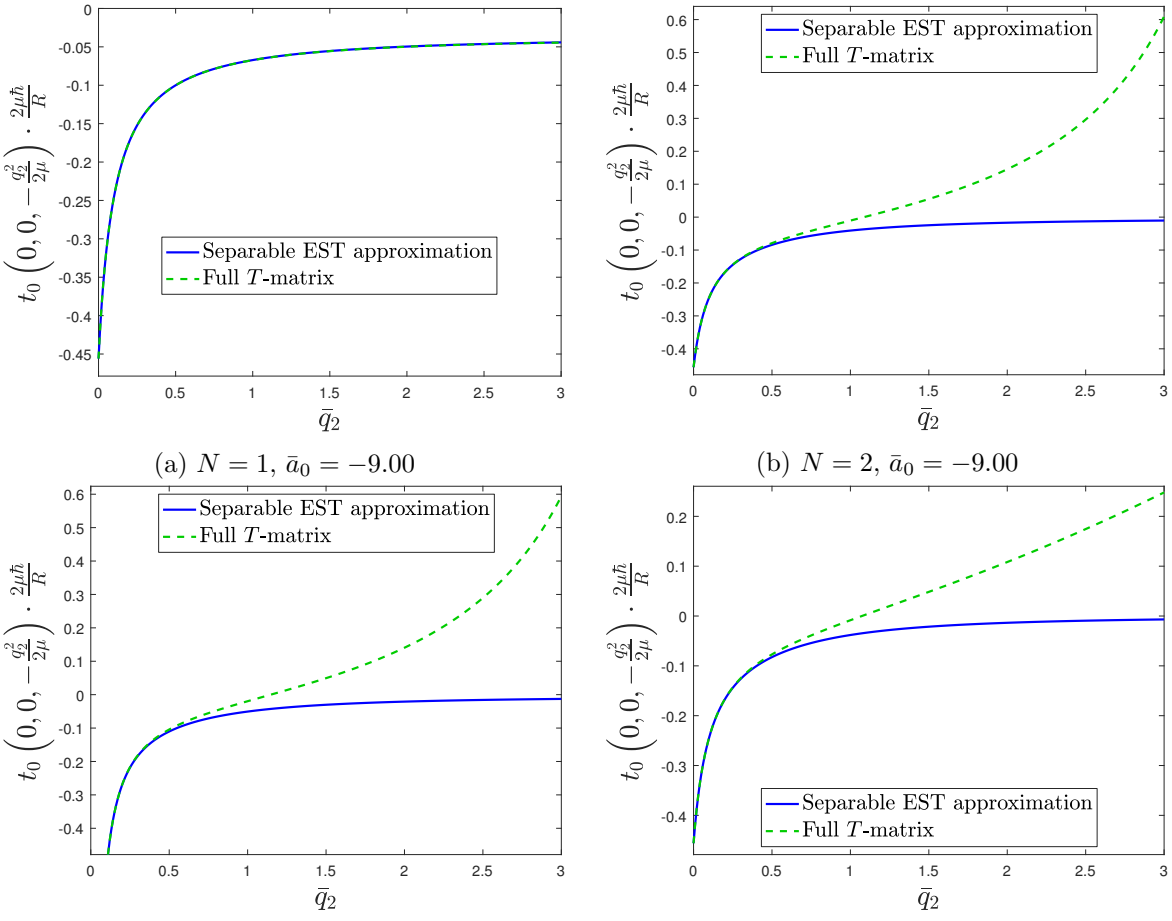


(a) $N = 1$, $\bar{a}_0 = -9.00$

(b) $N = 2$, $\bar{a}_0 = -9.00$

(c) $N = 2$, $\bar{a}_0 = -900$

(d) $N = 100$, $\bar{a}_0 = -9.00$

Figure 5.8: Comparison of the off-shell partial-wave component $t_0(0,0,z)$ corresponding to the square well potential with the one-term approximation of the EST method as a function of $z$. The depth of the square well is chosen such that the $N$th $s$-wave dimer state is almost bound.

## 5.5 Comparison of the separable expansions

We have considered several approaches to expand the off-shell partial-wave components $t_l(p, p', z)$ into terms which are separable in $p$ and $p'$. Table 5.1 summarizes the most important properties of these methods. One useful property which is shared by method I and II is that each two-body bound state with angular momentum quantum number $l$ corresponds to only one specific form factor $g_{nl}(p, z)$. This can be seen from the expansion coefficient $\tau_{nl}(z)$ which only has a pole exactly at the two-body binding energy of the $n$th dimer state with quantum number $l$. Therefore one can study the effect of these deeper bound states on the weakly bound Efimov trimers by including and excluding the corresponding terms in the expansion of $t_l(p, p', z)$.

Furthermore, method I and II provide approximations for the potential $V$ for which the binding energy of the weakly bound $s$-wave dimer state is exactly the same as the one of the full potential $V$. This allows us to use these methods for calculating the Efimov states at small positive scattering lengths close to the atom-dimer threshold. However, the one-term EST approximation of the potential supports a dimer state whose binding energy deviates from the one corresponding to the potential $V$ at small positive scattering lengths. This can be seen from Fig. 6 of Ref. [49] and Fig. 2 of Ref. [54] in which van der Waals potentials are considered. Therefore we will not use the one-term EST approximation to study whether the second Efimov state crosses the atom-dimer threshold.

Another useful property of method II is the fact that the form factors do not depend on the depth of the well and therefore also not on the $s$-wave scattering length $a_0$ for fixed range $R$. This can be seen from Eq. (5.11) which simply shows that any prefactor of the potential only affects the eigenvalues $\eta_{nl}(z)$. As a result, for the calculations of the Efimov states at fixed three-body energy $E$ one only needs to calculate the form factors once for all relevant energies $z$ as one varies the scattering length $\bar{a}_0$. A similar nice property applies to the EST approach (method III) in which the form factors do not depend on the energy $z$. Therefore one could perform three-body calculations at fixed scattering length and search for solutions to the three-body equations by varying the three-body energy $E$ without calculating the form factors more than once. The form factors of method I depend on both the scattering length and the two-body energy $z$, so that the computation time is the largest for three-body calculations involving this method. The form factors of the UPE (method IIb) are a special case. They are independent of the $s$-wave scattering length (for fixed range $R$) and the energy $z$, which reduces the computation time for solving the three-body equation significantly since the form factors need only to be calculated once. However, the three-body equation is changed due to the presence of nonsymmetric terms in the expansion of $t_l(p, p', z)$.

We have confirmed that the separable expansions of method I and II converge to the analytical expression given by Eq. (4.3). The number of terms which are needed to achieve convergence depends on the depth of the well (or equivalently the scattering length) and the considered energy. As discussed before, the separable expansion of $t_l(p, p', z)$ obtained by using method II converges slow at large negative energies below the depth of the well, whereas the convergence is much faster for method I and the UPE at these energies. Therefore method I has better convergence properties than method II. The convergence of the EST-method depends on which wave functions are chosen to be reproduced by the approximated potential. It is difficult to make this choice in general, so that the EST-approach lends itself best to

yielding a separable approximation for the off-shell components $t_l(p, p', z)$.

Finally, we compare in Fig. 5.9 the full $s$-wave component $t_0(p, p', z)$ of the square well potential supporting almost 50 $s$-wave dimer states with some approximations using methods II and III. This figure shows that the one-term EST approximation works well at small momenta and small negative energies, but it fails for $|\bar{p}_z| \gtrsim 0.5$. The Weinberg series is a better substitute for $t_0(p, p', z)$ when enough terms are used in the expansion. The failure of the single-term EST approximation for $|\bar{p}_z| \gtrsim 0.5$ occurs when at least one dimer state is bound. When the potential does not support any bound states, the function $t_0(p, p', z)$ does not have any zeros as a function of $z$ and the EST approximation is a fine substitute for $t_0(p, p', z)$.

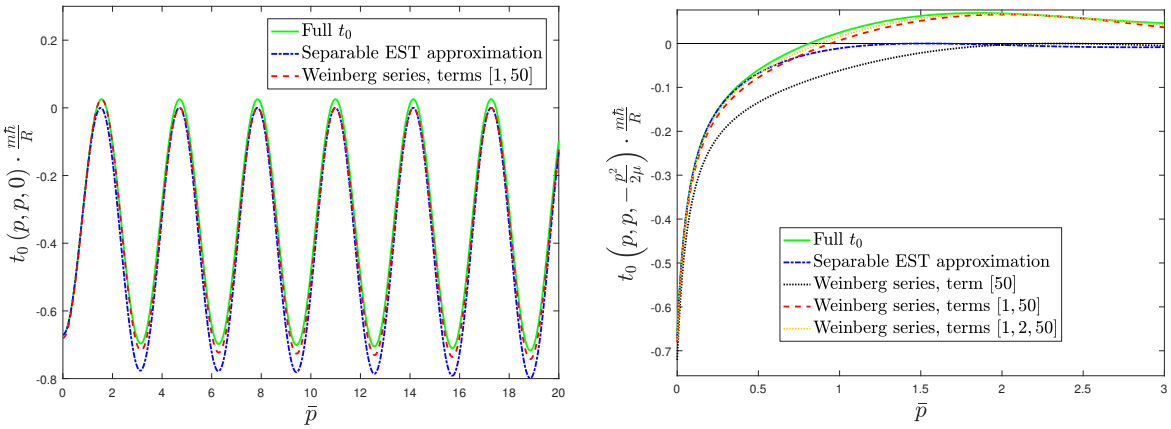


Figure 5.9: Comparison of the off-shell partial-wave components $t_0(p, p, 0)$ and $t_0(p, p, -\frac{p^2}{2\mu})$ corresponding to the square well potential with the approximations using the Weinberg series and the one-term EST approximation. The square brackets indicate which terms of the Weinberg series are used to approximate $t_0$. The depth of the square well is chosen such that the 50th $s$-wave dimer state is almost bound and $\bar{a}_0 = -13.23$.

Table 5.1: Comparison of the different separable expansions of the partial-wave components $t_l(p, p', z)$.

| Method | Advantages | Disadvantages |
|---|---|---|
| I | - each term contains one pole corresponding to a two-body bound state of the potential; the two-body binding energies are the same as for the non-separable potential<br>- the expansion converges slightly faster than the one of method II | - $t_l(p, p', z)$ must be known explicitly<br>- the form factors depend on both the energy $z$ and the depht $q_0$<br>- for deeper potentials many terms are needed to reproduce the scattering length corresponding to the original potential (except for very large scattering lengths) |
| II | - each term contains one pole corresponding to a two-body bound state of the potential; the two-body binding energies are the same as for the non-separable potential<br>- the form factors do not depend on the depth $q_0$ | - for deeper potentials many terms are needed to reproduce the scattering length corresponding to the original potential (except for very large scattering lengths)<br>- the series converges slowly for energies below the depth of the well (not relevant for a deep potential) |
| IIb | - the form factors do not depend on the depth $q_0$ and the energy $z$ | - the expansion of $t_l(p, p', z)$ contains nonsymmetric terms which changes the three-body equation<br>- for deeper potentials many terms are needed to reproduce the scattering length corresponding to the original potential (except for very large scattering lengths) |
| III | - the form factors do not depend on the energy $z$<br>- $\bar{a}_0$ is exactly the same as for the non-separable potential; the low-energy two-body physics is very well described by one-separable term (even for deep potentials) | - it is difficult to determine the second term of the expansion<br>- the separable appoximation fails for $\lvert\bar{p}_z\rvert \gtrsim 0.5$ when the square well supports at least one dimer state |

## 5.6 Comparison with van der Waals potentials

So far we have applied the different expansion methods to the square well potential. Now we apply these methods to some potentials which decay as $-C_6/r^6$ for large $r$. The dispersion coefficient $C_6$ determines the van der Waals length by $r_{vdW} = \frac{1}{2}\left(\frac{mC_6}{\hbar^2}\right)^{1/4}$.

First, we compare the form factors of the square well potential with the ones of several van der Waals potentials by using method II. The considered potentials are the soft-core van der Waals potential $V_{SC}(r)$ given by

$$V_{SC}(r) = -\frac{C_6}{r^6 + \sigma^6} \tag{5.46}$$

and the inner-core van der Waals potential $V_{IC}(r)$ given by

$$V_{IC}(r) = \begin{cases} C_6 v & 0 \leq r < \sigma \\ -\frac{C_6}{r^6} & r \geq \sigma. \end{cases} \tag{5.47}$$

This potential is the same as the hard-core van der Waals potential considered by Ref. [55] for $v \to \infty$.

It is clear from Eq. (5.11) that the form factors of these van der Waals potential do not depend on $C_6$ in the same way that the form factors of the square well potential are independent of the depth $V_0$. The form factors of the van der Waals potentials and the square well potential depend only on the length scales $\sigma$ and $R$ respectively. So when three-body calculations are performed for the van der Waals potentials, time is saved when the $s$-wave two-body scattering length is expressed in units of $\sigma$, so that the form factors do not have to be calculated as a function of the scattering length. The scattering length can be varied by adjusting the value of $C_6$.

Fig. 5.10 compares the form factors obtained for the potentials $V_{SC}(r)$, $V_{IC}(r)$ and $V_{SW}(r)$ at $z = 0$. The units are chosen such that the figure applies to all possible scattering lengths. The same data is also shown in Fig. 5.11 except we have used the van der Waals length to make the form factors and momenta dimensionless. In order to do this we have fixed the scattering length such that $1/a_0 = 0$. This figure is similar to Fig. 1 of Ref. [54] and it shows that the rescaled form factors of the van der Waals potentials look exactly the same in the range $0 \leq pr_{vdW}/\hbar \lesssim 40$, which indicates that this small-momentum regime reflects the part of the potential which is similar for both potentials, namely the van der Waals tail $-\frac{C_6}{r^6}$. The behavior of the form factors at small momenta is most relevant for the calculation of the three-body parameter, which indicates that Efimov physics corresponding to van der Waals potentials is universal [54].

Another interesting thing to note is that the inner barrier of $V_{IC}(r)$ has the effect of increasing the momentum at which $g_{nl}(p, 0)$ is damped out. This simply reflects the fact that the $n$th eigenvalue $\eta_{n,0}(0)$ of the soft-core van der Waals potential is larger than the eigenvalue $\eta_{n,0}(0)$ of $V_{IC}(r)$ with a repulsive barrier. In other words, the potential $V_{IC}(r)$ has to be made deeper than $V_{SC}(r)$ in order to bind the $n$th $s$-wave dimer state.

The form factors $g_{nl}(p, 0)$ of deep square well potentials are much smaller at small momenta $\bar{p}$ compared to the form factors of the considered van der Waals potentials. This is caused by the occurence of one big peak which suppresses the rest of the form factors due to the

normalization condition of Eq. (5.12). The big peak occurs near $\bar{p} \simeq \frac{(2n-1)\pi}{2}$ which is just the depth $\bar{q}_0$ at which the $n$th potential resonance occurs. This big peak reflects the large probability density for relative momenta near $\bar{q}_0$ at distances $r < R$. For van der Waals potentials, the probability density for finding two particles at small relative distances $r \lesssim r_{vdW}$ is suppressed (see Fig. 1.5), so that the probability density for two particles, which scatter at zero energy, to have large relative momenta is small. So the form factors corresponding to potentials involving a van der Waals tail do not have an extremely large peak at large momenta.

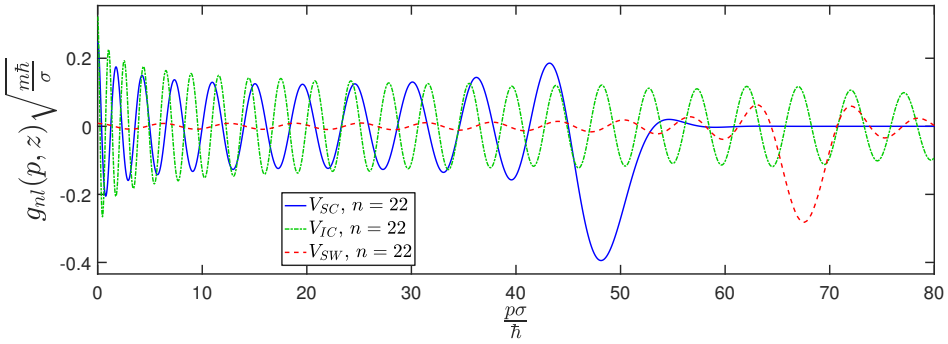


Figure 5.10: Form factors at $z = 0$ corresponding to the 22th $s$-wave two-body bound state of the potentials $V_{SC}$, $V_{IC}$ (with $v = 100\sigma^{-6}$) and $V_{SW}$ (i.e., $n = 22$ and $l = 0$) calculated by using method II. The form factor corresponding to $V_{SW}$ is plotted as $\frac{1}{2}g_{nl}(p,z)\sqrt{\frac{m\hbar}{R}}$ versus $\frac{pR}{\hbar}$.

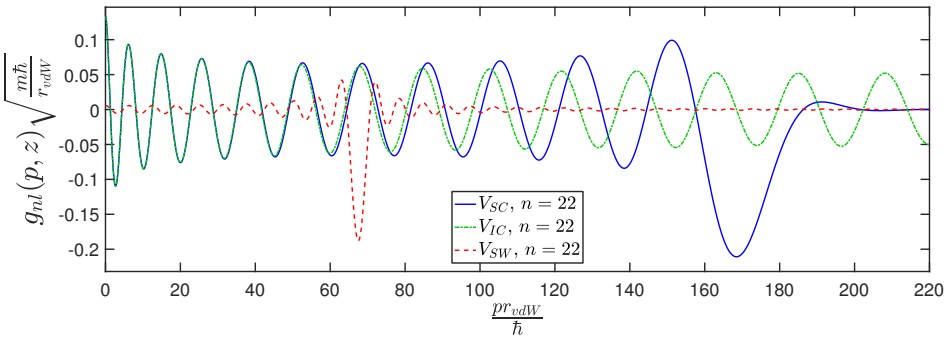


Figure 5.11: Form factors at $z = 0$ corresponding to the 22th $s$-wave two-body bound state of the potentials $V_{SC}$, $V_{IC}$ (with $v = 100\sigma^{-6}$) and $V_{SW}$ (i.e., $n = 22$ and $l = 0$). The potentials support exactly 22 $s$-wave bound states and the inverse scattering length $1/a_0$ is set to zero. The form factor corresponding to $V_{SW}$ is plotted as $\frac{1}{3}g_{nl}(p,z)\sqrt{\frac{m\hbar}{R}}$ versus $\frac{pR}{\hbar}$.

Now we compare the one-term EST approximation for the inner-core van der Waals potential with the corresponding Weinberg series. The comparison is shown in Fig. 5.12. Since this potential contains a repulsive barrier, the eigenvalues $\eta_{nl}(z)$ of the Weinberg series cannot only take on positive values, but also negative values. In this case we label the positive eigenvalues in the same way as before and we label the negative eigenvalues with negative values of $n$ such that $|\eta_{nl}(z)|$ decreases for increasing $|n|$. Fig. 5.12 shows that the one-term EST approximation works fine at small negative energies, but not for $\frac{pr_{vdW}}{\hbar} \gtrsim 0.5$ which is

quite similar as we have seen for the square well potential in Fig. 5.9. The cause for this failure is similar as for the square well potential. The EST approximation for $t_0(p,p,-\frac{p^2}{2\mu})$ cannot change sign, whereas the actual component $t_0(p,p,-\frac{p^2}{2\mu})$ does change sign.

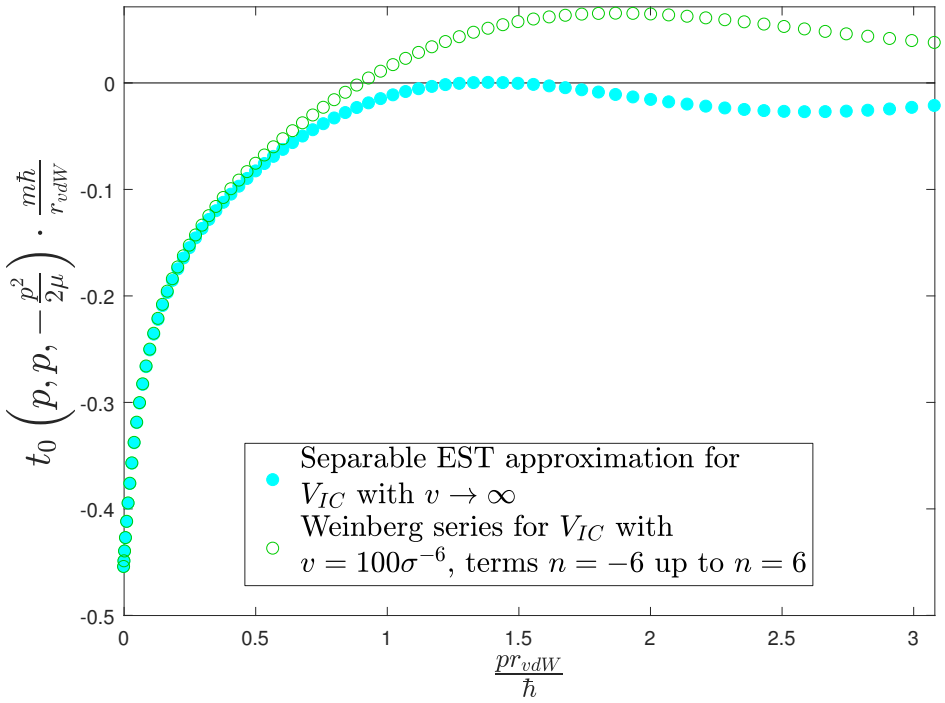


Figure 5.12: The off-shell partial-wave component $t_0(p,p,-\frac{p^2}{2\mu})$ corresponding to the inner-core van der Waals potential is approximated with the Weinberg series and the one-term EST approximation. The first $s$-wave dimer state is almost bound and the scattering length is $a_0 = -9.00\ r_{vdW}$.

The form factors of the square well potential and the van der Waals potential differ a lot as we have seen from Fig. 5.11. As a result, the function $\tau(z)$ corresponding to the EST method is also strongly affected as can be seen from Eq. (5.41). Fig. 5.13 shows this function for the square well potential and the inner-core van der Waals potential at the same value of the scattering length near the first and second potential resonance. For $N=1$ the differences are less big than for $N=2$. At $\bar{p}=3$ the curves differ by a factor 1.5 for $N=1$, whereas this factor is 5.0 for $N=2$. This difference in $\tau(z)$ between the square well and the van der Waals potential is caused by the big peak of the form factors of the square well potential which suppresses the small momentum part of the form factors after normalizing. This can easily be seen from Eqs. (5.41) and (5.42). Combining these equations results in

$$\tau(z) = \frac{1}{4\pi^2\mu}\left(\hbar\frac{|g(0)|^2}{a_0} - \frac{2}{\pi}\int_0^\infty \frac{z}{z-\frac{p^2}{2\mu}}|g(p)|^2\,dp\right)^{-1} \tag{5.48}$$

or

$$\frac{\tau(z)}{\tau(0)} = \left(1 - \frac{2}{\pi\hbar}\frac{a_0}{|g(0)|^2}\int_0^\infty \frac{z}{z-\frac{p^2}{2\mu}}|g(p)|^2\,dp\right)^{-1} \tag{5.49}$$

from which we see that the factor $\frac{a_0}{|g(0)|^2}$ makes sure that $\tau(z)$ drops off fast for the square well potential for $N \geq 2$.

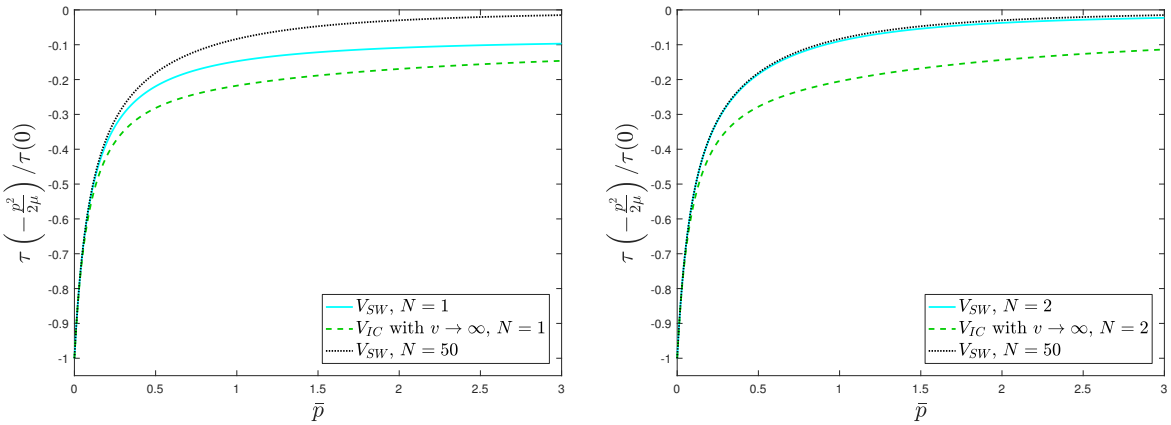


Figure 5.13: The EST-function $\tau(z)$ corresponding to the square well potential and the inner-core van der Waals potential with $v \to \infty$. The scattering length is $a_0 = -9.00\, r_0$ where $r_0 = R$ for $V_{SW}$ and $r_0 = r_{vdW}$ for $V_{IC}$. The potential resonance is indicated by $N$. The dimensionless momentum $\bar{p}$ is simply $\frac{pr_0}{\hbar}$.

## 5.7 Applicability for studying Efimov physics

The analysis of the different separable expansion methods presented in this Chapter allows us to determine the usefulness of these methods to study Efimov physics associated with square well potentials. Methods I-III are all expected to be useful for calculations of the Efimov states near the first potential resonance. However, only method I and II reproduce the correct dimer state energy at all values of the scattering length, so that these methods should be used to study the crossing of the deepest Efimov states with the atom-dimer threshold.

For deeper potentials, the Efimov resonances are embedded into the continuum associated with deeper two-body bound states. Consequently, the separable approximation (using any method) fails or it may only be valid in a smaller energy regime. Naidon *et al.* [59] have shown that the separable EST-approximation of many potentials (including van der Waals potentials) works very well to determine the three-body properties of the Efimov resonances. Therefore, we should certainly consider this approximation for the square well potential. Furthermore, although the separable expansion of method I converges faster than the separable expansion of method II, we do not recommend this method in the case of deep square well potentials because it is computationally more extensive. Moreover, since the form factors of method I and II (and IIb) are quite similar (and are exactly the same at zero energy), the number of terms which are necessary to approximate the two-body $T$-matrix of deep square well potentials will be quite similar. Therefore we will not consider method I and IIb for deep square well potentials. On the other hand, for a shallow square well potential supporting one bound state, method I allows us to calculate the three-body properties using less expansion terms, so that it is useful for such potentials. We will not perform any three-body calculations using the unitary pole expansion (method IIb) because it requires a different form of the three-body equations.

So far we have compared the different expansion methods only on the two-body level. We will expand this analysis on the three-body level in Chapter 7. It is not obvious that a separable approximation of the two-body $T$-matrix results in the correct three-body parameter because the three-body equation involves an integration over all negative energies below the energy $E$ of the three-body system. So even if a separable approximation holds very well close to $E$, it may not describe the three-body physics correctly.

# 6. Numerical model

The three-body equations presented in Chapter 3 need to be solved numerically. In this Chapter we describe how these numerical calculations are performed. We also analyze the three-body equations by considering how different terms of the separable expansion of $t_l(p, p', z)$ shift the energies of the Efimov states. For this purpose we introduce some new terminology. We will call the separable term in the expansion of the partial-wave component $t_0(p, p', z)$ which corresponds to the $s$-wave dimer state causing the potential resonance the resonant term and label it with $n = n_r$ and $l = 0$. This term is the dominant term of this expansion when considering energies close enough to the corresponding $s$-wave dimer energy because $\tau_{n_r,0}(z) \gg \tau_{n,0}(z)$ for $n \neq n_r$ and small energies $z$. We call the other terms in the expansion of $t_0(p, p', z)$ the nonresonant terms.

## 6.1 Three-body bound state calculations

The three-body equation which we need to solve is given by Eq. (3.15). We choose a finite number of components $\tilde{\phi}_{ln}(q, E)$ to be nonzero which reduces the set of three-body equations to a finite set of coupled one-dimensional integral equations. This approximation can be justified by studying the convergence of the numerical results as a function of the number of components $\tilde{\phi}_{ln}(q, E)$ taken into account. We will only consider $s$-wave and $d$-wave interactions, i.e., $l = 0$ and $l = 2$. We indicate the number of separable terms which are used to approximate the partial-wave components $t_0(p, p', z)$ and $t_2(p, p', z)$ by $N_s$ and $N_d$ respectively.

The usual method to numerically solve an integral equation, which is known as the Nyström method [80], is to introduce a grid for the momentum variables $q$ and $q'$ according to some quadrature rule, so that the value of an integral can be approximated as a linear combination of values of the integrand evaluated at some specific points $q_i$ and weighted by a specific number $w_i$ [80], i.e.,

$$\int_a^b f(q)\, dq = \sum_{i=1}^{N_q} w_i f(q_i). \tag{6.1}$$

This approximation is better when the number of grid points $N_q$ increases. We do not want to use equally spaced points $q_i$ if the only important contribution to the integrand is located in some small region of the range $[a, b]$. This is also the case for the integral in Eq. (3.15) due to the factor $\tau_{n_r,0}(Z_q)$. Furthermore, the form factors $g_{nl}(p, z)$ with small values of $n$ only contribute for small momenta.

We choose the method Gaussian quadrature to calculate the location of the abscissas $q_i$ and the corresponding weighting functions $w_i$ because then the sum in Eq. (6.1) converges exponentially fast to the value of the integral as the number of grid points $N_q$ increases, so that it is the most efficient method for smooth, nonsingular functions [80]. More theory on Gaussian quadratures can be found in Ref. [80]. We choose the Gauss-Legendre quadrature rule to calculate the abscissas and weights for integrals on the range $[-1, 1]$. This means that the abscissas $q_i$ are just the $N_q$ roots of the Legendre polynomial $P_{N_q}(q)$ and the weights are given by [80]

$$w_i = \frac{2}{(1 - q_i^2)[P'_{N_q}(q_i)]^2}. \tag{6.2}$$

We transform these abscissas and weights on $[-1, 1]$ to the abscissas $\tilde{q}_i$ and weights $\tilde{w}_i$ on the infinite range $[0, \infty]$ via [80]

$$\tilde{q}_i = \alpha \left( \frac{2}{q_i + 1} - 1 \right) \tag{6.3}$$

and

$$\tilde{w}_i = \frac{2\alpha w_i}{(q_i + 1)^2}. \tag{6.4}$$

This means that we have two momentum grid variables, $N_q$ and $\alpha$, which can be tuned to get converged results. The parameter $\alpha$ determines the location and spacing of the abscissas $\tilde{q}_i$.

Now we can define the column vector $\underline{q}$ which contains the momenta $\tilde{q}_1, \tilde{q}_2, \tilde{q}_3, ....$ Since we have discretized the absolute values of the momenta $\mathbf{q}$ and $\mathbf{q}'$, we can write the set (3.15) of coupled integral equations in matrix form as

$$\begin{pmatrix} \tilde{\phi}_1(\underline{q}, E) \\ \tilde{\phi}_2(\underline{q}, E) \\ \tilde{\phi}_3(\underline{q}, E) \\ \vdots \end{pmatrix} = \begin{pmatrix} F_{11}(\underline{q}, \underline{q}^T) & F_{12}(\underline{q}, \underline{q}^T) & F_{13}(\underline{q}, \underline{q}^T) & \cdots \\ F_{21}(\underline{q}, \underline{q}^T) & F_{22}(\underline{q}, \underline{q}^T) & F_{23}(\underline{q}, \underline{q}^T) & \cdots \\ F_{31}(\underline{q}, \underline{q}^T) & F_{32}(\underline{q}, \underline{q}^T) & F_{33}(\underline{q}, \underline{q}^T) & \cdots \\ \vdots & \vdots & \ddots & \end{pmatrix} \begin{pmatrix} \tilde{\phi}_1(\underline{q}, E) \\ \tilde{\phi}_2(\underline{q}, E) \\ \tilde{\phi}_3(\underline{q}, E) \\ \vdots \end{pmatrix}. \tag{6.5}$$

In this equation, we have replaced the label '$ln$' by the numbers 1, 2, 3, ... These numbers refer to each single equation given by Eq. (3.15). The superscript $T$ denotes the transpose of a matrix. Furthermore, $\tilde{\phi}_i(\underline{q}, E)$ indicates a column vector consisting of the values $\tilde{\phi}_i(q_1, E)$ up to $\tilde{\phi}_i(q_{N_q}, E)$ and the element $F_{ij}(\underline{q}, \underline{q}^T)$ is a matrix, namely

$$\left(F_{ij}(\underline{q}, \underline{q}^T)\right) = \begin{pmatrix} F_{ij}(\tilde{q}_1, \tilde{q}_1) & \cdots & F_{ij}(\tilde{q}_1, \tilde{q}_{N_q}) \\ \vdots & \ddots & \vdots \\ F_{ij}(\tilde{q}_{N_q}, \tilde{q}_1) & \cdots & F_{ij}(\tilde{q}_{N_q}, \tilde{q}_{N_q}) \end{pmatrix}. \tag{6.6}$$

The matrix element $F_{ij}(q_a, q_b)$ is given by

$$F_{ij}(q_a,q_b) = -4\pi du \sum_{n=1}^{N_u} \frac{\Delta_{l_i}\Delta_{l_j} q_b^2 dq_b}{E - \frac{1}{m}\left(q_a^2 + q_a q_b u_n + q_b^2\right)} P_{l_i}\left(\frac{\frac{1}{2}q_a + q_b u_n}{\sqrt{\frac{1}{4}q_a^2 + q_b^2 + q_a q_b u_n}}\right) \\ \tau_i\left(E - \frac{3}{4m}q_a^2\right) g_i\left(\sqrt{\frac{1}{4}q_a^2 + q_b^2 + q_a q_b u_n}, E - \frac{3}{4m}q_a^2\right)(2l_j+1) \\ P_{l_j}\left(\frac{\frac{1}{2}q_b + q_a u_n}{\sqrt{q_a^2 + \frac{1}{4}q_b^2 + q_a q_b u_n}}\right) g_j\left(\sqrt{q_a^2 + \frac{1}{4}q_b^2 + q_a q_b u_n}, E - \frac{3}{4m}q_b^2\right). \tag{6.7}$$

The momenta $q_a$ and $q_b$ are just elements of the set of abscissas $\{\tilde{q}_i\}$ defined in Eq. (6.3) and $dq_b$ is just the $b$th element of the set of weights $\{\tilde{w}_i\}$ defined in Eq. (6.4). Furthermore, the angular integration is executed by means of Riemann summation. We have defined the angular variable $u$ as $u \equiv \cos\left(\hat{\mathbf{q}} \cdot \widehat{\mathbf{q}'}\right)$ which takes on values in the range $[-1, 1]$. We have chosen for the middle Riemann sum in which $du$ is the step size of the angular integration and $N_u = \frac{2}{du}$ is the number of steps which are used to approximate the angular integration. So the $n$th value $u_n$ is given by $u_n = -1 + (n - \frac{1}{2})du$.

Eq. (6.5) can be written as $\tilde{t}_i = \sum_j \tilde{F}_{ij}\tilde{t}_j$ which is just an eigenvalue equation in which the vectors $\underline{\tilde{t}}$ are eigenvectors of the matrix $\tilde{F}$ with eigenvalue 1. The matrix $\tilde{F}$ is called the kernel. In order to find the three-body binding energies $E = -\frac{3\bar{q}_3^2}{4m}$ at some fixed scattering length we can simply vary the momentum $\bar{q}_3$ for a fixed depth $\bar{q}_0$ and calculate the determinant of $I - \tilde{F}$ where $I$ is the identity matrix. A solution to the three-body equation exists whenever

$$\det\left(I - \tilde{F}\right) = 0. \tag{6.8}$$

Alternatively, we can vary the depth $\bar{q}_0$ at a fixed value of the momentum $\bar{q}_3$ and then calculate the value of the determinant. When the determinant changes sign, we use the secant method to accurately find the depth $\bar{q}_0$ at which the zero occurs.

As we have seen before, the dimensionless depth $\bar{q}_0$ determines the scattering length of the square well potential. Therefore we can calculate the Efimov spectrum by calculating the zeros of the determinant $\det\left(I - \tilde{F}\right)$ for a set of scattering lengths around the potential resonance of interest.

## 6.2 Analysis of the kernel using the Weinberg series

Here we analyze the 'symmetrized' kernel of the three-body equations given in Eq. (F.20). We use the Weinberg series to expand the two-body $T$-matrix. The kernel of each integral equation is given by

$$K_{nl}(q,q',E) = \sum_{l'=0,\text{even}}^{\infty} \sum_{n'=1}^{\infty} K_{nln'l'}(q,q',E) \tag{6.9}$$

where

$$K_{nln'l'}(q,q',E) = -\int d\widehat{\mathbf{q}'} \frac{2q'qP_l(\hat{\mathbf{q}}\cdot\widehat{\frac{1}{2}\mathbf{q}+\mathbf{q}'})}{E-\frac{1}{m}(q^2+\mathbf{q}\cdot\mathbf{q}'+q'^2)}\sqrt{\tau_{nl}(E-\frac{3}{4m}q^2)}g_{nl}(|\frac{1}{2}\mathbf{q}+\mathbf{q}'|,E-\frac{3}{4m}q^2)$$
$$(2l'+1)P_{l'}(\widehat{\mathbf{q}+\tfrac{1}{2}\mathbf{q}'}\cdot\widehat{\mathbf{q}'})\sqrt{\tau_{n'l'}(E-\frac{3}{4m}q'^2)}g_{n'l'}(|\mathbf{q}+\frac{1}{2}\mathbf{q}'|,E-\frac{3}{4m}q'^2). \tag{6.10}$$

The functions $K_{nln'l'}(q,q',E)$ are symmetric in $q$ and $q'$ if $n=n'$ and $l=l'$. Note that when we only consider $s$-wave interactions ($l=0$), the Legendre polynomials are just constants, i.e. $P_0(x)=1$.

A very interesting feature of the function $K_{nln'l'}(q,q',E)$ is that the small-momentum region, i.e. $\bar{q},\bar{q}' \lesssim 5$, is most important for the three-body calculations even when the form factor $g_{nl}(p,z)$ has a big peak at large $p$. We will show this in more detail in Section 6.2.2, but here we will briefly consider why this is the case. When the three-body energy is close to the energy of a dimer state labeled by $n_r$ and $l_r$, the functions $\tau_{n_rl_r}(E-\frac{3}{4m}q^2)$ and $\tau_{n_rl_r}(E-\frac{3}{4m}q'^2)$ are very big at small values of $q$ and $q'$ respectively. So we see that large values of $q$ and $q'$ do not contribute much to the calculation of the three-body parameters and to the calculation of the higher excited Efimov states whose energies are very small and which are located very close to the $s$-wave dimer state. This also means that one needs to define the momentum grid denser for $\bar{q},\bar{q}' \ll 1$ if one wants to calculate the energies of the higher excited Efimov states. Furthermore, since the form factors $g_{nl}(p,z)$ for $l\neq 0$ are zero at $p=0$, these form factors have little overlap at small values of $q$ and $q'$ with the resonant form factor for which $l_r=0$. Therefore these terms are not expected to contribute much and $s$-wave interactions dominate.

In Section 5.3 we have seen that the form factors $g_{nl}(p,z)$ of the square well potential at zero energy have a big peak near $\bar{p}\simeq\frac{(2n-1)\pi}{2}$ (except for $n=1$) and are small at $\bar{p}=0$. The effect of this big peak is less important than one might expect. This is simply caused by the fact that the functions $\tau_{n_r,0}(E-\frac{3}{4m}q^2)$ and $\tau_{n_r,0}(E-\frac{3}{4m}q'^2)$ of the resonant term (which corresponds to the $s$-wave dimer state which causes the resonance) are very small at large $q$ and $q'$ respectively.

Now we consider the coupling terms. The most dominant coupling terms will be the coupling between the resonant term (indicated by $n_r$) and the other terms due to the large value of $\tau_{n_rl_r}$ corresponding to the resonant term. Since $\tau_{n_rl_r}$ drops off to zero as $q$ or $q'$ increases, it is the small-momentum region which dominates those coupling terms. Furthermore, the lowest-order terms ($n=1,2,...$) couple most strongly to the resonant term because the form factors corresponding to those terms have the biggest values for small momenta, whereas the prefactors $|\tau_{nl}(0)|$ for almost all $n<n_r$ (except for values of $n$ close to $n_r$) are on the order of $\frac{1}{4\pi}$ because the corresponding values of $\eta_{nl}(0)$ are much larger than 1 (see Eq. (5.13)).

We can quantify the coupling strength with the parameter $\Gamma(z)=\frac{\sqrt{|\tau_{nl}(z)|}g_{nl}(0,z)}{\sqrt{|\tau_{n_rl_r}(z)|}g_{n_rl_r}(0,z)}$, where the index $r$ refers to the resonant term. Fig. 6.1 shows how this coupling strength looks at zero energy for $n_r=100$, $l_r=0$ and $l=0$. This figure clearly shows that lowest-order terms ($n=1,2,...$) couple most strongly to the resonant term.

Another important point which has to be considered is the poles in the factors $\tau_{nl}$ for

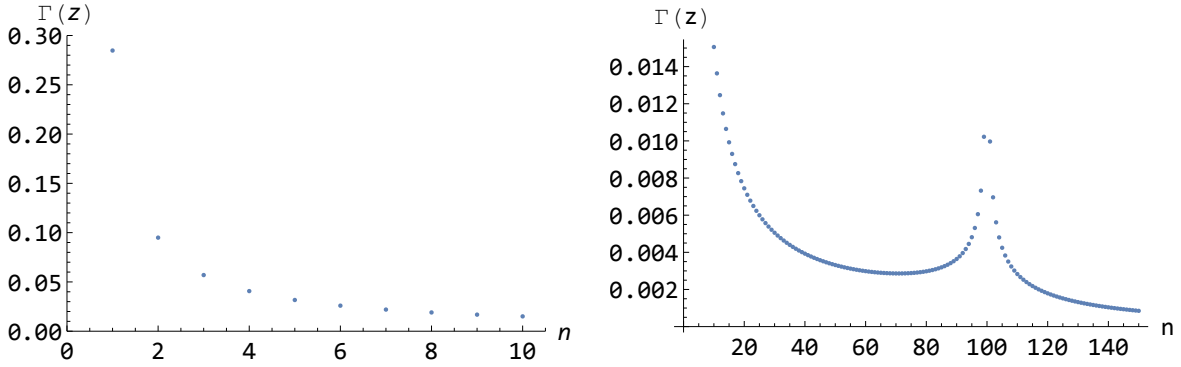


Figure 6.1: The coupling strength $\Gamma(z)$ as a function of $n$ at energy $z = 0$ and with $n_r = 100$, $l_r = 0$ and $l = 0$. The depth of the square well is chosen such that $\bar{a}_0 = -9.00$. The functions $g_{nl}$ and $\tau_{nl}$ are calculated by using the Weinberg series.

all $n \leq N_l$ which occur when the potential is deep enough to support $N_l$ two-body bound states with angular momentum quantum number $l$. Since integrating over a singularity can lead numerical errors, we need to be careful when we take these terms into account. In case of a deep square well potential many $s$-wave two-body bound states exist near the bottom of the well. Although the form factors of the resonant term are not zero at this value of the momentum, the prefactor $\tau_{n_r l_r}$ is almost zero at this value and the form factors $g_{n,0}$ corresponding to strongly bound $s$-wave dimer states are also close to zero at large momentum values. Therefore we expect that the poles corresponding to the strongly bound $s$-wave dimer states do not contribute much to the three-body calculation. The main effect of these poles is probably to give the Efimov states a width via the residue of the poles.

The situation is different for the weakliest bound $s$-wave dimer states. The poles corresponding to these two-body bound states occur at higher energies, so that $\tau_{n_r l_r}$ is not completely zero and also the form factors $g_{n,0}$ corresponding to these weakly bound $s$-wave dimer states are not zero. We will analyze the effect of these poles in more detail below when we investigate the eigenvalues of the kernel.

### 6.2.1 The diagonal of the kernel

An important feature of the function $K_{nln'l'}(q, q', E)$ is that it equals 0 when $q = 0$ or $q' = 0$ (except for $E = 0$). This is caused by the factor $\frac{q'q}{E - \frac{1}{m}(q^2 + \mathbf{q}\cdot\mathbf{q}' + q'^2)}$. This factor pronounces the diagonal of the $K_{nln'l'}(q, q', E)$, whereas it strongly suppresses the regions in which $q \ll 1$ or $q' \ll 1$ (except when both $q$ and $q'$ are small and $E$ is also close to zero). So by analyzing the diagonal of the submatrices of the kernel we gain a lot of knowledge about the kernel and we can see what values of $q'$ really contribute to the integrals in the three-body equations.

An interesting limit of the functions $K_{nlnl}(q, q', E)$ is the limit in which $q$, $q'$ and $E$ go to

zero. This limit can be easily calculated. For $l = 0$ it is given by

$$\lim_{q,q',E\to 0} K_{n0n0}(q,q',E) = -\int_{-1}^{1} 2\pi \frac{2}{\frac{1}{m}(2+u)} t_0(0,0,0)\, du \tag{6.11}$$

$$= -\frac{2\ln(3)}{\pi\hbar} a_{n,0}. \tag{6.12}$$

Here we have used Eq. (2.49). The scattering length $a_{n,0}$ is just the $n$th contribution to the $s$-wave scattering length (see Eq. (5.21)). Note that $\lim_{q,q'\to 0} K_{nlnl}(q,q',E) = 0$ for $E \neq 0$ or $l \neq 0$. Fig. 6.2a shows how $K_{nlnl}(q,q,E=0)$ decreases for different potential resonances of the square well potential using the Weinberg series which is described in Section 5.3.

When the momenta $q$ and $q'$ are nonzero, the specific behaviour of the partial-wave components $t_l(p,p',z)$ matters. In case of the square well potential we have seen that the form factors $g_{n,0}(p,z)$ exhibit a peak near $\bar{p} = \frac{(2n-1)\pi}{2}$. Since the form factors of the function $K_{nln'l'}(q,q',E)$ depend on $|\frac{1}{2}\mathbf{q} + \mathbf{q}'|$ and $|\frac{1}{2}\mathbf{q}' + \mathbf{q}|$, we expect that the peak of the form factors results in a broadened peak in the kernel due to the angular integration. Since $\frac{1}{2}q \leq |\frac{1}{2}\mathbf{q} + \mathbf{q}'| \leq \frac{3}{2}q$ for $q = q'$, the peak of the form factors will influence the diagonal $K_{n0n0}(q,q,E)$ for $\frac{2}{3}\frac{(2n-1)\pi}{2} \leq \bar{q} \leq (2n-1)\pi$. This can be clearly seen in Fig. 6.2b in which $K_{nlnl}(q,q,E=0)$ is shown as a function of $q$ for the square well potential. The peak clearly broadens as one considers higher values of $n$. The maximum of the peak also lowers as a function of $n$ due to the drop of $\tau_{n,0}\left(E - \frac{3}{4m}q^2\right)$ as $q$ increases. The three curves shown in Fig. 6.2b almost overlap for the values of $q$ which are not shown in this figure. Furthermore, if we compare Fig. 6.2b with Fig. 6.2a, we see that the peaks shown in Fig. 6.2b are very small compared to $K_{n0n0}(0,0,0)$.

In Fig. 6.2 we have only considered the functions $K_{n_r0n_r0}(q,q',E)$ where $n_r$ labels the resonant term in the separable expansion of $t_l(p,p',z)$. From this figure we can conclude that one needs to integrate at least to $\bar{q} = (2n_r - 1)\pi$ in order to have accurate results. However, if $n_r$ is large, the peak in the range $\frac{1}{3}(2n_r - 1)\pi \leq \bar{q} \leq (2n_r - 1)\pi$ is small compared to $K_{n_r0n_r0}(0,0,0)$, so that the contribution of the peak at large values of $q$ is not expected to contribute much to the calculation of the three-body parameter $a_-$.

### 6.2.2 The eigenvalues of the kernel

We have seen that a solution to the Faddeev equations exists when the kernel $\tilde{F}$ has an eigenvalue equal to 1. Now we study how the eigenvalues shift as one includes more terms in the expansion of $t_l(p,p',z)$ in which case the size of the kernel increases.

In this analysis we consider a set of two coupled integral equations which is represented in matrix form by

$$\begin{pmatrix} \tilde{\phi}_1(\underline{q},E) \\ \tilde{\phi}_2(\underline{q},E) \end{pmatrix} = \begin{pmatrix} F_{11}(\underline{q},\underline{q}^T) & \lambda F_{12}(\underline{q},\underline{q}^T) \\ \lambda F_{21}(\underline{q},\underline{q}^T) & F_{22}(\underline{q},\underline{q}^T) \end{pmatrix} \begin{pmatrix} \tilde{\phi}_1(\underline{q},E) \\ \tilde{\phi}_2(\underline{q},E) \end{pmatrix}. \tag{6.13}$$

Note that we have introduced a parameter $\lambda$ which equals 1 when we want to solve the three-body equations for the separable expansion of $t_0(p,p',z)$ which includes two terms. However, if the coupling parameter $\lambda$ equals 0, this set of three-body equations decouples. In our analysis, the number 1 in Eq. (6.13) corresponds to $l_1 = 0$ and $n_1 = n_r$ where $n_r$ is the

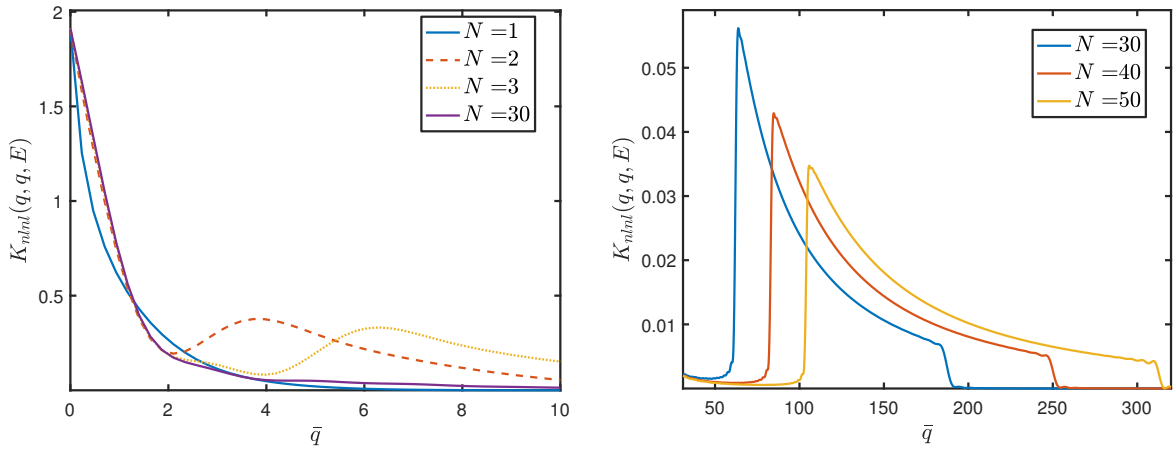


(a) $N = 1, 2, 3, 30$ (b) $N = 30, 40, 50$

Figure 6.2: The diagonal $K_{nlnl}(q, q, E)$ as a function of $q$ for the square well potential using the method described in Section 5.3 to calculate the form factors. The potential resonances are labeled by $N$. The plotted curves correspond to $n = N$ and $l = 0$. The considered energy of the three-body system is $E = 0$ and the considered contribution to the scattering length is $\bar{a}_{n,0} = -2.733$.

resonant term. We also choose $l_2 = 0$. The value of $n_2$ is varied. In all cases we calculate the eigenvalues of the kernel $\tilde{F}$ for $0 \leq \lambda \leq 1$. In this way we can study how the eigenvalues shift as we increase the coupling strength.

For $\lambda = 0$ the eigenvalues of the kernel $\tilde{F}$ are just the eigenvalues of the submatrices $\big(F_{11}(\underline{q}, \underline{q}^T)\big)$ and $\big(F_{22}(\underline{q}, \underline{q}^T)\big)$. So we start by choosing the depth $\bar{q}_0$ of the square well in such a way that the highest eigenvalue (which we call $f$) of $\big(F_{11}(\underline{q}, \underline{q}^T)\big)\big)$ is close to 1. This eigenvalue corresponds to the lowest Efimov state.

We define the shift $\Delta f$ of the considered eigenvalue as $\Delta f = f(\lambda = 1) - f(\lambda = 0)$. In Fig. 6.3a we show how the eigenvalues $f(\lambda)$ shift as a function of coupling parameter $\lambda$. A positive shift means that the trimer state becomes bound at a smaller depth $\bar{q}_0$, whereas a negative shift means that the depth $\bar{q}_0$ should be increased in order to bind the Efimov trimer. Fig. 6.3b shows how the corresponding functions $K_{nlnl}(q, q, E)$ look.

An overview of the shifts of the eigenvalues $f$ is given in Table 6.1 in which we study the coupling of the resonant term to the other terms and the effect of the chosen grid of $q$, which contains values in the range $0 < q \leq q_{max}$.

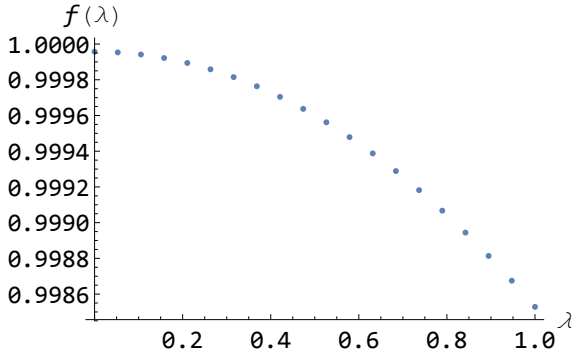


(a) Shift of $f$

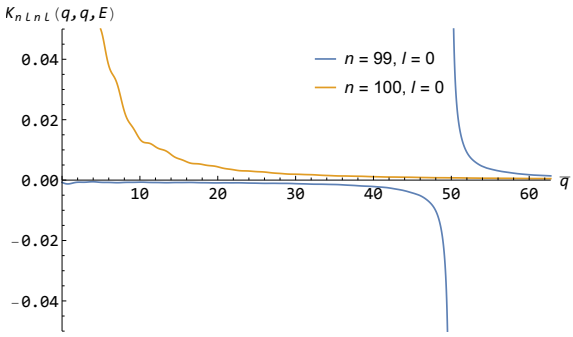


(b) Diagonal of $K_{nlnl}(q, q', E)$

Figure 6.3: The shift of the eigenvalue $f$ as the coupling parameter $\lambda$ increases (a) and the diagonal $K_{nlnl}(q, q, E)$ as a function of $q$ for the square well potential using the Weinberg series to calculate the form factors (b). Here $n_1 = 100$, $n_2 = 99$, $E = 0$ and $\bar{a}_{n_1 0} = -2.733$, which corresponds to $\bar{q}_0 = 312.6$.

Table 6.1: Shifts of the eigenvalues $f(\lambda)$ of the kernel $\tilde{F}$ at $E = 0$. When a pole is included in the calculation, the $q$-grid is chosen in such a way that it is symmetric around the pole. The Weinberg series is used expand $t_0(p, p', z)$. The grid for $q$ contains values in the range $0 < q \leq q_{max}$. The star $(*)$ indicates that these values are not relevant because the peak of the form factor $g_{1,0}(p, z)$ occurs at $p = 0$.

| $n_1$ | $n_2$ | $\bar{a}_{n_1 0}$ | $\bar{q}_{pole}$ | $(2n_2 - 1)\pi/3$ | $(2n_2 - 1)\pi$ | $\bar{q}_{max}$ | $f(0)$ | $f(1)$ | $\Delta f$ |
|---|---|---|---|---|---|---|---|---|---|
| 100 | 1 | $-2.733$ | 361 | $*$ | $*$ | 64 | 0.99995 | 0.37912 | $-0.62$ |
| 100 | 10 | $-2.733$ | 359 | 19.9 | 59.7 | 131 | 0.99995 | 0.99605 | $-3.9 \cdot 10^{-3}$ |
| 100 | 10 | $-2.733$ | 359 | 19.9 | 59.7 | 19 | 0.99989 | 0.99682 | $-3.1 \cdot 10^{-3}$ |
| 100 | 20 | $-2.733$ | 354 | 40.8 | 123 | 131 | 0.99995 | 0.99891 | $-1.0 \cdot 10^{-3}$ |
| 100 | 20 | $-2.733$ | 354 | 40.8 | 123 | 40 | 0.99994 | 0.99918 | $-7.6 \cdot 10^{-4}$ |
| 100 | 98 | $-2.733$ | 70.9 | 204 | 613 | 85 | 0.99996 | 0.99923 | $-7.3 \cdot 10^{-4}$ |
| 100 | 98 | $-2.733$ | 70.9 | 204 | 613 | 50 | 0.99996 | 0.99922 | $-7.4 \cdot 10^{-4}$ |
| 100 | 99 | $-2.733$ | 49.9 | 206 | 619 | 40 | 0.99996 | 0.99853 | $-1.4 \cdot 10^{-3}$ |
| 100 | 99 | $-2.733$ | 49.9 | 206 | 619 | 64 | 0.99996 | 0.99853 | $-1.4 \cdot 10^{-3}$ |
| 100 | 101 | $-2.733$ | – | 210 | 631 | 85 | 0.99995 | 1.00130 | $1.3 \cdot 10^{-3}$ |
| 100 | 102 | $-2.733$ | – | 213 | 638 | 85 | 0.99995 | 1.00061 | $6.6 \cdot 10^{-4}$ |

First of all, we want to note that the results of the shift $\Delta f$ in Table 6.1 behave similarly as the coupling strength $\Gamma$ shown in Fig. 6.1. This means that it is the small-momentum region which couples $n_1$ and $n_2$ most strongly. This can be easily understood by noting that $\tau_{n_1 0}(-\frac{3}{4m}q^2)$ is the largest for small values of $q$. Consequently, the coupling between $n_1 = 100$ and $n_2 = 1$ leads to the largest shift of $f$.

Secondly, the results for $n_2 = 98$ and $n_2 = 99$ in Table 6.1 clearly show that the poles hardly shift the eigenvalues of the kernel. This is caused by the symmetry of the poles. Therefore we can neglect the poles when calculating the Efimov trimers. Note that we have only considered the principal value integral and neglected the residue of the kernel at the

singular points.

Furthermore, the results of Table 6.1 also show the effect of the 'bump' which is just the big peak of the form factors $g_{n_20}$ broadened by the angular integration. If $\bar{q}_{max} > (2n_2 - 1)\pi$, then the bump is included in the calculation. However, if $\bar{q}_{max} < (2n_2 - 1)\pi/3$, the peak of the form factor $g_{n_20}$ is not included in the calculation. The results for $n_2 = 10$ and $n_2 = 20$ show that the peak of $g_{n_20}$ becomes less important as $n_2$ increases. For $n_2 = 10$ the contribution to the shift of the eigenvalue is $-8 \cdot 10^{-4}$, whereas for $n_2 = 20$ it is $-2.4 \cdot 10^{-4}$. This decrease of the effect of the bump is also caused by the fact that the bump shifts to larger values of $q$ as $n_2$ increases and the function $\tau_{n_10}(-\frac{3}{4m}q^2)$ decreases for increasing $q$.

Another interesting result shown in Table 6.1 is that $\Delta f$ has approximately the same absolute value, but opposite sign for $n_2 = 99$ and $n_2 = 101$ and also for $n_2 = 98$ and $n_2 = 102$. Therefore we expect that these pairs cancel each other's effect, so that their net contribution to $\Delta f$ is much smaller. We have tested this by considering the following coupled set of equations

$$\begin{pmatrix} \tilde{\phi}_1(\underline{q}, E) \\ \tilde{\phi}_2(\underline{q}, E) \\ \tilde{\phi}_3(\underline{q}, E) \end{pmatrix} = \begin{pmatrix} F_{11}(\underline{q}, \underline{q}^T) & \lambda F_{12}(\underline{q}, \underline{q}^T) & \lambda F_{13}(\underline{q}, \underline{q}^T) \\ \lambda F_{21}(\underline{q}, \underline{q}^T) & F_{22}(\underline{q}, \underline{q}^T) & \lambda F_{23}(\underline{q}, \underline{q}^T) \\ \lambda F_{31}(\underline{q}, \underline{q}^T) & \lambda F_{32}(\underline{q}, \underline{q}^T) & F_{33}(\underline{q}, \underline{q}^T) \end{pmatrix} \begin{pmatrix} \tilde{\phi}_1(\underline{q}, E) \\ \tilde{\phi}_2(\underline{q}, E) \\ \tilde{\phi}_3(\underline{q}, E) \end{pmatrix}. \tag{6.14}$$

where $n_1 = 100$, $n_2 = 99$ and $n_3 = 101$. Again we choose $\bar{a}_{n_10} = -2.733$ and $\bar{q}_{max} = 64$. The resulting shift of the eigenvalue is $\Delta f = -8 \cdot 10^{-5}$, which is indeed very small.

We have also performed some calculations which indicate how much these terms with $n$ close to $n_r$ contribute to the value of $\bar{a}_-$. The results are given in Table 6.2. It is clear that the effect of these terms on the value of $\bar{a}_-$ is small for this deep square well potential. What is more important, we see that the total effect of $n = 99$ and $n = 101$ is zero which agrees with our expectation based on Table 6.1.

Finally, we want to note that in Table 6.1 we have only studied the coupling between the resonant term and the other terms (labeled by $n_2$) of the separable expansion of $t_0$. The above analysis in which we considered Eq. (6.14) can be used to confirm that the coupling between terms $n_2$ and $n_3$ is not important. If we calculate the eigenvalues of

$$\begin{pmatrix} F_{11}(\underline{q}, \underline{q}^T) & \lambda F_{12}(\underline{q}, \underline{q}^T) & \lambda_{13} F_{13}(\underline{q}, \underline{q}^T) \\ \lambda F_{21}(\underline{q}, \underline{q}^T) & F_{22}(\underline{q}, \underline{q}^T) & \lambda F_{23}(\underline{q}, \underline{q}^T) \\ \lambda_{31} F_{31}(\underline{q}, \underline{q}^T) & \lambda F_{32}(\underline{q}, \underline{q}^T) & F_{33}(\underline{q}, \underline{q}^T) \end{pmatrix} \tag{6.15}$$

and set $\lambda = 1$, then we get the same eigenvalues $f$ for $\lambda_{13} = \lambda_{31} = 0$ and $\lambda_{13} = \lambda_{31} = 1$. Of course, we have not investigated all coupling terms, but it is clear that the coupling terms between the resonant term and the other terms are most important.

Table 6.2: Value of $\bar{a}_{-,0}$ corresponding to the 100th potential resonance of the square well potential as a function of the terms $n$ which are taken into account in the separable expansion of $t_0(p, p', z)$ (all other partial-wave components $t_{l\neq 0}$ are neglected). The $q$-grid contains 100 values and $\bar{q}_{max} = 33.2$. The $q$-grid does not contain any values near the poles which occur at larger values of $\bar{q}$. The purpose of this table is to show the effect of the terms labeled by $n = 98, 99, 101$ and 102 on the three-body parameter. The calculation of the exact three-body parameter also requires the inclusion of $n = 4, 5, 6, ...$ as we will see in Section 7.2.

| terms $n$ | $N_{terms}$ | $\bar{a}_{-,0}$ |
|---|---|---|
| $[100]$ | 1 | $-2.733$ |
| $[1-3, 100]$ | 4 | $-17.14$ |
| $[1-3, 99, 100]$ | 5 | $-17.18$ |
| $[1-3, 100, 101]$ | 5 | $-17.10$ |
| $[1-3, 99-101]$ | 6 | $-17.14$ |
| $[1-3, 98-101]$ | 8 | $-17.16$ |
| $[1-3, 99-102]$ | 8 | $-17.12$ |
| $[1-3, 98-102]$ | 8 | $-17.14$ |
| $[1-3, 97-102]$ | 10 | $-17.15$ |
| $[1-3, 98-103]$ | 10 | $-17.13$ |
| $[1-3, 97-103]$ | 10 | $-17.14$ |

## 6.3 Calculation of the three-body resonances

The theory presented in Section 3.1 deals with three-body bound states consisting of identical spinless bosons which only exist below the two-body ground state energy $E_{2b,0}$. It is important to realize that solutions to Eq. (3.3) only exist for three-particle bound states [75]. When the potential supports at least one dimer state, the Efimov trimers are not bound states, but resonant states which exist for complex energies, $E = E_R - \frac{1}{2}\Gamma i$ where $E_{2b,0} < E_R < 0$. We assume that these Efimov resonances have zero width, so that we can use Eq. (3.15) to search for solutions for real energies $E$. Recently, the lifetime of the Efimov trimers of $^{85}$Rb have been measured [41]. These measurements found that this lifetime $\tau$ is rougly 100 $\mu$s, so that the width is on the order of $\frac{\hbar}{\tau} = 2.5 \cdot 10^{-4}\ E_{vdW}$ which is indeed very small compared to the van der Waals energy $E_{vdW} = \frac{\hbar^2}{m r_{vdW}^2}$.

Since we search for solutions of Eq. (3.15) with real energies $E$, we only evaluate the principal value part of the integrals and neglect the residues which are associated with the poles of the two-body $T$-matrix. In fact, the singularities related to the bound states of the square well occur at large negative energies when the depth of the square well is chosen deep enough. For example, for the 40th, 50th and 60th potential resonance of the square well potential at $\bar{a}_0 = -10$, the first pole is located at $E = -\frac{q_2^2}{m}$ where $\bar{q}_2 = 26.78$, 30.13 and 33.15 respectively. We have analyzed the effect of these singularities on the solutions of Eq. (3.15) in Section 6.2 and we have shown that these singularities at large negative energies hardly shift the solutions of Eq. (3.15). Therefore we solve this equation for deep square well potentials by using an integration grid which is cut off before each pole and we use the same method as described in Section 6.1 to solve the three-body equation for real energies $E$.

The bumps in the kernel resulting from the big peaks of the form factors (see the analysis in Section 6.2) are also included in the calculation for all terms labeled by $n \lesssim n_r/2$. When $n \gtrsim n_r/2$ it is not possible to include the full bump of the function $K_{nlnl}(q, q', E)$ without including the poles of these functions. The effect of neglecting some parts of the bump for large values of $n$ is not so big. After all, the bump of the function $K_{nlnl}(q, q', E)$ becomes less important for the higher order terms (i.e., higher $n$) of the expansion. So it is a good approximation to neglect the bumps for these terms. Note that this approximation only holds for very deep potentials. For example, if we would consider the 5th potential resonance, it is not justified to neglect the bumps of the 3th and 4th term. However, the inclusion of these bumps requires inclusion of the poles which increases the difficulty of obtaining the three-body parameter $\bar{a}_{-,0}$ for this shallow potential. Therefore, we focus on deep square well potentials of which the highest $s$-wave dimer state occurs at large negative energies.

## 6.4 Elastic atom-dimer scattering calculations

The scattering process between a free particle and the lowest dimer state is described by Eq. (3.28). This scattering process is elastic, so that the $s$-wave atom-dimer scattering length $a_{ad}$ will be real. The set of equations given by Eq. (3.28) involves a singularity caused by the factor $\tau_{1,0}(E - \frac{3}{4m}q'^2)$. For the determination of the $s$-wave atom-dimer scattering length only the principal value part of the singular integral matters because the residue turns out

to be zero in the limit $q_{ad} \to 0$[3]. Note that this is only the case when the dimer occupies the ground state. We solve Eq. (3.28) for small values of $q_{ad}$, namely $\frac{q_{ad}}{\hbar} a_0 = 10^{-5}$, so that the kinetic energy at which the atom and dimer scatter is much smaller than the binding energy of the dimer. So we consider atom-dimer scattering at energy $E = E_{2b} + \frac{3}{4m} q_{ad}^2$ in which $\frac{3}{4m} q_{ad}^2 \ll |E_{2b}|$. After solving the set of equations given by Eq. (3.28) the $s$-wave atom-dimer scattering length can be calculated from the amplitudes $A_{nl}(q, q_{ad})$ by Eq. (3.30).

The procedure to solve Eq. (3.28) is similar as the one for the calculation of the three-body bound states. First, we define a grid for the momenta $q$ and $q'$, so that Eq. (3.28) turns into a big matrix equation. This momentum grid is chosen vary carefully because of the singularity in the factor $\tau_{1,0}(E - \frac{3}{4m} q'^2)$. Therefore we discretize the values of $q$ and $q'$ in two different ways. The vector $A_{1,0}(q, q_{ad})$ is calculated on a grid which contains hundreds of grid points near $q = q_{ad}$ (symmetrically chosen around the singularity) and a sparser grid at larger momenta. The momentum grid for the additional components $A_{n,l}(q, q_{ad})$ (in which $n, l \neq 1, 0$) does not need to contain the same amount of points as the momentum grid for the component $A_{1,0}(q, q_{ad})$. Therefore we choose a grid which is sparser at small momenta for the additional components compared to the grid for $A_{1,0}(q, q_{ad})$. The two grids can be written as column vectors and are here indicated by $\underline{q}$ and $\underline{q}_s$. So $\underline{q}$ is a column vector containing the momenta $q_1, q_2, q_3, ....$ Similary, $\underline{q}_s$ is the 'special' column vector containing much more grid points near the singularity.

Since we have now discretized the relevant momenta, we can write the set (Eq. (3.28)) of coupled integral equations in matrix form as

$$\begin{pmatrix} A_1(\underline{q}_s, q_{ad}) \\ A_2(\underline{q}, q_{ad}) \\ A_3(\underline{q}, q_{ad}) \\ \vdots \end{pmatrix} = 2 \begin{pmatrix} U_{1,1}(\underline{q}_s, q_{ad}) \\ U_{2,1}(\underline{q}, q_{ad}) \\ U_{3,1}(\underline{q}, q_{ad}) \\ \vdots \end{pmatrix} + \begin{pmatrix} K_{11}(\underline{q}_s, \underline{q}_s^T) & K_{12}(\underline{q}_s, \underline{q}^T) & K_{13}(\underline{q}_s, \underline{q}^T) & \cdots \\ K_{21}(\underline{q}, \underline{q}_s^T) & K_{22}(\underline{q}, \underline{q}^T) & K_{23}(\underline{q}, \underline{q}^T) & \cdots \\ K_{31}(\underline{q}, \underline{q}_s^T) & K_{32}(\underline{q}, \underline{q}^T) & K_{33}(\underline{q}, \underline{q}^T) & \cdots \\ \vdots & \vdots & \ddots & \end{pmatrix} \begin{pmatrix} A_1(\underline{q}_s, q_{ad}) \\ A_2(\underline{q}, q_{ad}) \\ A_3(\underline{q}, q_{ad}) \\ \vdots \end{pmatrix}. \tag{6.16}$$

In this equation, we have replaced the label '$nl$' by the numbers 1, 2, 3, ... These numbers refer to each single equation given by Eq. (3.28). In particular, the number 1 represents the quantum numbers $n = 1$ and $l = 0$. Furthermore, the superscript $T$ denotes the transpose of a matrix. The angular integration, which is hidden in $U_{i,1}$ and $K_{ij}$, is again executed by means of Riemann summation. The matrix equation given by Eq. (6.16) can also be summarized as

$$\underline{A} = 2\, \underline{U} + \underline{\underline{K}}\, \underline{A}. \tag{6.17}$$

The matrix $\underline{\underline{K}}$ is called the kernel. This equation can be solved for the vector $\underline{A}$ from which we obtain the subvector $A_1(\underline{q}_s, q_{ad})$. The atom-dimer scattering length can simply be obtained from Eq. (3.30).

[3]Note that we use the symbol $q_{ad}$ to indicate the momentum $q_0$ in Eq. (3.28). We changed the notation because $q_0$ is also used to define the depth of the square well potential.

One of the difficulties involves the calculation of $\tau_{1,0}(z)$ at energies $z$ very close to the two-body binding energy. Since we choose hundreds of closely spaced grid points near the singularity, we have to be careful to avoid numerical errors. We solve this problem by noting that the $T$-matrix is very separable at energies close to the two-body binding energy and can be approximated by Eq. (F.31) combined with Eq. (F.48). We have tested the energy regime in which this approximation is valid at scattering lengths in the range $1 \leq \bar{a}_0 \leq 100$. At energies $|\bar{E} - \bar{E}_{2b,0}| < 10^{-8}$ we can safely use this approximation. So for values of $q'$ satisfying $|\frac{3}{4}(\bar{q}_{ad}^2 - \bar{q}'^2)| < 10^{-8}$, we calculate the $\tau_{1,0}(E_{2b,0} + \frac{3}{4m}(q_{ad}^2 - q'^2))$ by using Eq. (F.48) and use the form factor $g_{1,0}(|\frac{1}{2}\mathbf{q}' + \mathbf{q}|, E_{2b,0})$.

The form factors of the square well potential can be found analytically for certain separable expansion methods such as the Weinberg series (Section 5.3). However, the form factors corresponding to the spectral representation of the $T$-matrix (Section 5.2) need to be calculated numerically. Fortunately, it is not needed to calculate the form factors numerically at energies $|\bar{E} - \bar{E}_{2b,0}| < 10^{-8}$ because in this energy range we can approximate the form factors $g_{1,0}(p, z)$ by $g_{1,0}(p, E_{2b,0})$ which are known analytically for the square well potential. The only thing which should be carefully considered is that the form factors should fulfill a certain normalization condition like Eq. (5.4). For example, if $I$ refers to the spectral representation of the $T$-matrix (Section 5.2) and $II$ refers to the Weinberg series (Section 5.3), we can write

$$g_{1,0}^{I}(p, E_{2b,0}) = X g_{1,0}^{II}(p, E_{2b,0}), \text{ where} \tag{6.18}$$

$$X = \left( \int_0^\infty \left( g_{1,0}^{II}(p, E_{2b,0}) \right)^2 dp \right)^{-\frac{1}{2}}. \tag{6.19}$$

Finally, we should note that the value $\bar{q}_{ad} = 10^{-5}\frac{1}{\bar{a}_0}$ is small enough to calculate the atom-dimer scattering length up to at least 4 significant figures. We have tested this by performing atom-dimer scattering calculations for different values of $\bar{q}_{ad}$, from which we conclude that the atom-dimer scattering calculations are converged to at least 4 significant figures (except very close to an atom-dimer resonance at which $a_{ad}$ diverges). The collision energy is not chosen to be much smaller than $\frac{3}{4} \cdot 10^{-10}\frac{\hbar^2}{m a_0^2}$ because numerical round-off errors would occur. We have also performed convergence tests for the momentum grids and the angular integration to make sure that we can trust our results for $a_{ad}$ up to 3 significant figures.

# 7. Results and discussion

Now we focus on the Efimov states corresponding to the potential resonances of the square well potential. Firstly, we investigate the effects of $d$-wave interactions by considering a shallow square well potential supporting only one $s$-wave dimer state. We also focus on the different methods described above to expand the two-body $T$-matrix. The atom-dimer scattering length is also calculated to study whether the first excited Efimov state unbinds. Secondly, we consider deep square well potentials and investigate the convergence of the three-body parameter. In all cases scattering lengths are calculated from the scattering length of the square well potential given by Eq. (4.2), in order to ensure the proper comparison between the methods, even when the approximated potentials have a slightly different scattering length. We indicate the number of separable terms which are used to approximate the partial-wave components $t_0(p, p', z)$ and $t_2(p, p', z)$ by $N_s$ and $N_d$ respectively.

## 7.1 Results for the shallow square well

Fig. 7.1 shows the energies of the lowest three Efimov states as a function of the inverse $s$-wave scattering length near the first potential resonance of the square well potential. The corresponding three-body parameters are given in Table 7.1. Fig. 7.1 shows that not only the first Efimov state does not converge to the two-body threshold, but also the second Efimov state does not cross the threshold although it gets very close to it. This can be seen from the inset in Fig. 7.1 in which the relative energy difference between the energies of the $s$-wave dimer state and the second Efimov state is shown as a function of the inverse scattering length. The non-crossing of the ground Efimov state with the atom-dimer threshold is also the case for shallow van der Waals potentials [52, 54, 55] and is consistent with a variational principle [45] which constrains the ground-state energy of three identical bosons, interacting via spherically symmetric pair potentials such as the square well potential, to always lie below the ground-state energy of two of such bosons, more precisely $E_{3b,0} \leq 3E_{2b,0}$. Ref. [45] states three conditions which are all sufficient to ensure that this inequality holds. Two of these conditions apply to the square well potential, so that the variational principle is also valid for this potential. The ground Efimov state of the square well potential satisfies this constraint as can be seen from Fig. H.1 which shows the relative energy difference between the binding energies of the first $s$-wave dimer state and the first two Efimov states as a function of the scattering length. For all interaction strengths considered, this relative energy difference is larger than 2/3 for the ground Efimov state, which is consistent with the constraint $E_{3b,0} \leq 3E_{2b,0}$.

The non-crossing of the first excited Efimov state has been seen before in a numerical study on the first three potential resonances of the Lennard-Jones potential [52] in which this

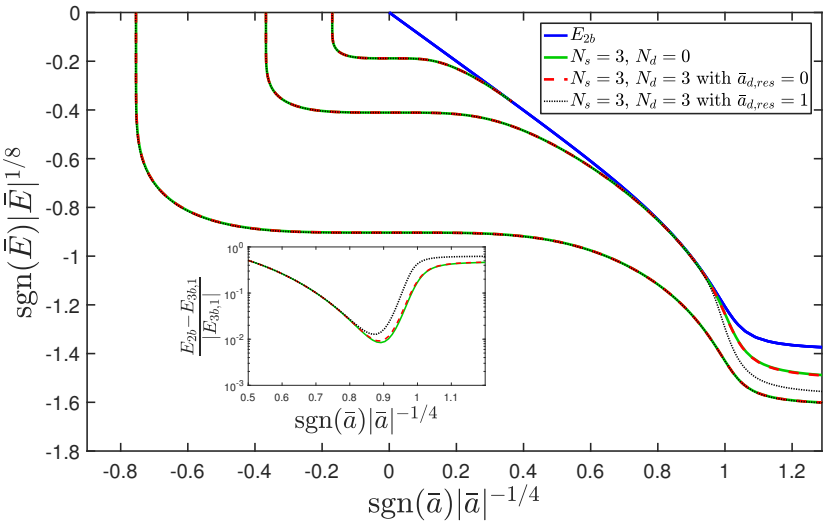


Figure 7.1: Energy of the lowest three Efimov states calculated near the first potential resonance of the square well potential by using method I for $N_s = 3$ and $N_d = 0$ and for $N_s = 3$ and $N_d = 3$. The black dotted curves indicate the calculation for which the $d$-wave resonance occurs at $\bar{a} = 1$ instead of $\bar{a} = 0$. The blue line is the binding energy corresponding to the $s$-wave dimer state. The inset shows the relative energy difference between the energies of the $s$-wave dimer state and the second Efimov state as a function of the inverse scattering length.

effect was attributed to strong $d$-wave interactions near $a = 1\ r_{vdW}$ [52, 53] although this hypothesis could not be confirmed because the $d$-wave interactions cannot be excluded in the adiabatic hyperspherical representation used by Ref. [52]. Our method allows us to include or exclude $d$-wave interactions. Fig. 7.1 also compares the calculation in which only $s$-wave effects are included with the one in which both $s$-wave and $d$-wave interactions are taken into account. The resulting curves clearly overlap from which we conclude that the effect of the $d$-wave interactions on the Efimov states is small in case of this shallow square well potential. This is not surprising since the $d$-wave dimer is bound at $\bar{a} = 0$. For single-channel interactions with a van der Waals tail, $-C_6 r^{-6}$, the $d$-wave dimer always becomes bound at a scattering $a = 4\pi/[\Gamma(1/4)]^2 \approx 0.956\ r_{vdW}$ as predicted by Gao [72]. This prediction has been confirmed by Wang *et al.* [53] using the Lennard-Jones potential as two-body interaction.

In order to investigate the effect of strong $d$-wave interactions which are present in case of van der Waals potentials at small positive scattering lengths we artificially increase the strength of the $d$-wave interactions by making the depth $V_0$ of the well larger for the $d$-wave component $t_2(p, p', z)$ in the three-body calculation. In this way the $d$-wave resonance is closer to the $s$-wave resonance. Fig. 7.1 also compares the energies of the Efimov states for calculations involving the weak (unmodified) $d$-wave interactions and the strong (modified) $d$-wave interactions in which the $d$-wave resonance occurs at $\bar{a} = 1.00$. The increase of the strength of the $d$-wave interactions has almost no effect on the ground Efimov state because this state is too far away from the $d$-wave dimer state. However, the first excited Efimov state is really affected at small positive scattering lengths by this increased $d$-wave interaction strength. The energy of this trimer state is decreased. So strong $d$-wave effects can be the cause of the non-crossing of the second Efimov state with the two-body threshold for the potential resonances of the Lennard-Jones potential as seen in Ref. [52].

The way which has so far been used most to calculate the energies of the Efimov states by means of the Faddeev equations is to approximate the $s$-wave two-body $T$-matrix by one separable term and to solve the resulting integral equation. This method is believed to work well when the non-separable function $t_0(p, p', z)$ is separable in the regime in which the Efimov states are located. This function $t_0(p, p', z)$ is more separable for energies $z$ closer to a two-body $s$-wave bound state. In Fig. 7.2 we compare the Efimov spectrum corresponding to the full $s$-wave $T$-matrix with the one corresponding to the single-term approximation of $t_0(p, p', z)$. This figure shows that the second Efimov trimer is strongly affected by the non-separable terms of the two-body $T$-matrix. In both cases the second Efimov state does not cross the atom-dimer threshold as can be seen from the inset, but it stays much closer to the two-body threshold at small positive scattering lengths when the off-shell two-particle $T$-matrix is approximated by a function which is fully separable in the incoming and outgoing momenta. The reason why the use of the separable approximation fails at large negative energies close to the dimer threshold is not obvious as the off-shell two-body $T$-matrix is highly separable in this regime. The cause of this failure is related to the Green's function $G_0$ which is present in the Faddeev equations, Eq. (3.3). The factor $\frac{q'^2}{E-\frac{1}{m}(q^2+\mathbf{q}\cdot\mathbf{q}'+q'^2)}$ in Eq. (F.21) clearly suppresses the small-momenta part, i.e., $q' \ll 1$, in which $\tau_{n_r,0}\left(E-\frac{3}{4m}q'^2\right)$ is the biggest[4]. When the three-body energy $E$ is not close to zero, this suppression is much more effective. As a result, the dominance of the resonant term is reduced and the separable approximation for $t_0(p, p', z)$ is not sufficient to calculate the first excited Efimov state accurately at energies rougly below $-\frac{\hbar^2}{2\mu R^2}$.

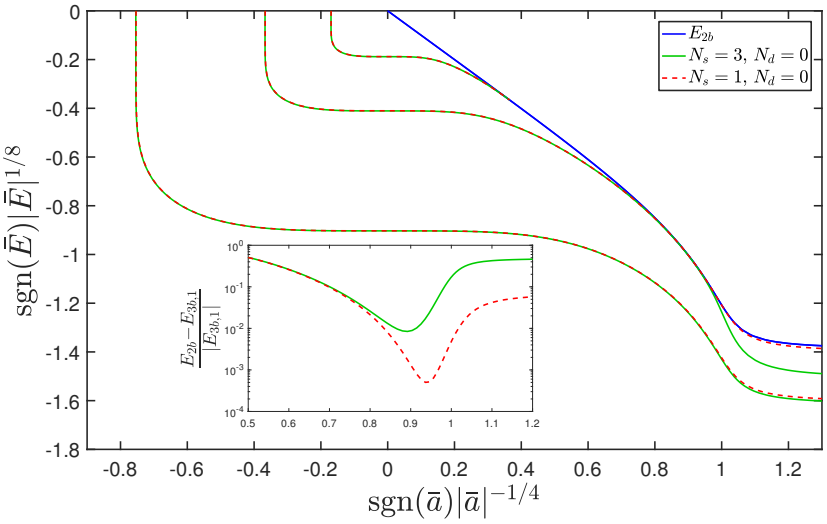


Figure 7.2: Energy of the lowest three Efimov states calculated near the first potential resonance of the square well potential by using method I for $N_s = 3$ and $N_s = 1$. In both cases $N_d$ is set to zero. The blue line is the binding energy corresponding to the $s$-wave dimer state. The inset shows the relative energy difference between the energies of the $s$-wave dimer state and the second Efimov state as a function of the inverse scattering length.

Based on this reasoning, one would expect that the separable approximation would also fail in the calculation of the ground Efimov state at large negative energies. However, the

[4]The parameter $n_r$ labels the resonant term as discussed in Chapter 6.

energy of the ground Efimov state at small positive scattering lengths is quite similar for both calculations shown in Fig. 7.2. We attribute this effect to the variational principle [45] stating that $E_{3b,0} \leq 3E_{2b,0}$, so that the energy of the ground Efimov state, which is close to this limiting value, cannot increase much at small positive scattering lengths for a decreasing number of terms of the separable expansion. Even though this variational principle is proven for energy-independent potentials [45, 81], its proof is based on the two-body ground state wave function of two identical spinless bosons interacting via a spherically symmetric potential which is the same for the square well potential and its separable approximation obtained by method I or II. Fig. H.2 confirms that the variational principle is also satisfied for this separable interaction potential.

Table 7.1 summarizes the three-body parameters near the first pole of the $s$-wave scattering length calculated from methods I, II and III. The wave number $\kappa_n^*$ corresponds to the energy $E_n^* = -\frac{(\hbar\kappa_n^*)^2}{2\mu}$ of the $n$th trimer state at diverging scattering length. The three-body parameters calculated from method I converge the fastest as more expansion terms are included. The results of method II converge less fast because the form factors do not depend on the scattering length for fixed range $R$. Furthermore, method I provides the best one-term approximation, followed by method III and II respectively. This result is not expected to hold in general, but only for the first potential resonance. The EST approximation is expected to be the best one-term approximation for deeper potentials because it reproduces the correct zero-energy two-body scattering state. Table 7.1 also shows that the relative difference between the calculations with and without $d$-wave effects is smaller than $10^{-3}$, so that $d$-wave effects should also be considered depending on the required accuracy. Again we expect that this result only holds for the first potential resonance. The $d$-wave effects will be larger for deeper potentials which also support $d$-wave dimer states.

The non-crossing of the second Efimov state is also reflected in the $s$-wave atom-dimer scattering length shown in Fig. 7.3. This figure shows only one atom-dimer resonance which occurs at $\bar{a}_{*,2} = 54.5$ and corresponds to the crossing of the bound state energy of the second excited Efimov state with the two-body binding energy. Another interesting feature occurs at small positive scattering lengths. The value of $a_{ad}$ calculated by using the full partial-wave component $t_0(p, p', z)$ shows a maximum at $\bar{a} = 2.00$, but it does not diverge. This indicates that the first excited Efimov state approaches the atom-dimer threshold closely for decreasing $a$, but it does not become unbound. As $a$ decreases further, the binding energy of this trimer state, $E_b = E_{2b} - E_{3b}$, increases.

Table 7.2 summarizes our computed values of the three-body parameter $a_*$. Here $a_{*,1}$ is defined as the value of $a$ at which $a_{ad}$ is maximum, wherease $a_{*,2}$ is defined as the value of $a$ at which the $a_{ad}$ diverges. The separable approximation of method I approximates $t_0(p, p', z)$ better than the separable approximation of method II, especially at large negative energies. This is reflected by the computed values of $a_{*,2}$ as shown in Table 7.2. However, Fig. 7.3 shows that the second Efimov state approaches the two-body threshold closer when using the separable approximation of method I compared to method II. This confirms that the accurateness of the separable approximation of the two-body $T$-matrix is not the reason why the separable calculations fail at small positive scattering lengths. The failure is rooted in the three-body equations themselves as we have discussed above.

The geometric scaling factors $\frac{a_{-,1}}{a_{-,0}} = 17.8$ and $\frac{a_{*,2}}{a_{*,1}} = 27.3$ deviate from the universal value $e^{\pi/s_0} \approx 22.69$ [15], which is just a finite-range effect. It depends on the particular shape

Table 7.1: Values of the three-body parameters $\bar{a}_{-,n}$ and $\bar{\kappa}^*_n$ corresponding to the first potential resonance of the square well potential using different methods and different number of terms to expand $t_0(p,p',z)$ and $t_2(p,p',z)$. In all cases the scattering length is calculated from Eq. (4.2). Method I$^*$ refers to method I in which the $d$-wave resonance is artificially shifted from $\bar{a}=0$ to $\bar{a}=1.000$.

| method | $N_s$ | $N_d$ | $\bar{a}_{-,0}$ | $\bar{a}_{-,1}$ | $\bar{\kappa}^*_0$ | $\bar{\kappa}^*_1$ |
|---|---|---|---|---|---|---|
| I | 1 | 0 | -3.102 | -55.23 | 0.6647 | $2.831\cdot10^{-2}$ |
| I | 2 | 0 | -3.092 | -54.96 | 0.6654 | $2.845\cdot10^{-2}$ |
| I | 3 | 0 | -3.091 | -54.94 | 0.6655 | $2.846\cdot10^{-2}$ |
| I | 4 | 0 | -3.091 | -54.93 | 0.6655 | $2.846\cdot10^{-2}$ |
| I | 5 | 0 | -3.090 | -54.93 | 0.6655 | $2.846\cdot10^{-2}$ |
| I | 3 | 1 | -3.088 | -54.91 | 0.6661 | $2.848\cdot10^{-2}$ |
| I | 3 | 2 | -3.088 | -54.91 | 0.6662 | $2.848\cdot10^{-2}$ |
| I | 3 | 3 | -3.088 | -54.91 | 0.6662 | $2.848\cdot10^{-2}$ |
| I$^*$ | 3 | 3 | -3.072 | -54.78 | 0.6689 | $2.854\cdot10^{-2}$ |
| II | 1 | 0 | -3.163 | -55.79 | 0.6536 | $2.804\cdot10^{-2}$ |
| II | 2 | 0 | -3.104 | -55.09 | 0.6631 | $2.838\cdot10^{-2}$ |
| II | 3 | 0 | -3.095 | -54.98 | 0.6647 | $2.844\cdot10^{-2}$ |
| II | 4 | 0 | -3.092 | -54.95 | 0.6652 | $2.845\cdot10^{-2}$ |
| II | 5 | 0 | -3.091 | -54.94 | 0.6653 | $2.846\cdot10^{-2}$ |
| II | 10 | 0 | -3.090 | -54.93 | 0.6655 | $2.847\cdot10^{-2}$ |
| III | 1 | 0 | -3.106 | -55.51 | 0.6610 | $2.815\cdot10^{-2}$ |

of the interaction potential. For example, the deviation of these ratios from the universal value is bigger for the potential resonances Lennard-Jones potential for which these ratios are $\frac{a_{-,1}}{a_{-,0}}\approx 16.7$ and $\frac{a_{*,2}}{a_{*,1}}\approx 47.8$ [52].

We also compare our results for the shallow square well potential with those which we had obtained before in Ref. [61]. In this reference we have shown that it is possible to calculate the Efimov spectrum by substituting the non-separable partial-wave component $t_0(p,p',z)$ into the Skorniakov-Ter-Martirosian equation for three-body bound states which is just the three-body equation for separable potentials. This equation is given by

$$F(q,E)=2\int d\mathbf{q}'\frac{t_0\left(|\mathbf{q}+\frac{1}{2}\mathbf{q}'|,|\frac{1}{2}\mathbf{q}+\mathbf{q}'|,E-\frac{3}{4m}q'^2\right)}{E-\frac{1}{m}\left(q^2+\mathbf{q}\cdot\mathbf{q}'+q'^2\right)}F(q',E) \tag{7.1}$$

where $F(q,E)$ is related to the three-body bound state wave function. The angular integration can be performed analytically if we use the following approximations to remove the angular dependence in $t_0$:

$$\begin{aligned}|\mathbf{q}+\frac{1}{2}\mathbf{q}'|&\approx\sqrt{q^2+\frac{1}{4}q'^2},\\ |\frac{1}{2}\mathbf{q}+\mathbf{q}'|&\approx\sqrt{q'^2+\frac{1}{4}q^2}.\end{aligned} \tag{7.2}$$

This approximation has been used before by Debets [62] and Kroeze [63]. The approximation considered in Ref. [61] was slightly different. The comparison between the modified STM-equation and the correct three-body equations is given by Fig. 7.4 which shows the energies

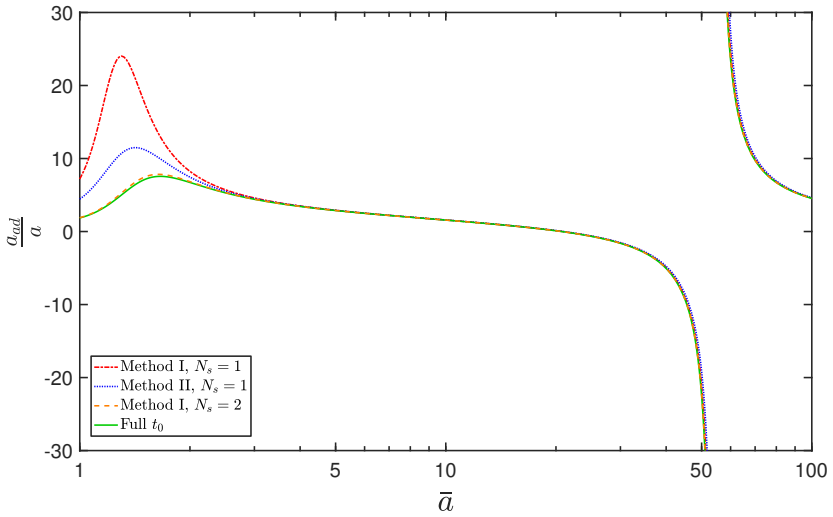


Figure 7.3: The $s$-wave atom-dimer scattering length as a function of the $s$-wave two-body scattering length $a$ for different approximations of $t_0(p, p', z)$. Only $s$-wave interactions are considered. The greene curve corresponds to calculations using method I with $N_s = 9$ and method II with $N_s = 10$.

Table 7.2: Values of the three-body parameters $\bar{a}_{*,n}$ corresponding to the first potential resonance of the square well potential using different methods and different number of terms to expand $t_0(p, p', z)$. In all cases $N_d$ is set to zero and only the $s$-wave part of the off-shell two-body $T$-matrix is considered. The scattering length is calculated from Eq. (4.2).

| method | $N_s$ | $\bar{a}_{*,1}$ | $\bar{a}_{*,2}$ |
|---|---|---|---|
| I | 1 | 1.33 | 54.8 |
| II | 1 | 1.53 | 55.3 |
| I | 2 | 1.93 | 54.6 |
| II | 2 | 1.94 | 54.7 |
| I | 10 | 2.00 | 54.5 |
| II | 10 | 2.00 | 54.5 |

of the lowest two Efimov states. The green curve is the result which has also been shown in Fig. 7.1. The black curve shows that Eq. (7.2) works quite well except at small positive scattering lengths for which we have seen above that the separable three-body equation is not valid. The three-body parameters corresponding to the black curve are $\bar{a}_{-,0} = -3.05$ and $\bar{a}_{-,1} = -53.8$ which deviate only 1-2% from the actual values given in Table 7.1. On the other hand, the use of Eq. (7.1) combined with the angular approximation of Eq. (7.2) is much less accurate as can be seen from Fig. 7.1. The three-body parameters corresponding to the red curve are $\bar{a}_{-,0} = -3.42$ and $\bar{a}_{-,1} = -65.1$ which deviate 10-20% from the actual values. The Efimov states are shifted so much that the second Efimov state crosses the threshold. This explains why Ref. [61] saw that the second trimer state unbinds into a dimer and free particle. So performing the angular integrals correctly is essential for an accurate calculation of the Efimov states.

So far we have shown the Efimov spectra which have been calculated by using method

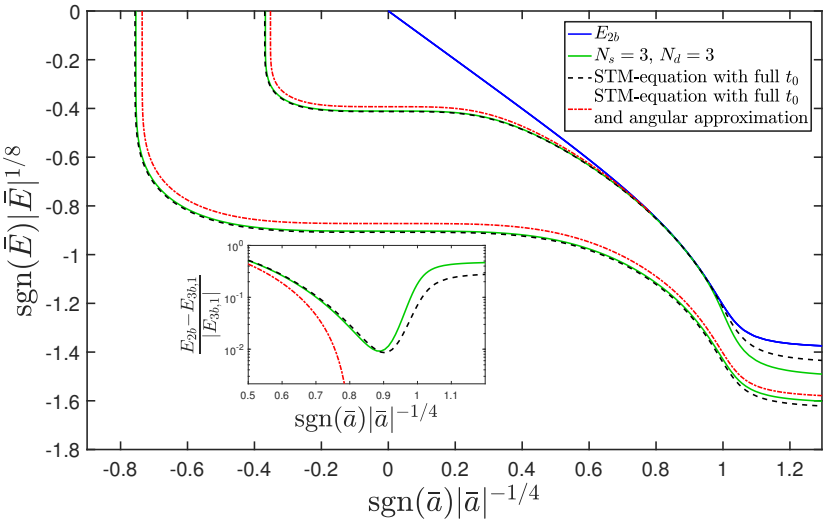


Figure 7.4: Energy of the lowest two Efimov states calculated near the first potential resonance of the square well potential by using method I for $N_s = 3$ and $N_d = 3$ and by using the approach considered by Ref. [61]. In this approach, the non-separable component $t_0(p, p', z)$ is substituted into the three-body equation for separable interactions (the homogeneous Skorniakov-Ter-Martirosian equation, Eq. (7.1)). The dash-dotted red line corresponds to a similar calculation in which the angular approximation of Ref. [62] (Eq. (7.2)) is used. The blue line is the binding energy corresponding to the $s$-wave dimer state. The inset shows the relative energy difference between the energies of the $s$-wave dimer state and the second Efimov state as a function of the inverse scattering length.

I to expand the two-body $T$-matrix in separable terms. We have repeated the three-body calculations involving only $s$-wave interactions by using the Weinberg series (method II) for the expansion of $t_0(p,p',z)$. These calculations have resulted in the same Efimov spectra as long as enough terms are taken into account in the separable expansion. Those calculations also show that the second Efimov state of the shallow square well potential stays below the atom-dimer threshold when we use the single-term approximation of the Weinberg series to approximate $t_0(p,p',z)$. This can be seen from Figs. H.3 and H.4. In order to illustrate the actual shape of the Efimov spectrum for separable interactions, we have chosen to change the $x$-axis of the Efimov spectrum shown in Figs. H.3 and H.4 with respect to the other figures presented here. The scattering length is not the scattering length of the square well potential, but it corresponds to the separable interaction. It is calculated from Eqs. (5.20) and (5.21). The separable interaction potential can only support one dimer state, so that the scattering length does not go to zero when $\bar{q}_0$ is increased. From Eqs. (5.20) and (5.21) it is clear that the scattering length cannot be smaller than $\frac{8}{\pi^2} = 0.811$ when we take only the first term in the considered separable expansion of $t_l(p,p',z)$ into account. Even though Fig. H.3 does not clearly show whether the first two Efimov states cross the atom-dimer threshold, Fig. H.4 does show the absence of an atom-dimer resonance corresponding to these trimer states. The variational principle, $E_{3b,0} \leq 3E_{2b,0}$ [45], is fulfilled for the considered depths of the square well. At $\bar{a} = 0.822$ the relative energy difference is $\frac{E_{2b,0}-E_{3b,0}}{|E_{3b,0}|} = 0.667$.

The EST method (method III) can also be used to approximate the partial-wave component $t_0(p,p',z)$ by a separable expression. Figs. H.5–7 show the Efimov spectra corresponding to the lowest three potential resonances of the separable potential obtained by the EST approach. In all those cases the ground Efimov state does not cross the atom-dimer threshold, whereas the first excited trimer state only stays slightly below the threshold for the first potential resonance. Based on the analysis of Section 5.4 we do not expect that the EST approach works well at energies which are not close to zero, so that the calculation of the trimer states near small positive $\bar{a}$ are not expected to correspond to a square well potential. This is reflected by the deviation of the two-body binding energies corresponding to square well potential and the EST approximation near $\bar{a} = 1$ as can be seen from Figs. H.5–7. However, this deviation occurs at smaller positive scattering lengths than for the soft-core van der Waals potential whose $s$-wave binding energy is compared to the one of the separable EST approximation in Figure 2 of Ref. [54]. The three-body parameters for the EST-method are summarized in Table 7.3. The validity of the one-term EST approximation for the $N$th potential resonance with $N \geq 2$ is questionable as we have seen in Section 5.4. In Section 7.2 we will test the validity of this approximation for deep square well potentials.

## 7.2 Results for the deep square well

Naidon *et al.* [59] have shown that the three-body parameter expressed in units of the effective range is universal for certain subclasses of interactions. They expect that the square well potential does not reveal any universality of the three-body parameter because the zero-energy two-body $s$-wave radial wave function does not show the suppression of the two-body probability inside the well. The analysis of Ref. [59] is based on separable approximations of the off-shell two-body $T$-matrix using the EST method. Although we have seen in Section 5.4 that the energy-dependence of the two-body $T$-matrix of square well potentials supporting

more than one bound state is not correctly approximated by the single-term EST approximation, we have tested the hypothesis of Ref. [59] by considering square well potentials of different depths. We have checked whether the three-body parameter converges when using the separable EST approximation. We have also gone beyond the separable approximation to test the validity of this approximation.

The results of these calculations involving separable $T$-matrices based on the EST-method are shown in Table 7.3. This table shows that the three-body parameter of the square well converges as a function of the number of two-body $s$-wave bound states when using the one-term EST approximation for $t_0(p, p', z)$. The convergence is slower for the square well potential than for the hard-core van der Waals potential considered in Ref. [55]. This is caused by the dominant peak in the form factors of the square well potential (see Fig. 5.6). For small $N$ this peak occurs at smaller momenta, so that its effect is big. The influence of the peak disappears when the depth of the well gets larger. So when the well is deep enough, the exact depth becomes irrelevant for the Efimov resonances which occur at small negative energies. The range $R$ is the only relevant length scale left, so that $\bar{a}_{-,0}$ converges as a function of the number of bound $s$-wave dimer states.

Although the three-body parameters for $N = 1$ can be calculated well by using the one-term EST approximation, this separable approximation does not reproduce the element $t_0(p, p', z)$ very well for deeper potentials at negative energies $z$ for which $|\bar{p}_z| \gtrsim 0.5$. Therefore it is hard to judge whether the obtained three-body parameters of the separable potential are similar to the those of deep square well potentials. Another important characteristic of the three-body parameters shown in Table 7.3 is the big difference between the three-body parameters for $N = 1$ and $N = 2$. Such a big jump is not the case for the hard-core van der Waals potential considered in Ref. [55]. This big jump of the three-body parameters is caused by the big difference in the form factors $g_1(p)$ and $g_2(p)$ at small momenta $p$ as shown in Fig. 5.6. The first zero of $g_1(p)$ occurs at $\bar{p} = 4.66$ for $\bar{a} = -3.106$, whereas the first zero of $g_2(p)$ occurs at $\bar{p} = 1.52$ for $\bar{a} = -12.58$. The other form factors $g_n(p)$ with $n > 1$ also have zeros which occur near $\bar{p} = 1.52$ at $\bar{a} = \bar{a}_{-,0}$. This value of $\bar{p}$ at which the first zero occurs is a factor 3.07 smaller for $n > 1$ than for $n = 1$. Thus the big difference in the three-body parameter between $N = 1$ and $N > 1$ simply reflects the difference of the form factors at small momenta. Li *et al.* [55] have used the one-term EST approximation to the hard-core van der Waals potential and did not observe a big difference in the three-body parameter between $N = 1$ and $N > 1$. However, the form factors $g_1(p)$ and $g_2(p)$ of this potential are quite similar at small momenta and so are the calculated three-body parameters for the first and second potential resonance.

The separable approximation of the $T$-matrix of square well potentials supporting more than one bound state is not valid at all energies which are relevant for calculating the three-body parameter as shown by Fig. 5.9. Therefore we now consider the 40th, 50th and 60th potential resonance of the square well potential and include many terms in the separable Weinberg series (method II). We only consider $s$-wave interactions, so $l = 0$. The terms are therefore completely specified by the label $n$ which we have defined for each separable expansion method discussed before.

Fig. 7.5 shows the value of $\bar{a}_{-,0}$ as a function of the terms $n$ which are taken into account in the separable expansion of $t_0(p, p', z)$. Some of these values are also given in Table 7.4. These results show that a lot of terms are necessary in order to determine the exact three-body

Table 7.3: Values for the three-body parameters $\bar{a}_{-,n}$ and $\bar{\kappa}_n^*$ corresponding to the $N$th potential resonance of the square well potential using the one-term EST approximation for $t_0(p, p', z)$.

| $N$ | $\bar{a}_{-,0}$ | $\bar{a}_{-,1}$ | $\bar{\kappa}_0^*$ | $\bar{\kappa}_1^*$ |
|---|---|---|---|---|
| 1 | -3.106 | -55.51 | 0.6610 | $2.815 \cdot 10^{-2}$ |
| 2 | -12.58 | -260.8 | 0.1332 | $5.835 \cdot 10^{-3}$ |
| 3 | -13.80 | -290.3 | 0.1193 | $5.235 \cdot 10^{-3}$ |
| 4 | -13.12 | -274.5 | 0.1262 | $5.539 \cdot 10^{-3}$ |
| 5 | -13.38 | -280.7 | 0.1233 | $5.415 \cdot 10^{-3}$ |
| 6 | -13.54 | -284.2 | 0.1219 | $5.348 \cdot 10^{-3}$ |
| 7 | -12.86 | -269.0 | 0.1288 | $5.654 \cdot 10^{-3}$ |
| 8 | -13.03 | -272.8 | 0.1270 | $5.573 \cdot 10^{-3}$ |
| 9 | -13.08 | -273.9 | 0.1265 | $5.551 \cdot 10^{-3}$ |
| 10 | -13.13 | -275.0 | 0.1259 | $5.528 \cdot 10^{-3}$ |
| ⋮ | ⋮ | ⋮ | ⋮ | ⋮ |
| 49 | -13.23 | -277.3 | 0.1249 | $5.482 \cdot 10^{-3}$ |
| 50 | -13.23 | -277.3 | 0.1249 | $5.482 \cdot 10^{-3}$ |
| ⋮ | ⋮ | ⋮ | ⋮ | ⋮ |
| $\infty$ | -13.24 | -277.4 | 0.1249 | $5.481 \cdot 10^{-3}$ |

The three-body parameter $\bar{\kappa}_0^*$ of an infinitely deep square well potential has also been calculated by Horinouchi and Ueda [82] by performing a functional renormalization-group analysis using the one-term EST approximation for the potential. They found $\kappa_0^* r_{eff} = 0.49(5)$ where $r_{eff} = R$. This result is not consistent with the value which we have obtained. It is hard to judge what is causing this difference because the methods are completely different.

parameter $\bar{a}_{-,0}$ of deep square well potentials and that the lowest-order terms ($n = 1, 2, ...$) of the expansion shift the value of $\bar{a}_{-,0}$ most which is consistent with the analysis shown in Section 6.2. This is caused by the fact that the form factors for small $n$ are the biggest at small momenta, whereas the differences in $\tau_{n,0}(z)$ at small $z$ are much smaller for $n < n_r$. Our calculations show that the three-body parameter of the 40th, 50th and 60th potential resonance is $\bar{a}_{-,0} \simeq -20$ with an estimated relative uncertainty of 5%. A higher accuracy is not possible because the poles prevent us from taking all big peaks of the form factors into account. Furthermore, the calculations become more sensitive to the chosen momentum grid as we make the set of coupled equations larger and more grid points must be chosen. The assumption of neglecting the widths of the Efimov states induces an extra uncertainty which we believe to be negligible.

Another interesting feature of the curves shown in Fig. 7.5 is that $\bar{a}_{-,0}$ is minimum when the lowest $n_r$ terms are taken into account and then increases when also terms labeled by $n > n_r$ are added to the expansion of $t_0(p, p', z)$. This effect is simply caused by the difference in sign of the functions $\tau_{n,0}(z)$ at $z = 0$ for $n < n_r$ compared to $n > n_r$.

The Weinberg series requires a lot of terms to get a converged result for the three-body parameter $\bar{a}_{-,0}$ of the deep square well potential. We expect that this result is more general and also holds for other potentials supporting many $s$-wave two-body bound states. For

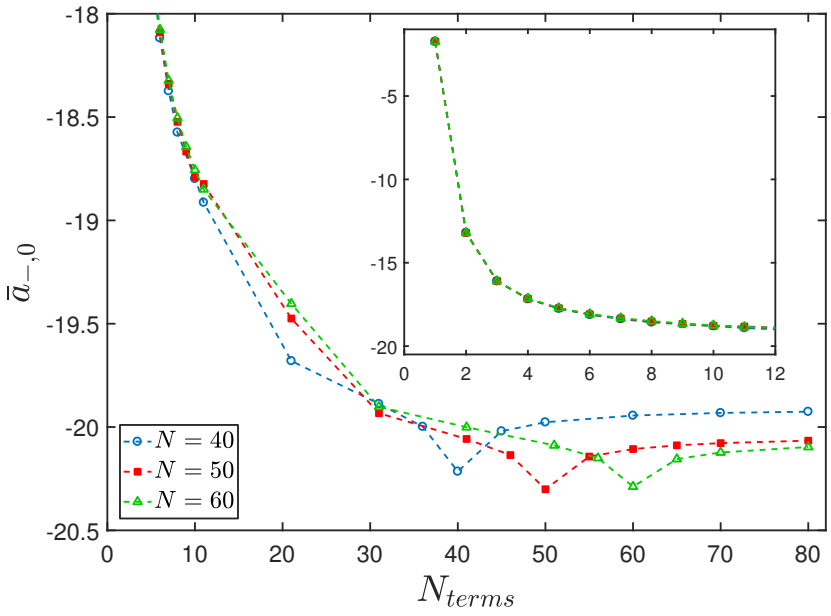


Figure 7.5: Value of $\bar{a}_{-,0}$ corresponding to the 40th, 50th and 60th potential resonance of the square well potential as a function of the number of terms, $N_{terms}$, which are taken into account in the Weinberg series of $t_0(p, p', z)$. $N_{terms} = 1$ corresponds to the term $[n_r]$ (where $n_r = N$), $N_{terms} = 2$ corresponds to the terms $[1, n_r]$, $N_{terms} = 3$ corresponds to the terms $[1, 2, n_r]$, etc.

attractive potentials with a repulsive barrier even more terms can contribute to the value of $\bar{a}_{-,0}$ because negative eigenvalues $\eta_{nl}(z)$ will also exist for those potentials. The contribution of these terms corresponding to negative eigenvalues $\eta_{nl}(z)$ will be larger when the barrier is bigger and wider because in those cases more negative eigenvalues exist which satisfy $|\eta_{nl}(z)| \gg 1$, so that the corresponding $\tau_{nl}(z)$ is approximately $-\frac{1}{4\pi}$ which follows from Eq. (5.13).

Finally, we consider the deep square well calculations performed by Debets [62] and Kroeze [63]. They solved the homogeneous STM-equation (Eq. (7.1)) in which the separable $s$-wave two-body $T$-matrix is replaced by the non-separable one of an infinitely deep square well potential. The angular dependence of this $T$-matrix was neglected by using the approximation given by Eq. (7.2). The resulting three-body parameter is $\bar{a}_{-,0} = -14.6$ [62, 63]. This value is quite close to the result of the one-term EST-approximation which is $\bar{a}_{-,0} = -13.23$. However, it still deviates a lot from the value obtained by using the Weinberg series. This suggests that it is really necessary to use the coupled set of three-body equations when considering deep square well potentials.

Similar as we have seen for the shallow square well potential, the three-body parameter of the infinitely deep square well potential also shifts due to the angular approximation of Eq. (7.2). We have calculated the three-body parameter of the 100th potential resonance of the square well potential using Eq. (7.1) with and without the angular approximation which resulted in $\bar{a}_{-,0} = -14.6$ and $\bar{a}_{-,0} = -14.1$ respectively. The relative difference is 3% which is smaller as for the shallow square well potential. So the angular approximation works slightly better for deep square well potentials.

Table 7.4: Value of $\bar{a}_{-,0}$ corresponding to the 40th, 50th and 60th potential resonance of the square well potential as a function of the terms which are taken into account in the separable expansion of $t_0(p, p', z)$ using the Weinberg series. The resonant term is indicated by $n_r$ and equals $N$ which labels the potential resonance. The singularities which occur at large negative energies $z$ are not included in the calculation. The relative uncertainty of the calculations involving 80 terms in the expansion is estimated to be 5%.

| terms | $\bar{a}_{-,0}$ $(N = 40)$ | $\bar{a}_{-,0}$ $(N = 50)$ | $\bar{a}_{-,0}$ $(N = 60)$ |
|---|---|---|---|
| $[n_r]$ | -1.73 | -1.73 | -1.73 |
| $[1, n_r]$ | -13.2 | -13.2 | -13.2 |
| $[1, 2, n_r]$ | -16.1 | -16.1 | -16.1 |
| $[1-3, n_r]$ | -17.2 | -17.2 | -17.1 |
| $[1-4, n_r]$ | -17.8 | -17.7 | -17.7 |
| $[1-5, n_r]$ | -18.1 | -18.1 | -18.1 |
| $[1-10, n_r]$ | -18.9 | -18.8 | -18.8 |
| $[1-80]$ | -19.9 | -20.1 | -20.1 |

# 8. Conclusions and outlook

This Chapter summarizes the main conclusions of our work, followed by an outlook to possible future research.

## 8.1 Conclusions

We have studied the Efimov effect for three-body systems involving identical bosons interacting via a pairwise square well potential. The three-body properties have been calculated by solving the Faddeev equations in the momentum-space representation. They are completely determined by the two-body interactions which enter the Faddeev equations via the off-shell two-body $T$-matrix. For a local interaction potential with a nonzero range, this $T$-matrix is non-separable in the incoming and outgoing relative momenta. Since the Faddeev equations are most easily solved when the two-body $T$-matrix is expanded in separable terms, we have analyzed the following expansion methods:

- Method I: the spectral representation of $t_l(p, p', z)$;
- Method II: the Weinberg series;
- Method III: the EST method.

Method I has not been studied before because this method is only useful when the off-shell two-body $T$-matrix is explicitly known, which is only the case for simple potentials such as the square well potential. We have found that this expansion method is quite similar to method II, but method I has slightly better convergence properties especially at large negative energies below the depth of the well. However, since the computation time to solve the three-body equations using method I is larger than for method II, we recommend to use method II. Method I and II are both suited to study Efimov physics near the atom-dimer theshold because the approximated potentials have exactly the same two-body binding energy as the actual potential. The EST method is different from method I and II, because it allows one to construct a separable potential which gives rise to the same zero-energy $s$-wave scattering state as the original potential. Consequently, this separable approximation is expected to be useful for determining the low-energy Efimov properties such as the three-body parameter $a_-$.

We have analyzed the difference between the square well potential and some van der Waals potentials on the two-body level. For all considered expansion methods, the form factors of the square well, labeled by $n = 2, 3, ...$, are characterized by a big peak occuring

near $\bar{p} \simeq \frac{(2n-1)\pi}{2}$. This momentum is just the depth $\bar{q}_0$ at which the $n$th potential resonance occurs. This big peak reflects the large probability density for two zero-energy scattering particles to have a relative momentum $\bar{p} \approx \bar{q}_0$ at short distances ($r < R$). For van der Waals potentials, the probability density for finding two particles at small relative distances $r \lesssim r_{vdW}$ is suppressed. This suppression leads to a far less pronounced peak at large momenta for van der Waals potentials as compared to the extreme square well case.

The three-body properties of the Efimov trimers have been analyzed in detail for the square well potential. These calculations have shown how accurate the different approximations and expansions for the two-body $T$-matrix are. For the shallow square well potential, we have found that the three-body parameters calculated from method I converge the fastest as more expansion terms are included. The results of method II converge less fast because the form factors do not depend on the scattering length for fixed range $R$. Furthermore, method I provides the best one-term approximation, followed by method III and II respectively. However, for potentials supporting more than one bound state the best separable approximation for the three-body calculations is provided by method III.

Our results for the shallow square well potential are consistent with those obtained by Ref. [61]. However, the results presented in this thesis are more accurate which is mainly caused by the fact that we did not make any approximations for the angular integration in the three-body equations. Therefore we could find —in contradiction to Ref. [61]— that the second Efimov state stays below the atom-dimer threshold even when we use a separable approximation for the potential. Furthermore, we have found that the approximation for the angular integration works better for the deep square well potential than for the shallow potential.

The non-crossing of the second Efimov state with the two-body threshold is a surprising result. So far this effect has only been seen in a recent numerical study on the first three potential resonances of the Lennard-Jones potential [52] in which this non-crossing was attributed to strong $d$-wave interactions at small positive scattering lengths. We have shown that the second Efimov state of the shallow square well potential stays below the two-body threshold even when $d$-wave interactions are excluded. Furthermore, we have found that strong $d$-wave interactions at positive scattering lengths have the effect of lowering the energy of the second Efimov state, so that $d$-wave effects may be the cause of the non-crossing of the second Efimov state for a shallow Lennard-Jones potential as seen by Ref. [52]. On the other hand, numerical studies on the potential resonances of van der Waals potentials which solve the Faddeev equations in the momentum-space representation have only considered separable approximations for the two-body $T$-matrix when determining whether the Efimov states cross the atom-dimer threshold. Therefore it should be confirmed whether the second Efimov trimer also unbinds into a free particle and a dimer for more realistic interatomic potentials when taking more than one separable term into account.

Moreover, we have shown that the separable approximation for the shallow square well potential using method I, II or III is insufficient to determine the three-body physics at large negative energies even at energies close to the two-body threshold. The failure of the separable approximation at negative energies for which $|E| \gtrsim \frac{\hbar^2}{2\mu R^2}$ is rooted in the free Green's function which is part of the Faddeev equations. This Green's function makes the contribution of the resonant term of the expansion of the $s$-wave $T$-matrix element, $t_0(p, p', z)$, less dominant. Therefore it is necessary to go beyond the separable approximation in this energy regime.

Since this effect is related to the three-body equations themselves and not to the details of the considered local potential, we expect that this conclusion also holds for other potentials which describe the atomic interactions more accurately.

Although the Efimov states can be calculated reasonably well for a shallow square well potential by using a separable approximation for $t_0(p, p', z)$, these approximations cannot simply be used for deep square well potentials. The one-term EST approximation results in a three-body parameter $a_{-,0}$ which strongly deviates from the one calculated by the Weinberg series which included many terms in the separable expansion of the two-body $T$-matrix. The EST approach results in $\bar{a}_{-,0} = -13.23$ which deviates 34% from the value $\bar{a}_{-,0} = -20$ which we obtained using the Weinberg series. This indicates that one should be careful when one wants to use the one-term EST approximation to calculate the Efimov resonances. The reason why this separable approximation fails is caused by the fact that the one-term EST approximation only approximates the partial-wave component $t_0(p, p', z)$ well at small energies $z$ for which $|\bar{p}_z| \lesssim 0.5$, whereas the three-body equations involve $t_0(p, p', z)$ at all values of $z$ below the three-body energy $E$ for which solutions are sought.

The results of Debets [62] and Kroeze [63] for the infinitely deep square well potential are in good agreement with those obtained in this work using the EST method. The relative difference of the results is rougly 10%. However, the value $\bar{a}_{-,0} = -14.6$ [62, 63] still deviates 27% from the one obtained by using the Weinberg series. The calculations of Ref. [62, 63] involved the full off-shell two-body $T$-matrix substituted into the three-body equation for separable potentials. The deviation from the results obtained by using the Weinberg series indicates that it is really necessary to solve the coupled set of three-body equations corresponding to the separable expansion of the $T$-matrix when considering deep square well potentials.

## 8.2 Outlook

The results of this study can be extended to more realistic interatomic potentials. It would be interesting to study the non-crossing of the second Efimov state for van der Waals potentials using the same procedure as we have used and to compare the results with those of Ref. [52] in order to determine whether this non-crossing is really caused by $d$-wave interactions.

Our analysis of the deep square well potential has shown that the separable approximation of the off-shell two-body $T$-matrix is insufficient to accurately calculate the three-body parameter. This conclusion could be verified by considering three-body recombination. The three-body parameter could be determined from the maxima in the recombination rate. This method is often used to obtain the three-body parameter, so that this approach could be used to test our results.

Furthermore, the validity of using the separable approximation for $t_0(p, p', z)$ in the three-body equations should be tested for other potentials as well, in particular for realistic interatomic potentials. In case of van der Waals potentials we expect that the one-term EST approximation based on the zero-energy scattering wave function does also not reproduce the correct $T$-matrix at all energies relevant for the calculation of the three-body parameter. This expectation is based on Fig. 5.12. The calculations performed by Ref. [49, 55, 59] suggested that the one-term EST approximation gives reasonable results for the three-body parameter for the considered van der Waals potentials. Further research should determine whether the

separable approximation is suitable for those potentials and would allow for a comparison with the square well scenario on an equal footing.

In this thesis we have only considered Efimov physics associated with potential resonances. The final goal should be to include the multichannel nature of atomic systems. Potential resonances can only be used as a simple model for broad Feshbach resonances for which the two scattering particles spend less time in the closed channel as compared to narrow Feshbach resonances. The single-channel model used in this work should therefore be upgraded to a multichannel model. Kroeze [63] has shown that it is possible to use the single-channel model as a basis when implementing the Feshbach formalism for the case in which the open-channel background scattering is non-resonant. This model should be expanded, so that it is possible to apply it to atomic systems with a narrow Feshbach resonance.

# Technology Assessment

Efimov physics is important for understanding the dynamics and stability of ultracold quantum gases in the strongly interacting regime. Three-body recombination and atom-dimer relaxation are two processes which lead to losses in the number of trapped atoms and dimers. The rate at which these two processes occur, is strongly affected by Efimov physics[5]. At positive scattering lengths three-body recombination minima exist due to the Efimov effect, which increases the lifetime of atoms in the trap. So the understanding of Efimov physics is relevant for promising applications which make use of ultracold trapped atoms, such as quantum simulators of interacting many-body systems [12]. This type of simulator allows us to study physical systems which cannot be modeled with a supercomputer.

Efimov physics is also important on a more fundamental level due to its universality. The Efimov effect is expected to occur in many physical systems including nucleons [17, 18], atoms [19] and magnons [20]. It may even apply to polymeric systems such as triple-stranded DNA [83, 84]. So Efimov physics is interesting for many different fields of physics.

[5]More information about these loss processes is given in Appendix A.

# Bibliography


[1] I. Bloch, J. Dalibard, and W. Zwerger, Rev. Mod. Phys. **80**, 885 (2008).

[2] H. Feshbach, Annals of Physics **5**, 357 (1958).

[3] H. Feshbach, Annals of Physics **19**, 287 (1962).

[4] U. Fano, Phys. Rev. **124**, 1866 (1961).

[5] A. G. Sitenko and O. D. Kocherga, *Scattering theory* (Springer, Berlin, 1991).

[6] S. Giorgini, L. P. Pitaevskii, and S. Stringari, Rev. Mod. Phys. **80**, 1215 (2008).

[7] V. Efimov, Physics Letters B **33**, 563 (1970).

[8] V. Efimov, Sov. J. Nucl. Phys **12**, 589 (1971), [Yad. Fiz. **12**, 1080 (1970)].

[9] D. Smith, E. Braaten, D. Kang, and L. Platter, Physical Review Letters **112**, 110402 (2014).

[10] A. Ludlow, M. Boyd, J. Ye, E. Peik, and P. Schmidt, Reviews of Modern Physics **87**, 637 (2015).

[11] D. Hall, M. Matthews, C. Wieman, and E. Cornell, Physical Review Letters **81**, 1543 (1998).

[12] I. Bloch, J. Dalibard, and S. Nascimbéne, Nature Physics **8**, 267 (2012).

[13] R. Lopes, C. Eigen, A. Barker, K. G. H. Viebahn, M. Robert-de Saint-Vincent, N. Navon, Z. Hadzibabic, and R. P. Smith, Phys. Rev. Lett. **118**, 210401 (2017).

[14] R. D. Amado and J. V. Noble, Phys. Rev. D **5**, 1992 (1972).

[15] E. Braaten and H.-W. Hammer, Physics Reports **428**, 259 (2006).

[16] P. Naidon and S. Endo, Reports on Progress in Physics **80**, 056001 (2017).

[17] A. S. Jensen, K. Riisager, D. V. Fedorov, and E. Garrido, Rev. Mod. Phys. **76**, 215 (2004).

[18] H.-W. Hammer and L. Platter, Annual Review of Nuclear and Particle Science **60**, 207 (2010).

[19] F. Ferlaino, A. Zenesini, M. Berninger, B. Huang, H. . Nägerl, and R. Grimm, Few-Body Systems **51**, 113 (2011).

[20] Y. Nishida, Y. Kato, and C. D. Batista, Nature Physics **9**, 93 (2013).

[21] B. D. Esry, C. H. Greene, and J. P. Burke, Phys. Rev. Lett. **83**, 1751 (1999).

[22] T. Kraemer, M. Mark, P. Waldburger, J. Danzl, C. Chin, B. Engeser, A. Lange, K. Pilch, A. Jaakkola, H.-C. Nägerl, et al., Nature **440**, 315 (2006).

[23] S. E. Pollack, D. Dries, and R. G. Hulet, Science **326**, 1683 (2009).

[24] P. Dyke, S. E. Pollack, and R. G. Hulet, Physical Review A **88** (2013).

[25] N. Gross, Z. Shotan, S. Kokkelmans, and L. Khaykovich, Physical Review Letters **103**, 163202 (2009).

[26] N. Gross, Z. Shotan, S. Kokkelmans, and L. Khaykovich, Physical Review Letters **105**, 103203 (2010).

[27] N. Gross, Z. Shotan, O. Machtey, S. Kokkelmans, and L. Khaykovich, Comptes Rendus Physique **12**, 4 (2011).

[28] T. B. Ottenstein, T. Lompe, M. Kohnen, A. Wenz, and S. Jochim, Physical Review Letters **101**, 203202 (2008).

[29] J. Huckans, J. Williams, E. Hazlett, R. Stites, and K. O'Hara, Physical Review Letters **102**, 165302 (2009).

[30] J. Williams, E. Hazlett, J. Huckans, R. Stites, Y. Zhang, and K. O'Hara, Physical Review Letters **103**, 130404 (2009).

[31] O. Machtey, Z. Shotan, N. Gross, and L. Khaykovich, Physical Review Letters **108**, 210406 (2012).

[32] T. Lompe, T. Ottenstein, F. Serwane, K. Viering, A. Wenz, G. Zürn, and S. Jochim, Physical Review Letters **105**, 103201 (2010).

[33] T. Lompe, T. B. Ottenstein, F. Serwane, A. N. Wenz, G. ZÃ$\frac{1}{4}$rn, and S. Jochim, Science **330**, 940 (2010).

[34] S. Nakajima, M. Horikoshi, T. Mukaiyama, P. Naidon, and M. Ueda, Physical Review Letters **105**, 023201 (2010).

[35] S. Nakajima, M. Horikoshi, T. Mukaiyama, P. Naidon, and M. Ueda, Physical review letters **106**, 143201 (2011).

[36] M. Zaccanti, B. Deissler, C. D'Errico, M. Fattori, M. Jona-Lasinio, S. Müller, G. Roati, M. Inguscio, and G. Modugno, Nature Physics **5**, 586 (2009).

[37] R. J. Wild, P. Makotyn, J. M. Pino, E. A. Cornell, and D. S. Jin, Physical Review Letters **108**, 145305 (2012).

[38] G. Barontini, C. Weber, F. Rabatti, J. Catani, G. Thalhammer, M. Inguscio, and F. Minardi, Physical Review Letters **103**, 043201 (2009).

[39] B. Huang, L. A. Sidorenkov, R. Grimm, J. M. Hutson, et al., Physical Review Letters **112**, 190401 (2014).

[40] M. Kunitski, S. Zeller, J. Voigtsberger, A. Kalinin, L. P. H. Schmidt, M. Schöffler, A. Czasch, W. Schöllkopf, R. E. Grisenti, T. Jahnke, et al., Science **348**, 551 (2015), ISSN 0036-8075.

[41] C. E. Klauss, X. Xie, C. Lopez-Abadia, J. P. D'Incao, Z. Hadzibabic, D. S. Jin, and E. A. Cornell, arXiv:1704.01206 [cond-mat.quant-gas] (2017).

[42] L. H. Thomas, Phys. Rev. **47**, 903 (1935).

[43] A. O. Gogolin, C. Mora, and R. Egger, Physical Review Letters **100**, 140404 (2008).

[44] H. Suno, B. D. Esry, C. H. Greene, and J. P. Burke, Phys. Rev. A **65**, 042725 (2002).

[45] L. W. Bruch and K. Sawada, Physical Review Letters **30**, 25 (1973).

[46] M. Berninger, A. Zenesini, B. Huang, W. Harm, H.-C. Nägerl, F. Ferlaino, R. Grimm, P. Julienne, and J. Hutson, Physical Review Letters **107**, 120401 (2011).

[47] S. Knoop, J. Borbely, W. Vassen, and S. Kokkelmans, Physical Review A **86**, 062705 (2012).

[48] J. Wang, J. P. D'Incao, B. D. Esry, and C. H. Greene, Physical Review Letters **108**, 263001 (2012).

[49] P. Naidon, S. Endo, and M. Ueda, Phys. Rev. A **90**, 022106 (2014).

[50] S. Knoop, F. Ferlaino, M. Mark, M. Berninger, H. Schöbel, H.-C. Nägerl, and R. Grimm, Nature Physics **5**, 227 (2009).

[51] A. Zenesini, B. Huang, M. Berninger, H. Nägerl, F. Ferlaino, and R. Grimm, Physical Review A **90** (2014).

[52] P. M. A. Mestrom, J. Wang, C. H. Greene, and J. P. D'Incao, Phys. Rev. A **95**, 032707 (2017).

[53] J. Wang, J. P. D'Incao, Y. Wang, and C. H. Greene, Phys. Rev. A **86**, 062511 (2012).

[54] P. Giannakeas and C. H. Greene, Few-Body Systems **58**, 20 (2016).

[55] J.-L. Li, X.-J. Hu, Y.-C. Han, and S.-L. Cong, Phys. Rev. A **94**, 032705 (2016).

[56] C. Chin, R. Grimm, P. Julienne, and E. Tiesinga, Reviews of Modern Physics **82**, 1225 (2010).

[57] A. J. Moerdijk, B. J. Verhaar, and A. Axelsson, Phys. Rev. A **51**, 4852 (1995).

[58] P. Törmä and K. Sengstock, *Quantum Gas Experiments: Exploring Many-body States*, vol. 3 (Imperial College Press, London, 2015).

[59] P. Naidon, S. Endo, and M. Ueda, Physical Review Letters **112**, 105301 (2014).

[60] A. S. Jensen, E. Garrido, and D. V. Fedorov, Few-Body Systems **22**, 193 (1997).

[61] P. M. A. Mestrom, Bachelor Thesis CQT2015-14, Eindhoven University of Technology (2015).

[62] V. E. Debets, Bachelor Thesis CQT2016-03, Eindhoven University of Technology (2016).

[63] R. M. Kroeze, Master Thesis CQT2016-04, Eindhoven University of Technology (2016).

[64] J. R. Taylor, *Scattering theory: The quantum theory on nonrelativistic collisions* (Wiley, 1972).

[65] S. Weinberg, Physical Review **131**, 440 (1963).

[66] R. D. Levine, *Quantum Mechanics of Molecular Rate Processes* (Oxford University Press, 1969).

[67] H. Cheng, E. Vilallonga, and H. Rabitz, Physical Review A **42**, 5232 (1990).

[68] J. J. Sakurai and S. F. Tuan, *Modern Quantum Mechanics* (Addison-Wesley, 1994).

[69] L. D. Faddeev and S. P. Merkuriev, *Quantum Scattering Theory for Several Particle Systems* (Springer Netherlands, Dordrecht, 1993).

[70] W. Schadow, C. Elster, and W. Glöckle, Few-Body Systems **28**, 15 (2000).

[71] V. F. Kharchenko and N. M. Petrov, Nuclear Physics, Section A **137**, 417 (1969).

[72] B. Gao, Phys. Rev. A **62**, 050702 (2000).

[73] P. M. A. Mestrom, Internship at JILA, Boulder, Colorado, USA CQT2016-15, Eindhoven University of Technology (2016).

[74] A. C. Pipkin, *A Course on Integral Equations* (Springer New York, New York NY, 1991).

[75] E. W. Schmid and H. Ziegelmann, *The quantum mechanical three-body problem* (Pergamon Press, Oxford, 1974).

[76] J. S. Levinger, A. H. Lu, and R. Stagat, Phys. Rev. **179**, 926 (1969).

[77] E. Harms, Physical Review C **1**, 1667 (1970).

[78] D. J. Ernst, C. M. Shakin, and R. M. Thaler, Physical Review C **8**, 46 (1973).

[79] Y. Koike, W. C. Parke, L. C. Maximon, and D. R. Lehman, Few-Body Systems **23**, 53 (1998).

[80] W. H. Press, B. P. Flannery, S. A. Teukolsky, and W. T. Vetterling, *Numerical recipes: The art of scientific computing* (Cambridge University Press, 2007), 3rd ed.

[81] T. K. Lim, K. Duffy, S. Nakaichi, Y. Akaishi, and H. Tanaka, The Journal of Chemical Physics **70**, 4782 (1979).

[82] Y. Horinouchi and M. Ueda, Physical Review Letters **114**, 025301 (2015).

[83] J. Maji, S. M. Bhattacharjee, F. Seno, and A. Trovato, New Journal of Physics **12**, 083057 (2010).

[84] T. Pal, P. Sadhukhan, and S. M. Bhattacharjee, Physical Review Letters **110**, 028105 (2013).

[85] N. P. Mehta, S. T. Rittenhouse, J. P. D'Incao, J. von Stecher, and C. H. Greene, Phys. Rev. Lett. **103**, 153201 (2009).

[86] J. P. D'Incao, J. Wang, Y. Wang, and C. H. Greene, *Universal relations in ultracold three-body observables associated with efimov physics*, poster, JILA and University of Colorado at Boulder.

[87] E. Nielsen and J. H. Macek, Phys. Rev. Lett. **83**, 1566 (1999).

[88] C. H. Greene, Physics Today **63**, 40 (2010).

[89] Y. Wang, J. P. D'Incao, and B. D. Esry, Adv. At. Mol. Opt. Phys. **62**, 1 (2013).

[90] K. F. Riley and M. P. Hobson, *Essential mathematical methods for the physical sciences* (Cambridge University Press, Cambridge, 2011).

[91] M. Abramowitz, I. A. Stegun, et al., *Handbook of mathematical functions* (Dover New York, 1965).

[92] F. W. Olver, *NIST handbook of mathematical functions* (Cambridge University Press, 2010).

[93] G. N. Watson, *A treatise on the theory of Bessel functions* (Cambridge University Press, 1995).

[94] R. Courant and D. Hilbert, *Methods of mathematical physics* (Wiley, Chichester, 1953).

# A. Experimental observables to determine the three-body parameters

The three-body parameters at positive scattering lengths, $a_+$ and $a_*$, are the values of the scattering length at which the three-body recombination minima and the atom-dimer resonances occur respectively, whereas $a_-$ indicates the negative scattering lengths at which maxima in the three-body recombination rate occur. In this Appendix the origin of these parameters is explained.

## A.1 Three-body recombination rate

Three-body recombination is a three-body collision in which two free particles undergo a transition to a two-body bound state [44]. The released kinetic energy is distributed between the free particle and the dimer. The high amount of kinetic energy which is released in this recombination process results in atomic losses in experiments with trapped atoms. The density $n_a$ of the trapped atoms is described by the following rate equation [44]:

$$\frac{dn_a}{dt} = -\frac{2K_3}{6} n_a^3 + 2D_3 n_a n_d. \tag{A.1}$$

Here $n_d$ is the dimer density, $K_3$ is the three-body recombination rate and $D_3$ is the rate for collision-induced dissociation, which is the inverse process of three-body recombination. Eq. (A.1) is valid when three-body inelastic collision events dominate $N$-body inelastic collisions events where $N \neq 3$. Furthermore, the second term on the right-hand side in Eq. (A.1) can often be neglected in experiments in which the dimer density $n_d$ is negligible compared to the atom density $n_a$. In this case, the three-body recombination rate can easily be obtained by measuring the loss rate of an ultracold gas of atoms in a trap. This loss rate is measured by recording the time evolution of the atom number. These measurements can be repeated for different values of the two-body scattering length by application of an external magnetic field. The gases are ultracold when the temperatures are in the sub-microkelvin regime.

The analytical expression for the three-body recombination rate $K_3$ in terms of the general $S$-matrix elements is given by [44]

$$K_3 = \sum_{i,f} \frac{192\pi^2(2J+1)\hbar}{\mu_{3b}k^4} \left|S_{f\leftarrow i}\right|^2. \tag{A.2}$$

The incident channels $i$ are the continuum channels and the final channels $f$ are the channels associated with an atom and a dimer. The wave number $k$ is related to the three-body energy

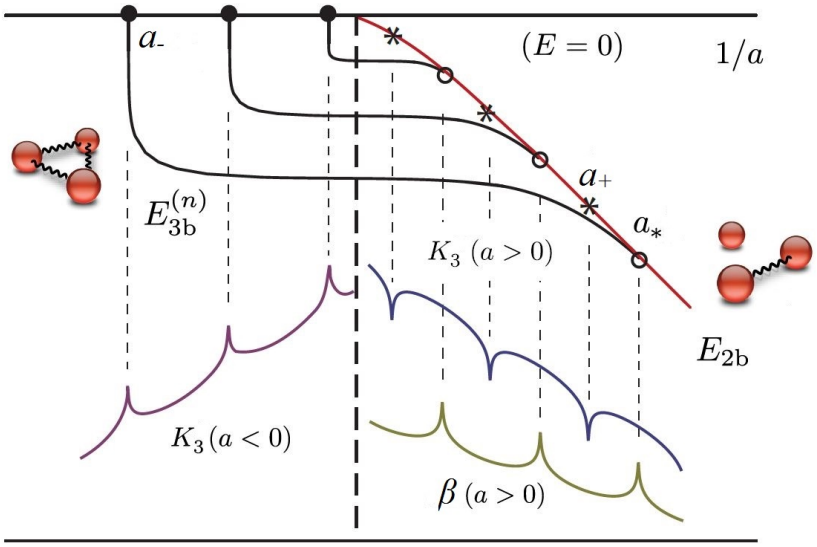


Figure A.1: The binding energy of the weakly bound Efimov trimer states, the three-body recombination rate $K_3$ and the inelastic atom-dimer scattering rate $\beta$ as a function of the inverse two-body scattering length $1/a$ (figure taken from ref. [86]). The two-body $s$-wave binding energy is indicated by the red curve. The three-body parameters are indicated by the filled circle ($a_-$), the star ($a_+$) and the open circle ($a_*$).

$E$ by $k = \sqrt{2\mu_{3b}E}/\hbar$ and $J$ is the total angular momentum quantum number. The three-body reduced mass is given by $\mu_{3b} = \frac{1}{\sqrt{3}}m$ for three particles of mass $m$.

The three-body recombination rate can be used to study the Efimov effect experimentally. It exhibits local extrema for specific scattering lengths $a$, namely the three-body parameters $a_-$ and $a_+$.

Near a pole in the $s$-wave two-body scattering length $a$, the recombination rate $K_3$ grows as $a^4$ for large $|a|$. This is the case for both positive and negative $a$, but the coefficient at negative scattering lengths is much larger [21]. Due to this strong dependence, three-body recombination is an important process in the ultracold limit [85]. On top of this $a^4$-scaling, recombination maxima occur at specific negative scattering lengths and recombination minima are present at specific positive scattering lengths. This is shown in Figure A.1.

The recombination maxima at negative scattering lengths are the result of a shape resonance effect [21] which is shown in Fig. A.2a. When the collision energy equals the quasi-bound state energy of the incoming continuum channel, the probability to tunnel through the barrier is strongly enhanced and the quasi-bound atoms are close together. In this regime ($R < |a|$) many avoided crossings with bound channels are located [21]. This results in a significant increase of the recombination rate $K_3$. At zero energy, infinitely many shape resonances occur when $a$ approaches $-\infty$ [21]. In this limit, the barrier height decreases as $1/a^2$, so that for finite energies $E$ the barrier falls below $E$ at some value of the scattering length $a$ and no shape resonances are possible anymore. So at positive energies only a finite number of recombination minima are present when $a$ approaches $-\infty$ [21]. The scattering lengths $a_-$ at which the Efimov states emerge from the three-body continuum can thus experimentally be determined by measuring the recombination rate as a function of the scattering length at

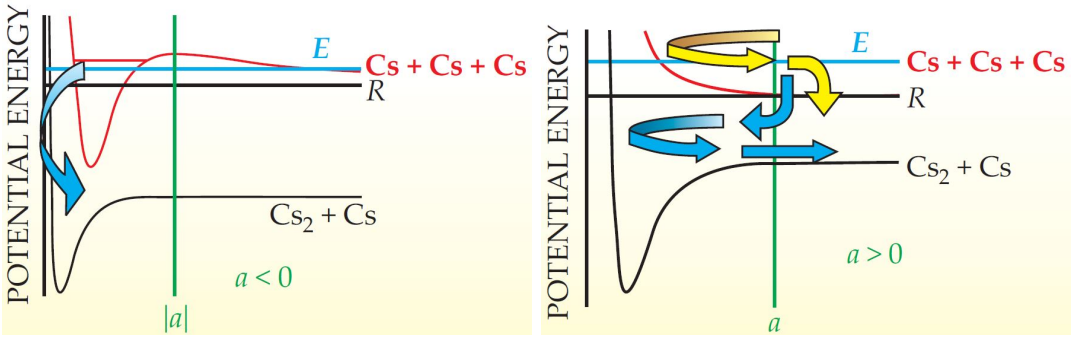


(a) $a < 0$ (b) $a > 0$

Figure A.2: The three-body recombination mechanisms at negative (a) and positive (b) scattering lengths leading to a maximum (a) or minimum (b) in $K_3$ (figure taken from ref. [88]). In each case, only two three-body potential curves $U_\nu(R)$ are shown as a function of the hyperradius $R$.

zero energy.

The recombination minima at positive scattering lengths have a different origin. They are the result of destructive interference between the two possible recombination paths [21, 87] as shown in Fig. A.2b. In one path, the system reflects from the potential cliff corresponding to the incoming channel and relaxes to the bound channel while the hyperradius $R$ is increasing. This bound channel corresponds to a weakly bound dimer state. In the second path, the system first relaxes to the bound channel while the particles approach each other and then bounces off the potential barrier corresponding to the bound channel. The transition from the continuum channel to the shallowest bound channel takes place at a hyperradius $R \approx 3a$ [21, 87] because that is where the absolute value of the non-adiabatic coupling terms between the three-body entrance channel and the shallowest $s$-wave bound channel are the largest [21]. It is clear that destructive interference would lead to a recombination rate of zero. However, if deeper bound channels are present, three-body recombination to these deeper channels results in a nonzero recombination rate for all two-body scattering lengths. A mimimum in the recombination rate can still be observed. The three-body parameters $a_{+,n}$ are the scattering lengths at which these recombination minima occur for zero three-body energy.

## A.2 Atom-dimer relaxation rate

The three-body parameter $a_*$ is the positive value of the scattering length for which an Efimov state causes a resonance in atom-dimer scattering [89]. During an atom-dimer collision, the dimer can relax into a more deeply bound two-body state. The kinetic energy of the atom and dimer increases during this process.

In experiments one can determine $a_*$ by preparing an ultracold sample of simultaneously trapped atoms and dimers and measuring the particle loss for various two-body scattering lengths. If the scattering length is tuned to $a_*$ by means of an applied magnetic field, a lot of atoms and dimers will gain kinetic energy due to the resonant enhancement of inelastic collisions between the atoms and dimers. As a result, their kinetic energy exceeds the trap

depth and the particle loss rate from the trap is large. If $n_D$ is the dimer density and $n_A$ is the atom density in the trap, then their time-dependence is described by

$$\frac{dn_D}{dt} = \frac{dn_A}{dt} = -\beta n_D n_A. \tag{A.3}$$

Here $\beta$ is the loss rate coefficient. It can be measured in experiments [50] and it will peak at $a = a_*$ as shown in Figure A.1. Note that particle loss by other inelastic collisions like dimer-dimer scattering also have to be taken into account in these experiments. If these processes are negligible, measuring the loss rate is equivalent to measuring the inelastic collision rate for the scattering process between a free atom and a dimer as described by Eq. (A.3). The experimental realization of an ultracold sample of trapped atoms and dimers is very challenging and special trap conditions are required [50].

Theoretically, the scattering process between an atom and a weakly bound $s$-wave dimer can be analyzed by calculating the following physical properties as a function of the two-body scattering length $a$: the atom-dimer scattering length $a_{ad}$, the elastic collision rate $\alpha$ and the inelastic collision rate $\beta$. Our definition of the atom-dimer scattering length $a_{ad}$ is given by

$$a_{ad} = -\lim_{k_{ad}\to 0} \frac{\tan\delta_{ad}}{k_{ad}^{2l+1}} \tag{A.4}$$

where the atom-dimer phase shift $\delta_{ad}$ is obtained from the $S$-matrix element $S_{i\leftarrow i} = e^{2i\delta_{ad}}$ associated with the incoming atom-dimer channel $i$. The wave number $k_{ad}$ is determined from the energy with respect to this channel by $k_{ad} = \sqrt{2\mu_{ad}(E + E_{2b})}/\hbar$. The reduced mass is given by $\mu_{ad} = \frac{2}{3}m$ and $E_{2b}$ is the binding energy of the dimer. The angular momentum quantum number $l$ specifies the orbital angular momentum of the dimer in the initial channel which is zero when the initial channel is the one correlated asymptotically with the weakly bound $s$-wave dimer.

The elastic and inelastic collision rates are defined by

$$\alpha = \frac{(2l'+1)\hbar\pi}{\mu_{ad}k_{ad}} \left|1 - S_{i\leftarrow i}\right|^2. \tag{A.5}$$

and

$$\beta = \sum_f \frac{(2l'+1)\hbar\pi}{\mu_{ad}k_{ad}} \left|S_{f\leftarrow i}\right|^2 \tag{A.6}$$

respectively. Here the final channels associated with an atom and deeply bound dimer are represented by $f$, whereas $i$ represents the initial channel. The relative angular momentum between the dimer and the third atom is described by the quantum number $l'$.

# B. Mathematics

This Appendix reviews some mathematical functions and their properties which are relevant for this thesis. We consider the spherical harmonics and the spherical Bessel functions which are relevant for solving the angular and radial part of the two-body Schrödinger equation respectively. More information can be found in [90–93].

## B.1 Some properties of the spherical harmonics

The spherical harmonics, denoted by $Y_l^m(\theta,\phi)$ or $Y_l^m(\hat{\mathbf{p}})$, form a complete set in the Hilbert space of square-integrable functions. These functions satisfy the following orthonormalization condition [90]:

$$\int_0^{2\pi}\int_0^{\pi} \left[Y_l^m(\theta,\phi)\right]^* Y_{l'}^{m'}(\theta,\phi)\sin(\theta)\,d\theta\,d\phi = \delta_{ll'}\delta_{mm'}. \tag{B.1}$$

The complex conjugate $[Y_l^m(\theta,\phi)]^*$, also indicated by $\bar{Y}_l^m(\theta,\phi)$, is simply given by

$$\left[Y_l^m(\theta,\phi)\right]^* = (-1)^m Y_l^{-m}(\theta,\phi). \tag{B.2}$$

Another important relationship obeyed by $Y_l^m(\theta,\phi)$ is the spherical harmonic addition theorem given by [90]

$$P_l(\hat{\mathbf{p}}\cdot\hat{\mathbf{p}}') = \frac{4\pi}{2l+1}\sum_{m=-l}^{l} Y_l^m(\hat{\mathbf{p}})\left[Y_l^m(\hat{\mathbf{p}}')\right]^*, \tag{B.3}$$

where $P_l(\hat{\mathbf{p}}\cdot\hat{\mathbf{p}}')$ are the Legendre polynomials.

## B.2 Spherical Bessel functions

The spherical Bessel functions $j_l(z)$ and $n_l(z)$ are two linearly independent solutions to the following differential equation:

$$\left(z^2\frac{\mathrm{d}^2}{\mathrm{d}z^2} + 2z\frac{\mathrm{d}}{\mathrm{d}z} + z^2 - l(l+1)\right)w(z) = 0, \tag{B.4}$$

where $l$ is an integer. The functions $j_l(z)$ and $n_l(z)$ are called the spherical Bessel functions of the first and second kind respectively. The functions $n_l(z)$ are also known as the spherical

Neumann functions. These spherical Bessel functions are related to the conventional Bessel functions by

$$\begin{aligned} j_l(z) &= \left(\frac{\pi}{2z}\right)^{1/2} J_{l+\frac{1}{2}}(z), \\ n_l(z) &= \left(\frac{\pi}{2z}\right)^{1/2} Y_{l+\frac{1}{2}}(z). \end{aligned} \tag{B.5}$$

Other useful functions related to the spherical bessel functions are the spherical Hankel functions which are also known as the spherical Bessel functions of the third kind. They are defined by

$$\begin{aligned} h_l^{(1)}(z) &= j_l(z) + i n_l(z), \\ h_l^{(2)}(z) &= j_l(z) - i n_l(z). \end{aligned} \tag{B.6}$$

## B.3 Riccati-Bessel functions

The Riccati-Bessel functions of the first and second kind, indicated by $\hat{j}_l(z)$ and $\hat{n}_l(z)$ respectively, are two linearly independent solutions to the following differential equation:

$$\left(\frac{\mathrm{d}^2}{\mathrm{d}z^2} - \frac{l(l+1)}{z^2} + 1\right) u(z) = 0, \tag{B.7}$$

where $l$ is an integer. This differential equation is obtained from Eq. (B.4) by substituting $w(z) = \frac{u(z)}{z}$. The functions $\hat{j}_l(z)$ and $\hat{n}_l(z)$ are related to the spherical Bessel functions and the ordinary Bessel functions by

$$\begin{aligned} \hat{j}_l(z) &= z j_l(z) = \left(\frac{\pi z}{2}\right)^{1/2} J_{l+\frac{1}{2}}(z), \\ \hat{n}_l(z) &= -z n_l(z) = -\left(\frac{\pi z}{2}\right)^{1/2} Y_{l+\frac{1}{2}}(z). \end{aligned} \tag{B.8}$$

. The Riccati-Bessel functions of the third kind are defined by

$$\begin{aligned} \hat{h}_l^{(1)}(z) &= z h_l^{(1)}(z) = \hat{j}_l(z) - i\hat{n}_l(z), \\ \hat{h}_l^{(2)}(z) &= z h_l^{(2)}(z) = \hat{j}_l(z) + i\hat{n}_l(z). \end{aligned} \tag{B.9}$$

# C. Multichannel scattering theory

In this Appendix we generalize the single-channel scattering theory presented in Section 2.1. The most important concepts which we need for the analysis of elastic atom-dimer scattering processes are the definition of the scattering amplitude and the two-body scattering length for cases in which the two bodies may be bound states of several particles. The theory presented in this Appendix is based on the textbook written by Taylor (1972) [64] in which more details can be found about multichannel scattering theory.

When more than two particles scatter, one can distinct different sets of particles that can enter or leave a collision. Each set defines a channel $\alpha$ with which a particular channel Hamiltonian $H^\alpha$ is associated. For example, the full Hamiltonian for three identical particles interacting in pairs is given by

$$H = H^0 + V = \sum_{i=1}^{3} \frac{\mathbf{p}_i^2}{2m_i} + V(\mathbf{r}_{12}) + V(\mathbf{r}_{23}) + V(\mathbf{r}_{31}), \tag{C.1}$$

where $\mathbf{r}_{ij} = \mathbf{r}_1 - \mathbf{r}_2$. The channel Hamiltonian corresponding to three free particles is given by $H^0$, whereas the channel Hamiltonian corresponding to a free particle $i$ and a bound state of particles $j$ and $k$ is given by $H^0 + V(\mathbf{r}_{jk})$.

When $n$ particles scatter from the in-channel $\alpha$, the state $|\psi\rangle$ at time $t$ is related to the state $|\psi_{\text{in}}\rangle$ by

$$e^{-iHt/\hbar}\,|\psi\rangle \xrightarrow{t\to-\infty} e^{-iH^\alpha t/\hbar}\,|\psi_{\text{in}}\rangle\,. \tag{C.2}$$

Similarly, we have

$$e^{-iHt/\hbar}\,|\psi\rangle \xrightarrow{t\to+\infty} e^{-iH^\alpha t/\hbar}\,|\psi_{\text{out}}\rangle\,. \tag{C.3}$$

The asymptotic condition states that for every vector in any channel subspace we can find a vector $|\psi\rangle$ which fulfills Eq. (C.2) or Eq. (C.3) [64]. As before, the asymptotic condition applies if the particle interactions $V(r)$ satisfy the usual asymptions.

The vector $|\psi\rangle$ is related to the vectors $|\psi_{\text{in}}\rangle$ and $|\psi_{\text{out}}\rangle$ by the channel Møller operators $\mathbf{\Omega}_+^\alpha$ and $\mathbf{\Omega}_-^\alpha$ respectively. These relations are given by

$$|\psi\rangle = \mathbf{\Omega}_+^\alpha\,|\psi_{\text{in}}\rangle = \lim_{t\to-\infty} e^{iHt/\hbar}e^{-iH^\alpha t/\hbar}\,|\psi_{\text{in}}\rangle \tag{C.4}$$

and

$$|\psi\rangle = \mathbf{\Omega}_-^\alpha\,|\psi_{\text{out}}\rangle = \lim_{t\to+\infty} e^{iHt/\hbar}e^{-iH^\alpha t/\hbar}\,|\psi_{\text{out}}\rangle\,. \tag{C.5}$$

In general, orbits exist that originate as a superposition $|\Psi_{\text{in}}\rangle$ of all open in-channels $\alpha$, so that Eq. (C.4) generalizes to

$$|\psi\rangle = \sum_{\alpha} \mathbf{\Omega}_{+}^{\alpha} |\psi_{\text{in}}^{\alpha}\rangle = \mathbf{\Omega}_{+} |\Psi_{\text{in}}\rangle . \tag{C.6}$$

Naturally, the scattering orbit will evolve into a superposition $|\Psi_{\text{out}}\rangle$ of all open out-channels $\alpha$, so that the generalization of Eq. (C.5) is given by

$$|\psi\rangle = \sum_{\alpha} \mathbf{\Omega}_{-}^{\alpha} |\psi_{\text{out}}^{\alpha}\rangle = \mathbf{\Omega}_{-} |\Psi_{\text{out}}\rangle . \tag{C.7}$$

The Møller operators $\mathbf{\Omega}_{+}$ and $\mathbf{\Omega}_{-}$ are isometric, so that the inverse of $\mathbf{\Omega}_{-}$ equals its Hilbert-adjoint operator $\mathbf{\Omega}_{-}^{\dagger}$. Consequently, Eqs. (C.6) and (C.7) can be combined to give

$$|\Psi_{\text{out}}\rangle = \mathbf{\Omega}_{-}^{\dagger} \mathbf{\Omega}_{+} |\Psi_{\text{in}}\rangle = \mathbf{S} |\Psi_{\text{in}}\rangle \tag{C.8}$$

where the scattering operator $\mathbf{S}$ has been defined as

$$\mathbf{S} = \mathbf{\Omega}_{-}^{\dagger} \mathbf{\Omega}_{+}. \tag{C.9}$$

The scattering operator maps each in-asymptote $|\Psi_{\text{in}}\rangle$ onto the corresponding out-asymptote $|\Psi_{\text{out}}\rangle$. Just as in single-channel scattering, the scattering operator $\mathbf{S}$ factors as

$$\mathbf{S} = 1_{cm} \otimes \Omega_{-}^{\dagger} \Omega_{+} \equiv 1_{cm} \otimes S. \tag{C.10}$$

The operator $S$ can be directly obtained from the relative Hamiltonian $H_{rel}$ and contains all of the physically interesting information. Thus from now on we will consider wave functions in the center-of-mass frame, and we will write the Hamiltonian $H_{rel} = H_{rel}^{0} + \sum_{\alpha} V_{\alpha}$ simply as $H$. The potentials $V_{\alpha}$ are just two-particle interaction potentials, so that $\sum_{\alpha} V_{\alpha} = \frac{1}{2} \sum_{i,j} V_{ij}$ where the sum is performed over all particles $i$ and $j$. The multichannel stationary scattering states can be defined in a similar way as the single-channel stationary scattering states given by Eq. (2.25), i.e., [64]

$$|\underline{p}, \alpha\pm\rangle \equiv \Omega_{\pm}^{\alpha} |\underline{p}, \alpha\rangle \tag{C.11}$$

where $\underline{p}$ denotes a set of $(n_{\alpha} - 1)$ relative momenta of the $n_{\alpha}$ bodies in channel $\alpha$. For example, for atom-dimer scattering the set $\underline{p}$ consists only of one relative momentum, namely the relative momentum $\mathbf{q}$ between the atom and the dimer, and $\alpha$ denotes a set of quantum numbers corresponding to the two-body bound state $\varphi_{\alpha}$. So in this particular case we have

$$|\underline{p}, \alpha\rangle = |\mathbf{q}\rangle |\varphi_{\alpha}\rangle. \tag{C.12}$$

The states $|\underline{p}, \alpha\pm\rangle$ are eigenstates of the full Hamiltonian $H$, whereas the states $|\underline{p}, \alpha\rangle$ are eigenstates of $H^{\alpha} = H - V^{\alpha}$ where $V^{\alpha}$ consists of all potentials that link different freely moving fragments in channel $\alpha$. The energy of the states $|\underline{p}, \alpha\pm\rangle$ and $|\underline{p}, \alpha\rangle$ is the same and consists of the kinetic energy of the state $|\underline{p}\rangle$ and the binding energy associated with the state $|\alpha\rangle$.

From Eq. (C.11) it can be proven that [64]

$$|\underline{p}, \alpha\pm\rangle = |\underline{p}, \alpha\rangle + G(E \pm i0) V^{\alpha} |\underline{p}, \alpha\rangle. \tag{C.13}$$

The Lippmann-Schwinger equation corresponding to the multichannel stationary scattering states $|\underline{p}, \alpha\pm\rangle$ is given by [64]

$$|\underline{p}, \alpha\pm\rangle = |\underline{p}, \alpha\rangle + G^{\alpha}(E \pm i0)V^{\alpha}|\underline{p}, \alpha\pm\rangle. \tag{C.14}$$

which is similar to Eq. (2.28). The Green's operator $G^{\alpha}$ is defined by $G^{\alpha}(z) \equiv (z - H^{\alpha})^{-1}$.

We can also define a transition operator $T^{\beta\alpha}(z)$ corresponding to the scattering process from the initial channel $\alpha$ to the final channel $\beta$. This multichannel $T$-operator is defined by

$$T^{\beta\alpha}(z) = V^{\alpha} + V^{\beta}G(z)V^{\alpha}. \tag{C.15}$$

Multiplying Eq. (C.15) on the left by $G^{\beta}(z)$ leads to

$$\begin{aligned} G^{\beta}(z)T^{\beta\alpha}(z) &= \left(G^{\beta}(z) + G^{\beta}(z)V^{\beta}G(z)\right)V^{\alpha} \\ &= G(z)V^{\alpha}. \end{aligned} \tag{C.16}$$

which can be substituted into Eq. (C.15) to obtain the Lippmann-Schwinger equations for the $T$-operators

$$T^{\beta\alpha}(z) = V^{\alpha} + V^{\beta}G^{\beta}(z)T^{\beta\alpha}(z). \tag{C.17}$$

So now we have formulated the Lippmann-Schwinger equation in terms of the stationary scattering states and in terms of transition operators $T^{\beta\alpha}(z)$.

The on-shell $T$-matrix element for scattering from channel $\alpha$ with energy $E$ to channel $\beta$ with the same energy $E$ is given by

$$\begin{aligned} \langle \underline{p}', \beta|T^{\beta\alpha}(E + i0)|\underline{p}, \alpha\rangle &= \langle \underline{p}', \beta|V^{\alpha} + V^{\beta}G(E + i0)V^{\alpha}|\underline{p}, \alpha\rangle \\ &= \langle \underline{p}', \beta|V^{\alpha} - V^{\beta}|\underline{p}, \alpha\rangle + \langle \underline{p}', \beta|V^{\beta}|\underline{p}, \alpha+\rangle \\ &= \langle \underline{p}', \beta|H^{\beta} - H^{\alpha}|\underline{p}, \alpha\rangle + \langle \underline{p}', \beta|V^{\beta}|\underline{p}, \alpha+\rangle \\ &= \left(E_{\underline{p}',\beta} - E_{\underline{p},\alpha}\right)\langle \underline{p}', \beta|\underline{p}, \alpha\rangle + \langle \underline{p}', \beta|V^{\beta}|\underline{p}, \alpha+\rangle \\ &= \langle \underline{p}', \beta|V^{\beta}|\underline{p}, \alpha+\rangle. \end{aligned} \tag{C.18}$$

Here we have explicitly used the fact that the energies corresponding to the states $|\underline{p}', \beta\rangle$ and $|\underline{p}, \alpha\rangle$ are equal. An alternative definition of the multichannel $T$-operator is given by

$$\tilde{T}^{\beta\alpha}(z) = V^{\beta} + V^{\beta}G(z)V^{\alpha} \tag{C.19}$$

which leads to exactly the same on-shell $T$-matrix elements given by Eq. (C.18). Furthermore, it can be proven that the on-shell $T$-matrix elements can also be calculated from

$$\langle \underline{p}', \beta|T^{\beta\alpha}(E + i0)|\underline{p}, \alpha\rangle = \langle \underline{p}', \beta - |V^{\beta}|\underline{p}, \alpha\rangle. \tag{C.20}$$

Moreover, we can relate the on-shell $T$-matrix to the $S$-matrix by [64]

$$\langle \underline{p}', \beta|S|\underline{p}, \alpha\rangle = \delta_{\beta\alpha}\delta(\underline{p}' - \underline{p}) - 2\pi i\delta(E_{\underline{p}',\beta} - E_{\underline{p},\alpha})\langle \underline{p}', \beta|T^{\beta\alpha}(E + i0)|\underline{p}, \alpha\rangle. \tag{C.21}$$

Now we turn our attention to multichannel scattering processes in which the initial channel $\alpha$ and the final channel $\beta$ both consists of two bodies. Each body may be a bound state

consisting of several particles and the two final bodies may be different as the two incoming bodies. In this case the sets of momenta $\underline{p}$ and $\underline{p}'$ reduce to the single momenta $\mathbf{q}$ and $\mathbf{q}'$ respectively. The differential scattering cross section for such a scattering process can then be calculated from the on-shell $T$-matrix element $\langle \mathbf{q}', \beta | T^{\beta\alpha}(E+i0) | \mathbf{q}, \alpha \rangle$ as [64]

$$\frac{d\sigma}{d\Omega}(\mathbf{q}', \beta \leftarrow \mathbf{q}, \alpha) = (2\pi)^4 \mu\mu' \hbar^2 \frac{q'}{q} |\langle \mathbf{q}', \beta | T^{\beta\alpha}(E+i0) | \mathbf{q}, \alpha \rangle|^2 \tag{C.22}$$

where $\mu$ and $\mu'$ are the reduced masses of the initial and final two-body system respectively. If we define the scattering amplitude $f(\mathbf{q}', \beta \leftarrow \mathbf{q}, \alpha)$ as

$$f(\mathbf{q}', \beta \leftarrow \mathbf{q}, \alpha) = -(2\pi)^2 \sqrt{\mu\mu'} \hbar \langle \mathbf{q}', \beta | T^{\beta\alpha}(E+i0) | \mathbf{q}, \alpha \rangle, \tag{C.23}$$

we can write Eq. (C.22) as

$$\frac{d\sigma}{d\Omega}(\mathbf{q}', \beta \leftarrow \mathbf{q}, \alpha) = \frac{q'}{q} |f(\mathbf{q}', \beta \leftarrow \mathbf{q}, \alpha)|^2. \tag{C.24}$$

An important physical parameter which is often used to characterize elastic scattering processes is the two-body scattering length. It can be related to the elastic scattering amplitude $f(\mathbf{q}', \alpha \leftarrow \mathbf{q}, \alpha)$ in which $q' = q$. In order to obtain this relation, we first expand the elastic scattering amplitude into spherical harmonics as

$$f(\mathbf{q}', \alpha \leftarrow \mathbf{q}, \alpha) \equiv 4\pi \sum_{l,m} Y_l^m(\hat{\mathbf{q}}) \bar{Y}_l^m(\hat{\mathbf{q}}') f_l(q). \tag{C.25}$$

The scattering length $a_l$ is related to $f_l(q)$ by

$$f_l(q) \underset{q \to 0}{\to} -a_l \left( \frac{q}{\hbar} \right)^{2l}. \tag{C.26}$$

Even though only $a_0$ has the dimensions of length, all parameters $a_l$ are referred to as the scattering length.

## C.1 Identical particles

So far we have considered scattering processes in which the involved particles are distinct. The theory can be extended to cases in which the particles are identical or in which part of the particles are identical. A detailed description of such scattering processes is given in Ref. [64].

One essential difference with respect to scattering processes involving distinguishable particles is that the number of channels is reduced. For example, the elastic scattering process,

$$i + (j,k) \to i + (j,k), \tag{C.27}$$

is physically indistinguishable from the rearrangement processes

$$i + (j,k) \to j + (k,i), \tag{C.28}$$
$$i + (j,k) \to k + (i,j), \tag{C.29}$$

when all particles are identical. Nonetheless, we can treat these three scattering processes mathematically distinct. The fact that these channels are physically indistinguishable is reflected in the wave function of this system. The wave function of a collection of identical particles should be symmetric (bosons) or antisymmetric (fermions) at all times $t$.

We would like to point out one special type of collisions, namely a collision between a single particle and a target containing $n$ particles. All $n+1$ particles are identical, spinless bosons. Furthermore, we assume that all out-channels have the same arrangements and are therefore physically indistinguishable. Therefore we label the incoming channel by $\alpha$ and the outgoing channel by $\alpha'$ where the prime indicates that the incoming and outgoing channels may only be mathematically distinct. The differential scattering cross section for such scattering processes can be calculated from

$$\frac{d\sigma}{d\Omega}(\mathbf{q}', \alpha' \leftarrow \mathbf{q}, \alpha) = \frac{q'}{q}|\hat{f}(\mathbf{q}', \alpha' \leftarrow \mathbf{q}, \alpha)|^2, \tag{C.30}$$

in which the scattering amplitude is given by

$$\hat{f}(\mathbf{q}', \alpha' \leftarrow \mathbf{q}, \alpha) = f_{di}(\mathbf{q}', \alpha' \leftarrow \mathbf{q}, \alpha) + n f_{ex}(\mathbf{q}', \alpha' \leftarrow \mathbf{q}, \alpha). \tag{C.31}$$

The direct amplitude $f_{di}(\mathbf{q}', \alpha' \leftarrow \mathbf{q}, \alpha)$ is the scattering amplitude for the direct scattering process

$$0 + (1\ 2\ \ldots\ n) \rightarrow 0 + (1\ 2\ \ldots\ n) \tag{C.32}$$

on the assumption that the particles are distinct. The exchange amplitude $f_{ex}(\mathbf{q}', \alpha' \leftarrow \mathbf{q}, \alpha)$ is the scattering amplitude for the rearrangement process

$$0 + (1\ 2\ \ldots\ n) \rightarrow 1 + (0\ 2\ \ldots\ n) \tag{C.33}$$

in which all particles are distinguishable. The direct and exchange amplitudes can be calculated from the theory presented above for distinct particles. This means that

$$f_{di}(\mathbf{q}', \alpha' \leftarrow \mathbf{q}, \alpha) = f(\mathbf{q}', \alpha \leftarrow \mathbf{q}, \alpha), \tag{C.34}$$
$$f_{ex}(\mathbf{q}', \alpha' \leftarrow \mathbf{q}, \alpha) = f(\mathbf{q}', \alpha' \leftarrow \mathbf{q}, \alpha). \tag{C.35}$$

where $f$ denotes the amplitude for distinct particles. Note that the channels $\alpha$ and $\alpha'$ on the right-hand-side of these equations refer to channels involving of non-symmetrized wave functions, so that the channels $\alpha$ and $\alpha'$ are different. However, the channels $\alpha$ and $\alpha'$ on the left-hand-side of these equations refer to channels involving of symmetrized wave functions and are therefore exactly the same.

# D. Exchange and permutation operators

The exchange operator $P_{ij}$ exchanges particles $i$ and $j$. Clearly, a symmetric pair potential $V_{ij}$ commutes with $P_{ij}$. Furthermore, $P_{ij}$ commutes with $P_{kl}$ only if $i \neq k$ and $j \neq l$ or if $i = l$ and $j = k$. For three particles, the former condition is irrelevant, but the latter condition means that $P_{ij} = P_{ji}$. Consequently, $P_{ij}^2 = 1$. Another important property of the exchange operator $P_{ij}$ is

$$P_{ij}P_{jk} = P_{jk}P_{ki}. \tag{D.1}$$

The operator $P_{ij}P_{jk}$ is the anticyclic permutation operator of three particles and is abbreviated as $P_-$. Similarly, $P_+ = P_{ik}P_{jk}$ is the cyclic permutation operator of the three particles.

Another useful operator is the permutation operator $P = P_+ + P_-$. The operator $P$ commutes with $P_{ij}$. After all,

$$\begin{aligned}[P, P_{jk}] &= PP_{jk} - P_{jk}P \\ &= (P_{ij}P_{jk} + P_{ik}P_{jk})P_{jk} - P_{jk}(P_{jk}P_{ik} + P_{jk}P_{ij}) \\ &= (P_{ij} + P_{ik}) - (P_{ik} + P_{ij}) = 0.\end{aligned} \tag{D.2}$$

So we have seen that $[P, P_{jk}] = 0$ and $[V_{jk}, P_{jk}] = 0$. However, $[P, V_{jk}] \neq 0$. Furthermore, $P$, $P_+$ and $P_-$ commute with the free Hamiltonian $H_0$ and therefore also with $G_0 = (z - H_0)^{-1}$.

# E. Free-particle states and the momentum-space representation of operators

This Appendix presents the two-body and three-body free-particle states. These states can be used to rewrite operators and wave functions in the momentum-space representation. We will also write the homogeneous part of the Faddeev equation for three identical bosons in the momentum-space representation.

## E.1 Free two-particle states

A free-particle state can be analyzed using either the plane wave basis $\{|\mathbf{p}\rangle\}$ or the spherical wave basis $\{|E,l,m\rangle\}$ which are both considered in this Appendix.

The eigenfunctions of the momentum operator $\frac{\hbar}{i}\nabla$ are the momentum eigenstates $|\mathbf{p}\rangle$. These states are also eigenfunctions of the free-particle Hamiltonian $H_0$. Their representation in position space is given by

$$\langle \mathbf{x}|\mathbf{p}\rangle = \frac{1}{(2\pi\hbar)^{3/2}} e^{i\mathbf{p}\cdot\mathbf{x}/\hbar} \tag{E.1}$$

which can be expanded in terms of partial waves as [5]

$$\begin{aligned}\langle \mathbf{x}|\mathbf{p}\rangle &= \frac{4\pi}{(2\pi\hbar)^{3/2}} \sum_{l=0}^{\infty} \sum_{m=-l}^{l} i^l j_l\left(\frac{pr}{\hbar}\right) Y_l^m(\hat{\mathbf{x}}) \bar{Y}_l^m(\hat{\mathbf{p}}) \\ &= \frac{1}{(2\pi\hbar)^{3/2}} \sum_{l=0}^{\infty} (2l+1) i^l j_l\left(\frac{pr}{\hbar}\right) P_l(\hat{\mathbf{p}}\cdot\hat{\mathbf{x}}).\end{aligned} \tag{E.2}$$

The momentum eigenvectors $|\mathbf{p}\rangle$ are not square-integrable. Therefore these functions do not belong to the Hilbert space and they do not represent physically realizable states. However, a normalized wave packet which is a superposition of momentum eigenvectors lives in the Hilbert space. The vectors $|\mathbf{p}\rangle$ obey the orthonormalization condition

$$\langle \mathbf{p}'|\mathbf{p}\rangle = \delta(\mathbf{p}'-\mathbf{p}). \tag{E.3}$$

Another important set of eigenvectors of the free Hamiltonian $H_0$ which are also eigenvectors of the angular momentum operators $\mathbf{L}^2$ and $L_z$ are the spherical wave states $|E,l,m\rangle$,

where $E$, $l(l+1)\hbar^2$ and $m\hbar$ are the corresponding eigenvalues of $H_0$, $\mathbf{L}^2$ and $L_z$ respectively. Here $m$ indicates the magnetic quantum number and not the mass of a particle. The free spherical wave states are normalized according to

$$\langle E', l', m'|E, l, m\rangle = \delta(E - E')\delta_{l'l}\delta_{m'm}. \tag{E.4}$$

The position-space representation of the spherical wave states $|E, l, m\rangle$ is given by [68]

$$\langle \mathbf{x}|E, l, m\rangle = i^l \left(\frac{2\mu}{\pi\hbar p}\right)^{1/2} \frac{1}{r}\hat{j}_l\left(\frac{pr}{\hbar}\right) Y_l^m(\hat{\mathbf{x}}), \tag{E.5}$$

whereas the momentum-space representation is given by

$$\langle \mathbf{p}|E, l, m\rangle = \left(\frac{1}{\mu p}\right)^{1/2} \delta\left(E - \frac{p^2}{2\mu}\right) Y_l^m(\hat{\mathbf{p}}). \tag{E.6}$$

## E.2 Momentum-space representation of the potential

The position-space representation of a local two-body potential is given by

$$\langle \mathbf{x}'|V|\mathbf{x}\rangle = V(\mathbf{x})\delta(\mathbf{x}' - \mathbf{x}), \tag{E.7}$$

whereas the momentum-space representation of such a potential is given by

$$\begin{aligned}\langle \mathbf{p}'|V|\mathbf{p}\rangle &= \iint \langle \mathbf{p}'|\mathbf{x}'\rangle\langle \mathbf{x}'|V|\mathbf{x}\rangle\langle \mathbf{x}|\mathbf{p}\rangle \, d\mathbf{x}\, d\mathbf{x}' \\ &= \int \langle \mathbf{p}'|\mathbf{x}\rangle V(\mathbf{x})\langle \mathbf{x}|\mathbf{p}\rangle \, d\mathbf{x}.\end{aligned} \tag{E.8}$$

If we substitute Eq. (E.2) and assume that the potential is spherically symmetric, we obtain

$$\begin{aligned}\langle \mathbf{p}'|V|\mathbf{p}\rangle &= \frac{(4\pi)^2}{(2\pi\hbar)^3}\sum_{l=0}^{\infty}\sum_{m=-l}^{l} \bar{Y}_l^m(\hat{\mathbf{p}})Y_l^m(\hat{\mathbf{p}}')\int V(r)j_l\left(\frac{pr}{\hbar}\right) j_l\left(\frac{p'r}{\hbar}\right) r^2 dr \\ &= \frac{4\pi\hbar^2}{(2\pi\hbar)^3 pp'}\sum_{l=0}^{\infty}(2l+1)P_l(\hat{\mathbf{p}}'\cdot\hat{\mathbf{p}})\int V(r)\hat{j}_l\left(\frac{pr}{\hbar}\right)\hat{j}_l\left(\frac{p'r}{\hbar}\right) dr \\ &= \sum_{l=0}^{\infty}(2l+1)P_l(\hat{\mathbf{p}}'\cdot\hat{\mathbf{p}})V_l(p,p').\end{aligned} \tag{E.9}$$

The partial-wave components of the potential, $V_l(p, p')$, are given by

$$V_l(p,p') = \frac{1}{2\pi^2\hbar pp'}\int V(r)\hat{j}_l\left(\frac{pr}{\hbar}\right)\hat{j}_l\left(\frac{p'r}{\hbar}\right) dr. \tag{E.10}$$

For the square well potential we find that these components are given by

$$\begin{aligned}V_l(p,p') &= \frac{-V_0}{2\pi^2\hbar pp'}\hbar\frac{\bar{p}\hat{j}_{l+1}(\bar{p})\hat{j}_l(\bar{p}') - \bar{p}'\hat{j}_l(\bar{p})\hat{j}_{l+1}(\bar{p}')}{\bar{p}^2 - \bar{p}'^2} \\ &= \frac{-V_0R^3}{2\pi^2\hbar^3\bar{p}\bar{p}'}\frac{\bar{p}\hat{j}_{l+1}(\bar{p})\hat{j}_l(\bar{p}') - \bar{p}'\hat{j}_l(\bar{p})\hat{j}_{l+1}(\bar{p}')}{\bar{p}^2 - \bar{p}'^2} \\ &= \frac{-\bar{q}_0^2R}{4\pi^2\mu\hbar\bar{p}\bar{p}'}\frac{\bar{p}\hat{j}_{l+1}(\bar{p})\hat{j}_l(\bar{p}') - \bar{p}'\hat{j}_l(\bar{p})\hat{j}_{l+1}(\bar{p}')}{\bar{p}^2 - \bar{p}'^2}.\end{aligned} \tag{E.11}$$

where the dimensionless momenta $\bar{p}$, $\bar{p}'$ and $\bar{q}_0$ are given by $\frac{pR}{\hbar}$, $\frac{p'R}{\hbar}$ and $\frac{q_0R}{\hbar}$ respectively.

## E.3 Momentum-space representation of the wave function

The wave function $|\psi\rangle$ can also be written in the momentum-space representation. In general, the wave function $\langle \mathbf{x}|\psi\rangle$ corresponding to a spherically symmetric potential can be expanded in position space as

$$\langle \mathbf{x}|\psi\rangle = \sum_{l=0}^{\infty}\sum_{m=-l}^{l}\frac{u_l(r)}{r}Y_l^m(\hat{\mathbf{x}}), \tag{E.12}$$

so that

$$\begin{aligned}
\langle \mathbf{p}|\psi\rangle &= \int \langle \mathbf{p}|\mathbf{x}\rangle\langle \mathbf{x}|\psi\rangle\, d\mathbf{x} \\
&= \frac{4\pi}{(2\pi\hbar)^{3/2}}\int \sum_{l=0}^{\infty}\sum_{m=-l}^{l}\sum_{l'=0}^{\infty}\sum_{m'=-l'}^{l'}(-i)^l j_l\left(\frac{pr}{\hbar}\right)\bar{Y}_l^m(\hat{\mathbf{x}})Y_l^m(\hat{\mathbf{p}})\frac{u_{l'}(r)}{r}Y_{l'}^{m'}(\hat{\mathbf{x}})\, d\mathbf{x} \\
&= \frac{4\pi}{(2\pi\hbar)^{3/2}}\int \sum_{l=0}^{\infty}\sum_{m=-l}^{l}(-i)^l j_l\left(\frac{pr}{\hbar}\right)Y_l^m(\hat{\mathbf{p}})\frac{u_l(r)}{r}r^2\, dr \\
&= \sum_{l=0}^{\infty}\sum_{m=-l}^{l}\frac{w_l(p)}{p}Y_l^m(\hat{\mathbf{p}}).
\end{aligned} \tag{E.13}$$

Here we have defined the functions $w_l(p)$ as

$$w_l(p) = \frac{4\pi}{(2\pi\hbar)^{3/2}}(-i)^l\int_0^{\infty}\hat{j}_l\left(\frac{pr}{\hbar}\right)u_l(r)\, dr. \tag{E.14}$$

We can also apply an operator on the state $|\psi\rangle$ and project the resulting state onto the plane-wave state $|\mathbf{p}\rangle$. For example, if we consider again a local spherically symmetric potential and define the state $|g\rangle = V|\psi\rangle$, we obtain analogous to Eq. (E.13) that

$$\langle \mathbf{p}|g\rangle = \sum_{l=0}^{\infty}\sum_{m=-l}^{l}g_l(p)Y_l^m(\hat{\mathbf{p}}), \tag{E.15}$$

where the functions $g_l(p)$ are defined as

$$g_l(p) = \frac{4\pi}{(2\pi\hbar)^{3/2}}(-i)^l\frac{1}{p}\int_0^{\infty}V(r)\hat{j}_l\left(\frac{pr}{\hbar}\right)u_l(r)\, dr. \tag{E.16}$$

In case of the square well potential these functions are given by

$$\begin{aligned}
g_l(p) &\propto -\frac{1}{p}\int_0^R V_0\hat{j}_l\left(\frac{pr}{\hbar}\right)\hat{j}_l\left(\frac{qr}{\hbar}\right)\, dr \\
&= -\frac{V_0\hbar}{p}\frac{q\hat{j}_{l+1}\left(\frac{qR}{\hbar}\right)\hat{j}_l\left(\frac{pR}{\hbar}\right) - p\hat{j}_{l+1}\left(\frac{pR}{\hbar}\right)\hat{j}_l\left(\frac{qR}{\hbar}\right)}{q^2-p^2} \\
&= -\frac{\hbar\bar{q}_0^2}{2\mu\bar{p}}\frac{\bar{q}\hat{j}_{l+1}(\bar{q})\,\hat{j}_l(\bar{p}) - \bar{p}\hat{j}_{l+1}(\bar{p})\,\hat{j}_l(\bar{q})}{\bar{q}^2-\bar{p}^2}
\end{aligned} \tag{E.17}$$

where $q = \sqrt{\frac{2\mu}{\hbar^2}(V_0+z)}$ and $z$ corresponds to the energy of the system whose state is given by $|\psi\rangle$.

## E.4 Three-particle momentum states

The three-particle momentum state $|\mathbf{q}_1, \mathbf{p}_1\rangle_1$ describes the system of three free noninteracting particles. Here $2\mathbf{q}_1$ is the relative momentum of particle 1 with respect to the center-of-mass of the two-particle system (2 3) and $2\mathbf{p}_1$ is the relative momentum between particles 2 and 3. The momenta $\mathbf{q}_2$, $\mathbf{p}_2$, $\mathbf{q}_3$ and $\mathbf{p}_3$ are defined in a similar way, but they correspond to different Jacobi vectors. Table E.1 gives the momenta of each particle for each asymptotic state corresponding to three free particles.

The states $|\mathbf{q}_1, \mathbf{p}_1\rangle_1$ and $|\mathbf{q}_2, \mathbf{p}_2\rangle_2$ in Table E.1 are the same when

$$\begin{aligned} \mathbf{p}_1 &= \frac{1}{2}(\mathbf{q}_2 - (\mathbf{p}_2 - \frac{1}{2}\mathbf{q}_2)) = \frac{3}{4}\mathbf{q}_2 - \frac{1}{2}\mathbf{p}_2 \text{ and} \\ \mathbf{q}_1 &= -\mathbf{p}_2 - \frac{1}{2}\mathbf{q}_2. \end{aligned} \tag{E.18}$$

Similarly, the states $|\mathbf{q}_1, \mathbf{p}_1\rangle_1$ and $|\mathbf{q}_3, \mathbf{p}_3\rangle_3$ are the same when

$$\begin{aligned} \mathbf{p}_1 &= \frac{1}{2}((-\mathbf{p}_3 - \frac{1}{2}\mathbf{q}_3) - \mathbf{q}_3) = -\frac{3}{4}\mathbf{q}_3 - \frac{1}{2}\mathbf{p}_3 \text{ and} \\ \mathbf{q}_1 &= \mathbf{p}_3 - \frac{1}{2}\mathbf{q}_3. \end{aligned} \tag{E.19}$$

The three-particle momentum states $|\mathbf{q}_1, \mathbf{p}_1\rangle_1$, $|\mathbf{q}_2, \mathbf{p}_2\rangle_2$ and $|\mathbf{q}_3, \mathbf{p}_3\rangle_3$ are equivalent, so that we can just use one of these states. Therefore we can define

$$|\mathbf{q}, \mathbf{p}\rangle \equiv |\mathbf{q}, \mathbf{p}\rangle_\alpha \tag{E.20}$$

where $\alpha$ can be chosen to be 1, 2 or 3. So by choosing $\alpha$, we do not need to bother about the indices anymore. We normalize the three-body momentum states according to

$$\langle \mathbf{q}', \mathbf{p}' | \mathbf{q}, \mathbf{p}\rangle = \delta(\mathbf{q}' - \mathbf{q})\delta(\mathbf{p}' - \mathbf{p}). \tag{E.21}$$

Table E.1: The momenta $\mathbf{P}_i$ of each particle $i$ in the center-of-mass frame for different representations of the momentum state corresponding to three free particles.

| Three-particle state | $\mathbf{P}_1$ | $\mathbf{P}_2$ | $\mathbf{P}_3$ |
|---|---|---|---|
| $\|\mathbf{q}_1, \mathbf{p}_1\rangle_1$ | $\mathbf{q}_1$ | $\mathbf{p}_1 - \frac{1}{2}\mathbf{q}_1$ | $-\mathbf{p}_1 - \frac{1}{2}\mathbf{q}_1$ |
| $\|\mathbf{q}_2, \mathbf{p}_2\rangle_2$ | $-\mathbf{p}_2 - \frac{1}{2}\mathbf{q}_2$ | $\mathbf{q}_2$ | $\mathbf{p}_2 - \frac{1}{2}\mathbf{q}_2$ |
| $\|\mathbf{q}_3, \mathbf{p}_3\rangle_3$ | $\mathbf{p}_3 - \frac{1}{2}\mathbf{q}_3$ | $-\mathbf{p}_3 - \frac{1}{2}\mathbf{q}_3$ | $\mathbf{q}_3$ |

## E.5 Momentum-space representation of three-body operators

In this thesis we solve the Faddeev equations in the momentum-space representation. This means that we write an operator $\hat{O}$ as

$$\hat{O} = \iiiint |\mathbf{q}', \mathbf{p}'\rangle\langle \mathbf{q}', \mathbf{p}'|\hat{O}|\mathbf{q}, \mathbf{p}\rangle\langle \mathbf{q}, \mathbf{p}|\, d\mathbf{q}\, d\mathbf{p}\, d\mathbf{q}'\, d\mathbf{p}'. \tag{E.22}$$

The elements $\langle \mathbf{q}', \mathbf{p}'|\hat{O}|\mathbf{q}, \mathbf{p}\rangle$ are called the matrix elements of the operator $\hat{O}$ in the momentum-space representation. The Faddeev equations involve the operators $G_0$, $T_\alpha$ and $P$ for which we will now evaluate the corresponding matrix elements.

Since the momentum states $|\mathbf{q}, \mathbf{p}\rangle$ are eigenstates of the free hamiltonian $H_0$, it follows that

$$\langle \mathbf{p}', \mathbf{q}'|G_0(E)|\mathbf{p}, \mathbf{q}\rangle = \frac{1}{E - E_{\mathbf{p},\mathbf{q}}} \delta\left(\mathbf{p}' - \mathbf{p}\right) \delta\left(\mathbf{q}' - \mathbf{q}\right). \tag{E.23}$$

The energy $E_{\mathbf{p},\mathbf{q}}$ is just

$$\begin{aligned} E_{\mathbf{p},\mathbf{q}} = \sum_{i=1}^{3} \frac{1}{2m} \mathbf{P}_i^2 &= \frac{1}{2m} \left( |\mathbf{q}|^2 + \left|\mathbf{p} - \frac{1}{2}\mathbf{q}\right|^2 + \left|-\mathbf{p} - \frac{1}{2}\mathbf{q}\right|^2 \right) \\ &= \frac{1}{2m} \left( \frac{3}{2} q^2 + 2p^2 \right). \end{aligned} \tag{E.24}$$

Furthermore,

$$\langle \mathbf{p}, \mathbf{q}|T_\alpha(E)|\mathbf{p}', \mathbf{q}'\rangle = \langle \mathbf{p}|T_\alpha|\mathbf{p}'\rangle \delta\left(\mathbf{q} - \mathbf{q}'\right). \tag{E.25}$$

Since $T_\alpha(E)$ is the two-body $T$-operator for two-particle scattering in the presence of the third particle, it is just equal to the ordinary two-body $T$-operator, $T(z)$, evaluated at energy $z = E - \frac{3}{4m} q^2$.

The momentum-space representation of the permutation operator $P$ can be determined from Table E.1. We find that

$$\begin{aligned} \langle \mathbf{q}, \mathbf{p}|P|\mathbf{q}', \mathbf{p}'\rangle &= \langle \mathbf{q}, \mathbf{p}| - \mathbf{p}' - \frac{1}{2}\mathbf{q}', -\frac{1}{2}\mathbf{p}' + \frac{3}{4}\mathbf{q}'\rangle \\ &\quad + \langle \mathbf{q}, \mathbf{p}|\mathbf{p}' - \frac{1}{2}\mathbf{q}', -\frac{1}{2}\mathbf{p}' - \frac{3}{4}\mathbf{q}'\rangle \\ &= \delta\left(\mathbf{p} + \frac{1}{2}\mathbf{p}' - \frac{3}{4}\mathbf{q}'\right) \delta\left(\mathbf{q} + \mathbf{p}' + \frac{1}{2}\mathbf{q}'\right) \\ &\quad + \delta\left(\mathbf{p} + \frac{1}{2}\mathbf{p}' + \frac{3}{4}\mathbf{q}'\right) \delta\left(\mathbf{q} - \mathbf{p}' + \frac{1}{2}\mathbf{q}'\right) \\ &= \delta\left(\mathbf{p} - \frac{1}{2}\mathbf{q} - \mathbf{q}'\right) \delta\left(\mathbf{p}' + \mathbf{q} + \frac{1}{2}\mathbf{q}'\right) \\ &\quad + \delta\left(\mathbf{p} + \frac{1}{2}\mathbf{q} + \mathbf{q}'\right) \delta\left(\mathbf{p}' - \mathbf{q} - \frac{1}{2}\mathbf{q}'\right). \end{aligned} \tag{E.26}$$

Now we can evaluate

$$\begin{aligned}\langle \mathbf{p},\mathbf{q}|T_\alpha(E)G_0(E)P|\Phi_\alpha\rangle = \int\cdots\int d\mathbf{p}'d\mathbf{q}'d\mathbf{p}''d\mathbf{q}''d\mathbf{p}'''d\mathbf{q}'''\langle \mathbf{p},\mathbf{q}|T_\alpha(E)|\mathbf{p}',\mathbf{q}'\rangle \\ \langle \mathbf{p}',\mathbf{q}'|G_0(E)|\mathbf{p}'',\mathbf{q}''\rangle\langle \mathbf{p}'',\mathbf{q}''|P|\mathbf{p}''',\mathbf{q}'''\rangle\langle \mathbf{p}''',\mathbf{q}'''|\Phi_\alpha\rangle.\end{aligned} \tag{E.27}$$

Taking Eqs. (E.23), (E.25) and (E.26) into account we find that Eq. (E.27) reduces to

$$\begin{aligned}\langle \mathbf{p},\mathbf{q}|T_\alpha(E)G_0(E)P|\Phi_\alpha\rangle = \int d\mathbf{q}'''\Bigg(\langle \mathbf{p}|T_\alpha(E)|\frac{1}{2}\mathbf{q}+\mathbf{q}'''\rangle\frac{1}{E-E_{(\frac{1}{2}\mathbf{q}+\mathbf{q}'''),\mathbf{q}}}\langle -\frac{1}{2}\mathbf{q}'''-\mathbf{q},\mathbf{q}'''|\Phi_\alpha\rangle \\ +\langle \mathbf{p}|T_\alpha(E)|-\frac{1}{2}\mathbf{q}-\mathbf{q}'''\rangle\frac{1}{E-E_{(-\frac{1}{2}\mathbf{q}-\mathbf{q}'''),\mathbf{q}}}\langle \frac{1}{2}\mathbf{q}'''+\mathbf{q},\mathbf{q}'''|\Phi_\alpha\rangle\Bigg).\end{aligned} \tag{E.28}$$

From Eq. (E.24) it follows that

$$E_{(\frac{1}{2}\mathbf{q}+\mathbf{q}'''),\mathbf{q}} = E_{(-\frac{1}{2}\mathbf{q}-\mathbf{q}'''),\mathbf{q}} = \frac{1}{m}\left(q^2+q'''^2+\mathbf{q}\cdot\mathbf{q}'''\right). \tag{E.29}$$

For three identical bosons the relation $\langle \frac{1}{2}\mathbf{q}'''+\mathbf{q},\mathbf{q}'''|\Phi_\alpha\rangle = \langle -\frac{1}{2}\mathbf{q}'''-\mathbf{q},\mathbf{q}'''|\Phi_\alpha\rangle$ holds, so that Eq. (E.28) simplifies to

$$\langle \mathbf{p},\mathbf{q}|T_\alpha(E)G_0(E)P|\Phi_\alpha\rangle = \int d\mathbf{q}'''\left(\frac{t_s\left(\mathbf{p},\frac{1}{2}\mathbf{q}+\mathbf{q}''',E-\frac{3}{4m}q^2\right)}{E-\frac{1}{m}\left(q^2+q'''^2+\mathbf{q}\cdot\mathbf{q}'''\right)}\langle\frac{1}{2}\mathbf{q}'''+\mathbf{q},\mathbf{q}'''|\Phi_\alpha\rangle\right), \tag{E.30}$$

where $t_s\left(\mathbf{p},\mathbf{p}',E\right)$ is the symmetrized two-body $T$-matrix which is defined as

$$t_s\left(\mathbf{p},\mathbf{p}',E\right) = \langle \mathbf{p}|T(E)|\mathbf{p}'\rangle + \langle \mathbf{p}|T(E)|-\mathbf{p}'\rangle. \tag{E.31}$$

# F. Partial wave expansion of the three-body equations

In this Appendix we perform a partial wave expansion on the three-body equations derived in Chapter 3. First, we consider the Faddeev equation for three-body bound states given by Eq. (3.11). Secondly, we consider Eq. (3.27) describing atom-dimer scattering processes.

## F.1 Three-body bound states

Here we analyze the three-body equation given by Eq. (3.11) for zero total angular momentum. For simplicity, we drop the index $\alpha$ in this equation. We expand the three-body wave function $\langle \mathbf{p}, \mathbf{q}|\Phi\rangle$ in terms of angular functions, so that we obtain an infinite set of two-dimensional integral equations for the expansion coefficients. This infinite set of equations is further reduced to an even larger set of one-dimensional integral equations after expanding the two-particle $T$-matrix in separable terms.

We will expand the wave function $\langle \mathbf{p}, \mathbf{q}|\Phi\rangle$ in the bispherical basis $Y_{l\lambda LM}(\hat{\mathbf{p}}, \hat{\mathbf{q}})$. In order to define this basis, we first define the operators $\vec{l}$ and $\vec{\lambda}$ as the orbital angular momentum operators, corresponding to the Jacobi vectors $\mathbf{r}_{23} = \mathbf{r}_2 - \mathbf{r}_3$ and $\mathbf{r}_{1,23} = \mathbf{r}_1 - \frac{1}{2}(\mathbf{r}_2 + \mathbf{r}_3)$ respectively, with respect to the center of mass of the pair of particles, i.e. $\frac{1}{2}(\mathbf{r}_2 + \mathbf{r}_3)$. So

$$\vec{l} = -i\hbar \mathbf{r}_{23} \times \nabla_{\mathbf{r}_{23}} \tag{F.1}$$

and

$$\vec{\lambda} = -i\hbar \mathbf{r}_{1,23} \times \nabla_{\mathbf{r}_{1,23}}. \tag{F.2}$$

The total angular momentum of the three-particle system is then $\mathbf{L} = \vec{l} + \vec{\lambda}$. The bispherical basis corresponding to total angular momentum $\mathbf{L}$ is given by [5, 69]

$$Y_{l\lambda LM}(\hat{\mathbf{p}}, \hat{\mathbf{q}}) = \sum_{m_l + m_\lambda = M} \langle l m_l \lambda m_\lambda | LM \rangle Y_l^{m_l}(\hat{\mathbf{p}}) Y_\lambda^{m_\lambda}(\hat{\mathbf{q}}) \tag{F.3}$$

where the functions $Y_l^{m_l}$ and $Y_\lambda^{m_\lambda}$ are spherical harmonics and the coefficients $\langle l m_l \lambda m_\lambda | LM \rangle$ are Clebsch-Gordan coefficients. The functions $Y_{l\lambda LM}(\hat{\mathbf{p}}, \hat{\mathbf{q}})$ are orthonormalized and form a complete set [5], so that the bispherical basis can be used to expand the wave function $\langle \mathbf{p}, \mathbf{q}|\Phi\rangle$ as

$$\langle \mathbf{p}, \mathbf{q}|\Phi(E)\rangle = \sum_{l,\lambda,L,M} Y_{l\lambda LM}(\hat{\mathbf{p}}, \hat{\mathbf{q}}) \Phi_{l\lambda L}(p, q, E). \tag{F.4}$$

Similar expansions can be found in Ref. [71], in Ref. [5] and in Chapter 7.2 and 7.3.1 of Faddeev's book [69].

For zero total angular momentum, the Clebsch-Gordan coefficients are given by

$$\langle l m_l \lambda m_\lambda | 00 \rangle = \delta_{l,\lambda} \delta_{m_l,-m_\lambda} \frac{(-1)^{l-m_l}}{\sqrt{2l+1}}, \tag{F.5}$$

so that Eq. (F.4) can be written as

$$\begin{aligned}
\langle \mathbf{p}, \mathbf{q} | \Phi(E) \rangle &= \sum_{l,\lambda} Y_{l\lambda 00}(\hat{\mathbf{p}}, \hat{\mathbf{q}}) \Phi_{l\lambda 0}(p, q, E) && \text{(F.6)} \\
&= \sum_{l,\lambda} \sum_{m_l + m_\lambda = 0} \langle l m_l \lambda m_\lambda | 00 \rangle Y_l^{m_l}(\hat{\mathbf{p}}) Y_\lambda^{m_\lambda}(\hat{\mathbf{q}}) \Phi_{l\lambda 0}(p, q, E) && \text{(F.7)} \\
&= \sum_{l} \sum_{m_l=-l}^{l} \frac{(-1)^{l-m_l}}{\sqrt{2l+1}} Y_l^{m_l}(\hat{\mathbf{p}}) Y_l^{-m_l}(\hat{\mathbf{q}}) \Phi_{ll0}(p, q, E) && \text{(F.8)} \\
&= \sum_{l} \sum_{m_l=-l}^{l} \frac{(-1)^{l}}{\sqrt{2l+1}} Y_l^{m_l}(\hat{\mathbf{p}}) \bar{Y}_l^{m_l}(\hat{\mathbf{q}}) \Phi_{ll0}(p, q, E). && \text{(F.9)}
\end{aligned}$$

In the last line we used $(-1)^m Y_l^{-m_l}(\hat{\mathbf{q}}) = \bar{Y}_l^{m_l}(\hat{\mathbf{q}})$ where the bar denotes the complex conjugate. Next, we substitute Eq. (F.9) into Eq. (3.11). We also use the partial wave expansion of the two-body $T$-matrix (Eq. (2.31)). This gives

$$\begin{aligned}
\sum_{l} \sum_{m_l=-l}^{l} \frac{(-1)^{l}}{\sqrt{2l+1}} Y_l^{m_l}(\hat{\mathbf{p}}) \bar{Y}_l^{m_l}(\hat{\mathbf{q}}) \Phi_{ll0}(p, q, E) = \int d\mathbf{q}'' \frac{1}{E - \frac{1}{m}(q^2 + \mathbf{q} \cdot \mathbf{q}'' + q''^2)} \\
\left( 2 \sum_{l'=0,\text{even}}^{\infty} (2l'+1) P_{l'}(\hat{\mathbf{p}} \cdot \widehat{\tfrac{1}{2}\mathbf{q} + \mathbf{q}''}) t_{l'}(p, |\frac{1}{2}\mathbf{q} + \mathbf{q}''|, E - \frac{3}{4m} q^2) \right) \\
\sum_{l''} \sum_{m_{l''}=-l}^{l''} \frac{(-1)^{l''}}{\sqrt{2l''+1}} Y_{l''}^{m_{l''}}(\widehat{\mathbf{q} + \tfrac{1}{2}\mathbf{q}''}) \bar{Y}_{l''}^{m_{l''}}(\widehat{\mathbf{q}''}) \Phi_{l''l''0}(|\mathbf{q} + \frac{1}{2}\mathbf{q}''|, q'', E)
\end{aligned} \tag{F.10}$$

This equation can be multiplied by $\bar{Y}_l^{m_l}(\hat{\mathbf{p}})$ and integrated over $\hat{\mathbf{p}}$. Taking the orthogonality of the spherical harmonics, $\int Y_l^{m_l}(\hat{\mathbf{p}}) \bar{Y}_{l'}^{m_{l'}}(\hat{\mathbf{p}}) d\hat{\mathbf{p}} = \delta_{ll'} \delta_{m_l m_{l'}}$, into account and using Eq. (B.3), it is easy to verify that Eq. (F.10) reduces to

$$\begin{aligned}
\frac{(-1)^{l}}{\sqrt{2l+1}} \bar{Y}_l^{m_l}(\hat{\mathbf{q}}) \Phi_{ll0}(p, q, E) = \int d\mathbf{q}'' \frac{1}{E - \frac{1}{m}(q^2 + \mathbf{q} \cdot \mathbf{q}'' + q''^2)} \\
\left( 8\pi \Delta_l \bar{Y}_l^{m_l}(\widehat{\tfrac{1}{2}\mathbf{q} + \mathbf{q}''}) t_l(p, |\frac{1}{2}\mathbf{q} + \mathbf{q}''|, E - \frac{3}{4m} q^2) \right) \\
\sum_{l''=0}^{\infty} \sum_{m_{l''}=-l''}^{l''} \frac{(-1)^{l''}}{\sqrt{2l''+1}} Y_{l''}^{m_{l''}}(\widehat{\mathbf{q} + \tfrac{1}{2}\mathbf{q}''}) \bar{Y}_{l''}^{m_{l''}}(\widehat{\mathbf{q}''}) \Phi_{l''l''0}(|\mathbf{q} + \frac{1}{2}\mathbf{q}''|, q'', E)
\end{aligned} \tag{F.11}$$

where $\Delta_l \equiv \frac{1}{2}\left(1 + (-1)^l\right)$. Clearly, $l$ must be even because odd values of $l$ are not present in the symmetrized two-body $T$-matrix. So $\Phi_{ll0}(p, q, E) = 0$ for odd values of $l$. Consequently,

$(-1)^l = 1$ and only the terms with even values of $l''$ contribute to the sum over $l''$ on the right-hand-side of this equation. To get a better overview, we can define the variable $\tilde{\Phi}_l(p,q,E) \equiv \frac{1}{\sqrt{2l+1}}\Phi_{ll0}(p,q,E)$. Now Eq. (F.11) looks like

$$\begin{aligned}\bar{Y}_l^{m_l}(\hat{\mathbf{q}})\tilde{\Phi}_l(p,q,E) = \int d\mathbf{q}'' \frac{1}{E-\frac{1}{m}\left(q^2+\mathbf{q}\cdot\mathbf{q}''+q''^2\right)} \\ \left(8\pi\Delta_l \bar{Y}_l^{m_l}(\widehat{\tfrac{1}{2}\mathbf{q}+\mathbf{q}''})t_l(p,|\frac{1}{2}\mathbf{q}+\mathbf{q}''|,E-\frac{3}{4m}q^2)\right) \\ \sum_{l''=0}^{\infty}\sum_{m_{l''}=-l''}^{l''} \Delta_{l''} Y_{l''}^{m_{l''}}(\widehat{\mathbf{q}+\tfrac{1}{2}\mathbf{q}''})\bar{Y}_{l''}^{m_{l''}}(\widehat{\mathbf{q}''})\tilde{\Phi}_{l''}(|\mathbf{q}+\frac{1}{2}\mathbf{q}''|,q'',E).\end{aligned} \tag{F.12}$$

The next step is to get rid of the factor $\bar{Y}_l^{m_l}(\hat{\mathbf{q}})$ on the left-hand-side of this equation. This can be done by multiplying Eq. (F.12) with $Y_l^{m_l}(\hat{\mathbf{q}})$ and summing over $m_l$. The resulting equation is

$$\begin{aligned}\sum_{m_l=-l}^{l} Y_l^{m_l}(\hat{\mathbf{q}})\bar{Y}_l^{m_l}(\hat{\mathbf{q}})\tilde{\Phi}_l(p,q,E) = \int d\mathbf{q}'' \frac{1}{E-\frac{1}{m}\left(q^2+\mathbf{q}\cdot\mathbf{q}''+q''^2\right)} \\ \left(8\pi\sum_{m_l=-l}^{l}\Delta_l Y_l^{m_l}(\hat{\mathbf{q}})\bar{Y}_l^{m_l}(\widehat{\tfrac{1}{2}\mathbf{q}+\mathbf{q}''})t_l(p,|\frac{1}{2}\mathbf{q}+\mathbf{q}''|,E-\frac{3}{4m}q^2)\right) \\ \sum_{l''=0}^{\infty}\sum_{m_{l''}=-l}^{l''} \Delta_{l''} Y_{l''}^{m_{l''}}(\widehat{\mathbf{q}+\tfrac{1}{2}\mathbf{q}''})\bar{Y}_{l''}^{m_{l''}}(\widehat{\mathbf{q}''})\tilde{\Phi}_{l''}(|\mathbf{q}+\frac{1}{2}\mathbf{q}''|,q'',E).\end{aligned} \tag{F.13}$$

which can be simplified by using Eq. (B.3) to

$$\begin{aligned}\tilde{\Phi}_l(p,q,E) = \int d\mathbf{q}'' \frac{1}{E-\frac{1}{m}\left(q^2+\mathbf{q}\cdot\mathbf{q}''+q''^2\right)}\left(2\Delta_l P_l(\hat{\mathbf{q}}\cdot\widehat{\tfrac{1}{2}\mathbf{q}+\mathbf{q}''})t_l(p,|\frac{1}{2}\mathbf{q}+\mathbf{q}''|,E-\frac{3}{4m}q^2)\right) \\ \sum_{l''=0}^{\infty}(2l''+1)\Delta_{l''}P_{l''}(\widehat{\mathbf{q}+\tfrac{1}{2}\mathbf{q}''}\cdot\widehat{\mathbf{q}''})\tilde{\Phi}_{l''}(|\mathbf{q}+\frac{1}{2}\mathbf{q}''|,q'',E).\end{aligned} \tag{F.14}$$

This set of equations is an infinite set of two-dimensional integral equations. This can easily be seen by introducing the $\delta$-function and adding an additional integration, so that

$$P_{l''}(\widehat{\mathbf{q}+\tfrac{1}{2}\mathbf{q}''}\cdot\widehat{\mathbf{q}''})\tilde{\Phi}_{l''}(|\mathbf{q}+\frac{1}{2}\mathbf{q}''|,q'',E) = \int d\mathbf{p}''\delta\left(\mathbf{p}''-\mathbf{q}-\frac{1}{2}\mathbf{q}''\right)P_{l''}(\widehat{\mathbf{p}''}\cdot\widehat{\mathbf{q}''})\tilde{\Phi}_{l''}(p'',q'',E). \tag{F.15}$$

Eq. (F.14) can be reduced to an infinite set of one-dimensional integral equations if $t_l(p,p',z)$ is written as a sum of terms which are separable in the incoming and outgoing momenta, namely

$$t_l(p,p',z) = -\sum_{n=1}^{\infty}\tau_{nl}(z)g_{nl}(p,z)g_{nl}(p',z). \tag{F.16}$$

There exists many ways in which this separable expansion can be done and it depends on the specific method whether the form factors $g_{nl}(p,z)$ are energy-dependent or not. We also assume that an orthonormalization condition for the form factors $g_{nl}(p,z)$ exists, i.e.,

$$\int_0^\infty k(p,z)g_{n'l}(p,z)g_{nl}(p,z)dp = \delta_{n'n} \tag{F.17}$$

where $k(p,z)$ is a function depending on $p$ and $z$. Chapter 5 discusses some methods to perform a separable expansion of $t_l(p,p',z)$ and it is shown that $k(p,z)=1$ for method I (the spectral representation) and $k(p,z)=\frac{p^2}{\frac{p^2}{2\mu}-z}$ for method II (the Weinberg series).

The expansion given by Eq. (F.16) can be substituted into Eq. (F.14). If we also define the quantities $\tilde{\phi}_{ln}(q,E)$ as the expansion coefficients of $\tilde{\Phi}_l(p,q,E)$ with respect to the orthonormal basis $\{g_{nl}(p,E-\frac{3}{4m}q^2)\}$, i.e. $\tilde{\Phi}_l(p,q,E)=\sum_{n=1}^\infty g_{nl}(p,E-\frac{3}{4m}q^2)\tilde{\phi}_{ln}(q,E)$, the resulting three-body equation is

$$\begin{aligned}\sum_{n=1}^\infty g_{nl}(p,E-\frac{3}{4m}q^2)\tilde{\phi}_{ln}(q,E) = -\int d\mathbf{q}''\frac{1}{E-\frac{1}{m}(q^2+\mathbf{q}\cdot\mathbf{q}''+q''^2)}2\Delta_l P_l(\hat{\mathbf{q}}\cdot\widehat{\tfrac{1}{2}\mathbf{q}+\mathbf{q}''})\\ \sum_{n'=1}^\infty \tau_{n'l}(E-\frac{3}{4m}q^2)g_{n'l}(p,E-\frac{3}{4m}q^2)g_{n'l}(|\frac{1}{2}\mathbf{q}+\mathbf{q}''|,E-\frac{3}{4m}q^2)\\ \sum_{l''=0}^\infty(2l''+1)\Delta_{l''}P_{l''}(\widehat{\mathbf{q}+\tfrac{1}{2}\mathbf{q}''}\cdot\widehat{\mathbf{q}''})\sum_{n''=1}^\infty g_{n''l''}(|\mathbf{q}+\frac{1}{2}\mathbf{q}''|,E-\frac{3}{4m}q''^2)\tilde{\phi}_{l''n''}(q'',E).\end{aligned} \tag{F.18}$$

When we multiply this equation with $k(p,z)g_{nl}(p,E-\frac{3}{4m}q^2)$, integrate over $p$ and use Eq. (F.17), Eq. (F.18) reduces to

$$\begin{aligned}\tilde{\phi}_{ln}(q,E) = -\int d\mathbf{q}''\frac{2\Delta_l P_l(\hat{\mathbf{q}}\cdot\widehat{\tfrac{1}{2}\mathbf{q}+\mathbf{q}''})}{E-\frac{1}{m}(q^2+\mathbf{q}\cdot\mathbf{q}''+q''^2)}\tau_{nl}(E-\frac{3}{4m}q^2)g_{nl}(|\frac{1}{2}\mathbf{q}+\mathbf{q}''|,E-\frac{3}{4m}q^2)\\ \sum_{l''=0}^\infty\sum_{n''=1}^\infty(2l''+1)\Delta_{l''}P_{l''}(\widehat{\mathbf{q}+\tfrac{1}{2}\mathbf{q}''}\cdot\widehat{\mathbf{q}''})g_{n''l''}(|\mathbf{q}+\frac{1}{2}\mathbf{q}''|,E-\frac{3}{4m}q''^2)\tilde{\phi}_{l''n''}(q'',E)\end{aligned} \tag{F.19}$$

which is an infinite set of one-dimensional integral equations. When the separable representation of two-body $T$-matrix (Eq. (F.16)) converges well, only a few terms of this expansion have to be considered. In this case the number of coupled equations is small enough to solve this set numerically.

Finally, we note that we could also symmetrize the integrand of Eq. (F.19) for the terms with $n=n''$ and $l=l''$ if we define the expansion of $\tilde{\Phi}_l(p,q,E)$ in a different way, namely $\tilde{\Phi}_l(p,q,E)=\frac{1}{q}\sum_{n=1}^\infty g_{nl}(p,E-\frac{3}{4m}q^2)\sqrt{\tau_{nl}(E-\frac{3}{4m}q^2)}\widetilde{\tilde{\phi}}_{ln}(q,E)$. Here we have defined some

new quantities $\widetilde{\widetilde{\phi}}_{ln}(q,E)$. The resulting three-body equation is

$$\begin{aligned}\widetilde{\widetilde{\phi}}_{ln}(q,E) = &-\int d\widehat{\mathbf{q}''}\, dq'' \frac{2q''q\Delta_l P_l(\hat{\mathbf{q}}\cdot\widehat{\frac{1}{2}\mathbf{q}+\mathbf{q}''})}{E-\frac{1}{m}(q^2+\mathbf{q}\cdot\mathbf{q}''+q''^2)}\sqrt{\tau_{nl}(E-\frac{3}{4m}q^2)}g_{nl}(|\frac{1}{2}\mathbf{q}+\mathbf{q}''|,E-\frac{3}{4m}q^2)\\ &\sum_{l''=0}^{\infty}\sum_{n''=1}^{\infty}(2l''+1)\Delta_{l''}P_{l''}(\widehat{\mathbf{q}+\tfrac{1}{2}\mathbf{q}''}\cdot\widehat{\mathbf{q}''})\sqrt{\tau_{n''l''}(E-\frac{3}{4m}q''^2)}g_{n''l''}(|\mathbf{q}+\frac{1}{2}\mathbf{q}''|,E-\frac{3}{4m}q''^2)\\ &\widetilde{\widetilde{\phi}}_{l''n''}(q'',E).\end{aligned} \tag{F.20}$$

Alternatively, we could define $\theta_{ln}(q,E) = \frac{\tilde{\phi}_{ln}(q,E)}{\tau_{nl}(E-\frac{3}{4m}q^2)}$, so that Eq. (F.19) can also be written as

$$\begin{aligned}\tilde{\theta}_{ln}(q,E) = &-\int d\mathbf{q}'\frac{2\Delta_l P_l(\hat{\mathbf{q}}\cdot\widehat{\frac{1}{2}\mathbf{q}+\mathbf{q}'})}{E-\frac{1}{m}(q^2+\mathbf{q}\cdot\mathbf{q}'+q'^2)}\tau_{nl}(E-\frac{3}{4m}q'^2)g_{nl}(|\frac{1}{2}\mathbf{q}+\mathbf{q}'|,E-\frac{3}{4m}q^2)\\ &\sum_{l'=0}^{\infty}\sum_{n'=1}^{\infty}(2l'+1)\Delta_{l'}P_{l'}(\widehat{\mathbf{q}+\tfrac{1}{2}\mathbf{q}'}\cdot\widehat{\mathbf{q}'})g_{n'l'}(|\mathbf{q}+\frac{1}{2}\mathbf{q}'|,E-\frac{3}{4m}q'^2)\tilde{\theta}_{l'n'}(q',E).\end{aligned} \tag{F.21}$$

## F.2 Atom-dimer scattering states

Now we follow a similar approach to the problem of atom-dimer scattering. The derivation of the equation is based on Ref. [71]. The equation to determine the wave function of the atom-dimer scattering state is given by Eq. (3.27). This three-body equation can also be expanded in the bispherical basis $Y_{l\lambda LM}(\hat{\mathbf{p}},\hat{\mathbf{q}})$. The angular momentum of the dimer, which is the scatterer of the third particle, is assumed to be zero [5]. We indicate this by $l_d = 0$. So if we define

$$\langle \mathbf{p},\mathbf{q}|\tilde{\Psi}(\mathbf{q}_0)\rangle = \sum_{l,\lambda,L,M}\psi_{l\lambda L}(p,q;q_0)Y_{l\lambda LM}(\hat{\mathbf{p}},\hat{\mathbf{q}})\bar{Y}_L^M(\hat{\mathbf{q}}_0) \tag{F.22}$$

and substitute this expansion in Eq. (3.27), we obtain

$$\begin{aligned}\sum_{l,\lambda,L,M}\psi_{l\lambda L}(p,q;q_0)Y_{l\lambda LM}(\hat{\mathbf{p}},\hat{\mathbf{q}})\bar{Y}_L^M(\hat{\mathbf{q}}_0) = &\,\varphi_{n_d,l_d}(p)\frac{\delta(q-q_0)}{q^2}Y_{l_d}^{m_d}(\hat{\mathbf{p}})\sum_{L,M}Y_L^M(\hat{\mathbf{q}})\bar{Y}_L^M(\hat{\mathbf{q}}_0)\\ &+\left(E-\frac{p^2}{m}-\frac{3q^2}{4m}\right)^{-1}\int d\mathbf{q}'2\sum_{l,m_l}\Delta_l 4\pi Y_l^{m_l}(\hat{\mathbf{p}})\bar{Y}_l^{m_l}(\widehat{\tfrac{1}{2}\mathbf{q}+\mathbf{q}'})t_l\left(p,|\frac{1}{2}\mathbf{q}+\mathbf{q}'|,E-\frac{3q^2}{4m}\right)\\ &\sum_{l',\lambda',L',M'}\psi_{l'\lambda'L'}(|\frac{1}{2}\mathbf{q}'+\mathbf{q}|,q';q_0)Y_{l'\lambda'L'M'}(\widehat{\tfrac{1}{2}\mathbf{q}'+\mathbf{q}},\hat{\mathbf{q}}')\bar{Y}_{L'}^{M'}(\hat{\mathbf{q}}_0).\end{aligned} \tag{F.23}$$

Multiplying this equation by $Y_L^M(\hat{\mathbf{q}}_0)\bar{Y}_l^{m_l}(\hat{\mathbf{p}})\bar{Y}_\lambda^{m_\lambda}(\hat{\mathbf{q}})$ and integrating over $\hat{\mathbf{q}}_0$, $\hat{\mathbf{p}}$ and $\hat{\mathbf{q}}$ results in

$$\begin{aligned}\langle lm_l\lambda m_\lambda|LM\rangle\psi_{l\lambda L}(p,q;q_0,E) &= \varphi_{n_d,l_d}(p)\frac{1}{q^2}\delta(q-q_0)\delta_{l,l_d}\delta_{m_l,m_d}\delta_{\lambda,L}\delta_{m_\lambda,M}\\ &+ 8\pi\Delta_l\left(E-\frac{p^2}{m}-\frac{3q^2}{4m}\right)^{-1}\iint \bar{Y}_l^{m_l}(\widehat{\tfrac{1}{2}\mathbf{q}+\mathbf{q}'})\bar{Y}_\lambda^{m_\lambda}(\hat{\mathbf{q}})t_l\left(p,|\frac{1}{2}\mathbf{q}+\mathbf{q}'|,E-\frac{3q^2}{4m}\right)\\ &\sum_{l'\lambda'}\psi_{l'\lambda'L}(|\frac{1}{2}\mathbf{q}'+\mathbf{q}|,q';q_0,E)Y_{l'\lambda'LM}(\widehat{\tfrac{1}{2}\mathbf{q}'+\mathbf{q}},\hat{\mathbf{q}}')\,d\mathbf{q}'\,d\hat{\mathbf{q}}.\end{aligned} \tag{F.24}$$

The next step is to multiply this equation by $\langle LM|lm_l\lambda m_\lambda\rangle$ and summing over $m_l$ and $m_\lambda$. We also use the orthogonality relation

$$\sum_{m_1,m_2}\langle JM|j_1m_1j_2m_2\rangle\langle j_1m_1j_2m_2|J'M'\rangle = \langle JM|J'M'\rangle = \delta_{J,J'}\delta_{M,M'}, \tag{F.25}$$

so that we end up with

$$\begin{aligned}\psi_{l\lambda L}(p,q;q_0,E) &= \sum_{m_l+m_\lambda=M}\langle LM|lm_l\lambda m_\lambda\rangle\varphi_{n_d,l_d}(p)\frac{1}{q^2}\delta(q-q_0)\delta_{l,l_d}\delta_{m_l,m_d}\delta_{\lambda,L}\delta_{m_\lambda,M}\\ &+ 8\pi\Delta_l\left(E-\frac{p^2}{m}-\frac{3q^2}{4m}\right)^{-1}\iint \bar{Y}_{l\lambda LM}(\widehat{\tfrac{1}{2}\mathbf{q}+\mathbf{q}'},\hat{\mathbf{q}})t_l\left(p,|\frac{1}{2}\mathbf{q}+\mathbf{q}'|,E-\frac{3q^2}{4m}\right)\\ &\sum_{l'\lambda'}\psi_{l'\lambda'L}(|\frac{1}{2}\mathbf{q}'+\mathbf{q}|,q';q_0,E)Y_{l'\lambda'LM}(\widehat{\tfrac{1}{2}\mathbf{q}'+\mathbf{q}},\hat{\mathbf{q}}')\,d\mathbf{q}'\,d\hat{\mathbf{q}}.\end{aligned} \tag{F.26}$$

Now we simplify this equation further by remembering that we assumed a dimer state with zero angular momentum, i.e., $l_d = 0$ and $m_d = 0$. The resulting atom-dimer scattering equation is given by

$$\begin{aligned}\psi_{l\lambda L}(p,q;q_0,E) &= \varphi_{n_d,0}(p)\frac{1}{q^2}\delta(q-q_0)\delta_{l,0}\delta_{\lambda,L}\\ &+ 8\pi\Delta_l\left(E-\frac{p^2}{m}-\frac{3q^2}{4m}\right)^{-1}\iint \bar{Y}_{l\lambda LM}(\widehat{\tfrac{1}{2}\mathbf{q}+\mathbf{q}'},\hat{\mathbf{q}})t_l\left(p,|\frac{1}{2}\mathbf{q}+\mathbf{q}'|,E-\frac{3q^2}{4m}\right)\\ &\sum_{l'\lambda'}\psi_{l'\lambda'L}(|\frac{1}{2}\mathbf{q}'+\mathbf{q}|,q';q_0,E)Y_{l'\lambda'LM}(\widehat{\tfrac{1}{2}\mathbf{q}'+\mathbf{q}},\hat{\mathbf{q}}')\,d\mathbf{q}'\,d\hat{\mathbf{q}}.\end{aligned} \tag{F.27}$$

The next step is to reduce this infinite set of two-dimensional integral equations to an infinite set of one-dimensional integral equations by introducing the expansion for the partial-wave off-shell components $t_l(p,p',z)$ given by Eq. (F.16). Before substituting this expansion into Eq. (F.27) we first consider the relation between the two-body wave function $\varphi_{nl}(p,E_{2b})$ and the form factor $g_{nl}(p,z)$.

The two-body $T$-matrix contains singularities at the binding energies of the pair of particles. Near any singular point, the $T$-matrix can be written as [69]

$$\langle \mathbf{p}'|T(z)|\mathbf{p}\rangle \simeq \frac{\langle \mathbf{p}'|\tilde{g}_{nl}\rangle\langle \tilde{g}_{nl}|\mathbf{p}\rangle}{z - E_{2b,nl}} \tag{F.28}$$

where the indices $n$ and $l$ specify the singularity since they are the principal and angular momentum quantum number of the two-body bound state respectively. The form factors $\langle \mathbf{p}|\tilde{g}_{nl}\rangle$ are defined as

$$\langle \mathbf{p}|\tilde{g}_{nl}\rangle = \int \langle \mathbf{p}|V|\mathbf{q}\rangle\langle \mathbf{q}|\varphi_{nl}\rangle \, d\mathbf{q} \tag{F.29}$$

where $\langle \mathbf{q}|\varphi_{nl}\rangle$ is the two-body bound state wave function in the momentum-space representation whose energy is $E_{2b,nl}$. This bound state wave function is normalized as $\langle \varphi_{nl}|\varphi_{n'l'}\rangle = \delta_{nn'}\delta_{ll'}$. Clearly, Eq. (F.29) can also be written as

$$\begin{aligned}\langle \mathbf{p}|\tilde{g}_{nl}\rangle &= \int \langle \mathbf{p}|E_{2b,nl} - H_0|\mathbf{q}\rangle\langle \mathbf{q}|\varphi_{nl}\rangle \, d\mathbf{q} \\ &= \left(E_{2b,nl} - \frac{p^2}{2\mu}\right)\langle \mathbf{p}|\varphi_{nl}\rangle.\end{aligned} \tag{F.30}$$

From Eq. (F.16) we also know that close to the singularity the $T$-matrix can also be approximated by

$$\langle \mathbf{p}'|T(z)|\mathbf{p}\rangle \simeq -\tau_{nl}(z)\langle \mathbf{p}'|g_{nl}(E_{2b,nl})\rangle\langle g_{nl}(E_{2b,nl})|\mathbf{p}\rangle \tag{F.31}$$

because for $|z - E_{2b,nl}| \ll 1$ the form factors depend much weaker on $z$ than the prefactor $\tau_{nl}(z)$. So we see from Eqs. (F.28), (F.30) and (F.31) that we can always write $\langle \mathbf{p}|\varphi_{nl}\rangle$ in terms of $\langle \mathbf{p}|g_{nl}(E_{2b,nl})\rangle$ as

$$\langle \mathbf{p}|\varphi_{nl}\rangle = X_{nl}\frac{\langle \mathbf{p}|g_{nl}(E_{2b,nl})\rangle}{E_{2b,nl} - \frac{p^2}{2\mu}} \tag{F.32}$$

where $X_{nl}$ is a constant which does not depend on $\mathbf{p}$. When $\varphi_{nl}(p)$ and $g_{nl}(p,z)$ are defined by $\langle \mathbf{p}|\varphi_{nl}\rangle = \varphi_{nl}(p)Y_l^m(\hat{\mathbf{p}})$ and $\langle \mathbf{p}|g_{nl}(z)\rangle = g_{nl}(p,z)Y_l^m(\hat{\mathbf{p}})$ respectively, we find that

$$\varphi_{nl}(p) = X_{nl}\frac{g_{nl}(p, E_{2b,nl})}{E_{2b,nl} - \frac{p^2}{2\mu}}. \tag{F.33}$$

Now we go back to the elastic atom-dimer scattering equation. Substituting Eq. (F.16) and Eq. (F.33) into Eq. (F.27) results in

$$\begin{aligned}\psi_{l\lambda L}(p,q;q_0,E) = X_{n_d,0}\frac{g_{n_d,0}(p,E_{2b})}{E_{2b} - \frac{p^2}{2\mu}}\frac{1}{q^2}\delta(q-q_0)\delta_{l,0}\delta_{\lambda,L} - 8\pi\Delta_l\left(Z_q - \frac{p^2}{m}\right)^{-1} \\ \iint \bar{Y}_{l\lambda LM}(\widehat{\tfrac{1}{2}\mathbf{q}+\mathbf{q}'},\hat{\mathbf{q}})\sum_n \tau_{nl}\left(Z_q\right)g_{nl}\left(p,Z_q\right)g_{nl}\left(|\frac{1}{2}\mathbf{q}+\mathbf{q}'|,Z_q\right) \\ \sum_{l'\lambda'}\psi_{l'\lambda' L}(|\frac{1}{2}\mathbf{q}'+\mathbf{q}|,q';q_0,E)Y_{l'\lambda' LM}(\widehat{\tfrac{1}{2}\mathbf{q}'+\mathbf{q}},\hat{\mathbf{q}}')\,d\mathbf{q}'\,d\hat{\mathbf{q}}\end{aligned} \tag{F.34}$$

where $Z_q = E - \frac{3q^2}{4m}$. Next, we define the functions $A_{nl\lambda L}(q, q_0)$ by writing the expansion coefficients $\psi_{l\lambda L}(p, q; q_0, E)$ as

$$\psi_{l\lambda L}(p,q;q_0,E) = \sum_n \Delta_l X_{n_d,0} \frac{g_{nl}(p,Z_q)}{Z_q - \frac{p^2}{m}} \{\delta_{n,n_d}\delta_{l,0}\delta_{\lambda,L}\frac{\delta(q-q_0)}{q^2} + 4\pi\tau_{nl}(Z_q)A_{nl\lambda L}(q,q_0)\}. \tag{F.35}$$

The functions $A_{nl\lambda L}(q, q_0)$ are closely related to the scattering amplitude as we will see below. Substitution of Eq. (F.35) into Eq. (F.34) results in

$$\begin{aligned}\sum_n \Delta_l X_{n_d,0} \frac{g_{nl}(p,Z_q)}{Z_q - \frac{p^2}{m}} \tau_{nl}(Z_q) A_{nl\lambda L}(q,q_0) = -2\Delta_l \left(Z_q - \frac{p^2}{m}\right)^{-1} \iint \bar{Y}_{l\lambda LM}(\widehat{\tfrac{1}{2}\mathbf{q}+\mathbf{q}'},\hat{\mathbf{q}}) \\ \sum_n \tau_{nl}(Z_q)\, g_{nl}(p,Z_q)\, g_{nl}\left(|\frac{1}{2}\mathbf{q}+\mathbf{q}'|, Z_q\right) \sum_{l'\lambda',n'} \Delta_{l'} X_{n_d,0} \frac{g_{n'l'}(|\frac{1}{2}\mathbf{q}'+\mathbf{q}|,Z_{q'})}{Z_{q'} - \frac{|\frac{1}{2}\mathbf{q}'+\mathbf{q}|^2}{m}} \\ \{\delta_{n',n_d}\delta_{l',0}\delta_{\lambda',L}\frac{\delta(q'-q_0)}{q'^2} + 4\pi\tau_{n'l'}(Z_{q'})A_{n'l'\lambda'L}(q',q_0)\} Y_{l'\lambda'LM}(\widehat{\tfrac{1}{2}\mathbf{q}'+\mathbf{q}},\hat{\mathbf{q}}')\, d\mathbf{q}'\, d\hat{\mathbf{q}}.\end{aligned} \tag{F.36}$$

This equation can be simplified by applying the orthogonalization condition of the form factors $g_{nl}(p, Z_q)$ given by Eq. (F.17). This results in

$$\begin{aligned}\Delta_l A_{nl\lambda L}(q,q_0) = -2\Delta_l \iint \bar{Y}_{l\lambda LM}(\widehat{\tfrac{1}{2}\mathbf{q}+\mathbf{q}'},\hat{\mathbf{q}}) g_{nl}\left(|\frac{1}{2}\mathbf{q}+\mathbf{q}'|,Z_q\right) \\ \sum_{l'\lambda',n'} \Delta_{l'} \frac{g_{n'l'}(|\frac{1}{2}\mathbf{q}'+\mathbf{q}|,Z_{q'})}{E - \frac{1}{m}(q^2+q'^2+\mathbf{q}\cdot\mathbf{q}')} \{\delta_{n',n_d}\delta_{l',0}\delta_{\lambda',L}\frac{\delta(q'-q_0)}{q'^2} \\ + 4\pi\tau_{n'l'}(Z_{q'})A_{n'l'\lambda'L}(q',q_0)\} Y_{l'\lambda'LM}(\widehat{\tfrac{1}{2}\mathbf{q}'+\mathbf{q}},\hat{\mathbf{q}}')\, d\mathbf{q}'\, d\hat{\mathbf{q}}.\end{aligned} \tag{F.37}$$

This equation can be represented in a nicer way if we define

$$\begin{aligned}U_{nl\lambda L,n'l'\lambda'L}(q,q',E) \equiv -\Delta_{l'}\Delta_l \iint \bar{Y}_{l\lambda LM}(\widehat{\tfrac{1}{2}\mathbf{q}+\mathbf{q}'},\hat{\mathbf{q}}) g_{nl}(|\frac{1}{2}\mathbf{q}+\mathbf{q}'|,Z_q) \\ \left(E - \frac{1}{m}\left(q^2+q'^2+\mathbf{q}\cdot\mathbf{q}'\right)\right)^{-1} g_{n'l'}(|\frac{1}{2}\mathbf{q}'+\mathbf{q}|,Z_{q'}) Y_{l'\lambda'LM}(\widehat{\tfrac{1}{2}\mathbf{q}'+\mathbf{q}},\hat{\mathbf{q}}')\, d\hat{\mathbf{q}}'\, d\hat{\mathbf{q}}.\end{aligned} \tag{F.38}$$

Eq. (F.37) can be written as

$$\begin{aligned}\Delta_l A_{nl\lambda L}(q,q_0) = 2U_{nl\lambda L,n_d0LL}(q,q_0,E) \\ + 8\pi \sum_{l'\lambda',n'} \int_0^\infty U_{nl\lambda L,n'l'\lambda'L}(q,q',E)\tau_{n'l'}(Z_{q'})A_{n'l'\lambda'L}(q',q_0)q'^2\, dq'.\end{aligned} \tag{F.39}$$

The same equation can be found in Ref. [71], in which the definition of $\tau_{nl}(z)$ is a factor $4\pi$ larger than the one used in this thesis.

When we consider ultracold collisions between the atom and the dimer, the value of $q_0$ is very small. In this case all amplitudes $A_{nl\lambda L}$ with $L \neq 0$ vanish [5]. The components with

$L = 0$ are fully specified by the indices $n$ and $l$ since $\lambda = l$ in this case. So if we define $A_{nl} \equiv A_{nll0}$, we end up with [71]

$$\begin{aligned} A_{nl}(q,q_0) &= 2U_{nl,n_d0}(q,q_0,E) \\ &\quad + 8\pi \sum_{n',l'} \int_0^\infty U_{nl,n'l'}(q,q',E)\tau_{n'l'}\left(E - \frac{3}{4m}q'^2\right) A_{n'l'}(q',q_0)q'^2\,dq'. \end{aligned} \tag{F.40}$$

The functions $U_{nl,n'l'}(q,q',E)$ are defined by

$$\begin{aligned} &U_{nl,n'l'}(q,q',E) \equiv U_{nll0,n'l'l'0}(q,q',E) \\ &\quad = \frac{1}{4\pi}\Delta_l\Delta_{l'}\sqrt{2l+1}\sqrt{2l'+1}\int P_l(\hat{\mathbf{q}}\cdot\widehat{\tfrac{1}{2}\mathbf{q}+\mathbf{q}'})P_{l'}(\hat{\mathbf{q}}'\cdot\widehat{\tfrac{1}{2}\mathbf{q}'+\mathbf{q}}) \\ &\quad \left(\frac{1}{m}\left(q^2+\mathbf{q}'\cdot\mathbf{q}+q'^2\right)-E\right)^{-1} g_{nl}\left(|\frac{1}{2}\mathbf{q}+\mathbf{q}'|,Z_q\right) g_{n'l'}\left(|\frac{1}{2}\mathbf{q}'+\mathbf{q}|,Z_{q'}\right) d\hat{\mathbf{q}}'. \end{aligned} \tag{F.41}$$

### F.2.1 The scattering amplitude

The physical parameter of interest is the scattering amplitude defined by Eq. (C.23). For three identical bosons of mass $m$, the reduced mass of the atom-dimer system is $\frac{2}{3}m$. Thus, in case of elastic atom-dimer scattering we use Eq. (C.31) and we find that the elastic scattering amplitude is given by

$$\begin{aligned} \hat{f}(\mathbf{q},\alpha' \leftarrow \mathbf{q}_0,\alpha) &= -\sum_\beta \lim_{q\to q_0}(2\pi)^2\frac{2}{3}m\hbar\langle\mathbf{q},\beta|T^{\beta\alpha}(E+i0)|\mathbf{q}_0,\alpha\rangle \\ &= -\sum_\beta \lim_{q\to q_0}(2\pi)^2\frac{2}{3}m\hbar\langle\mathbf{q},\beta|V^\beta|\Psi_\alpha(\mathbf{q}_0)\rangle \\ &= -\frac{1}{3}\sum_{\beta,\alpha} \lim_{q\to q_0}(2\pi)^2\frac{2}{3}m\hbar\langle\mathbf{q},\beta|V^\beta|\Psi_\alpha(\mathbf{q}_0)\rangle \\ &= -\frac{1}{3}\sum_\beta \lim_{q\to q_0}(2\pi)^2\frac{2}{3}m\hbar\langle\mathbf{q},\beta|V^\beta|\Psi(\mathbf{q}_0)\rangle \\ &= -\frac{1}{3}\sum_\beta \lim_{q\to q_0}(2\pi)^2\frac{2}{3}m\hbar\langle\mathbf{q},\beta|H-(H_0+V_\beta)|\Psi(\mathbf{q}_0)\rangle \\ &= -\frac{1}{3}\sum_\beta \lim_{q\to q_0}(2\pi)^2\frac{2}{3}m\hbar\left(E_{2b}+\frac{3}{4m}q_0^2-(E_{2b}+\frac{3}{4m}q^2)\right)\langle\mathbf{q},\beta|\Psi(\mathbf{q}_0)\rangle \\ &= -2\pi^2\hbar\lim_{q\to q_0}\left(q_0^2-q^2\right)\langle\mathbf{q},\alpha|\Psi(\mathbf{q}_0)\rangle \\ &= -2\pi^2\hbar\lim_{q\to q_0}\left(q_0^2-q^2\right)\langle\mathbf{q},\alpha|1+P_++P_-|\tilde{\Psi}_\alpha(\mathbf{q}_0)\rangle. \end{aligned} \tag{F.42}$$

If we represent the two-body bound state by $|\varphi\rangle$ and remove the index $\alpha$, this equation can also be written as

$$f_{ad}(\mathbf{q} \leftarrow \mathbf{q}_0) = -2\pi^2\hbar \lim_{q\to q_0} \left(q_0^2 - q^2\right) \Big( \langle \mathbf{q}, \varphi | \tilde{\Psi}(\mathbf{q}_0)\rangle + \int \langle \varphi | \frac{1}{2}\mathbf{q} + \mathbf{q}'\rangle \langle \mathbf{q}', -\mathbf{q} - \frac{1}{2}\mathbf{q}' | \tilde{\Psi}(\mathbf{q}_0)\rangle \, d\mathbf{q}' + \int \langle \varphi | -\frac{1}{2}\mathbf{q} - \mathbf{q}'\rangle \langle \mathbf{q}', \mathbf{q} + \frac{1}{2}\mathbf{q}' | \tilde{\Psi}(\mathbf{q}_0)\rangle \, d\mathbf{q}' \Big). \tag{F.43}$$

The second and third term vanish in the limit $q \to q_0$. So the scattering amplitude can be calculated from

$$f(\mathbf{q}, \mathbf{q}_0) = -2\pi^2\hbar \lim_{q\to q_0} \left(q_0^2 - q^2\right) \langle \mathbf{q}, \varphi | \tilde{\Psi}(\mathbf{q}_0, E)\rangle. \tag{F.44}$$

By using Eq. (F.22) we obtain

$$\begin{aligned} \langle \mathbf{q}, \varphi | \tilde{\Psi}(\mathbf{q}_0, E)\rangle &= \iint \langle \mathbf{q}, \varphi | \mathbf{p}', \mathbf{q}'\rangle \langle \mathbf{p}', \mathbf{q}' | \tilde{\Psi}(\mathbf{q}_0, E)\rangle \, d\mathbf{p}' \, d\mathbf{q}' \\ &= \iint \langle \varphi | \mathbf{p}'\rangle \delta(\mathbf{q} - \mathbf{q}') \langle \mathbf{p}', \mathbf{q}' | \tilde{\Psi}(\mathbf{q}_0, E)\rangle \, d\mathbf{p}' \, d\mathbf{q}' \\ &= \int \langle \varphi | \mathbf{p}'\rangle \langle \mathbf{p}', \mathbf{q} | \tilde{\Psi}(\mathbf{q}_0, E)\rangle \, d\mathbf{p}' \\ &= \int \bar{\varphi}_{n_d,0}(p') \bar{Y}_0^0(\hat{\mathbf{p}}') \sum_{l,\lambda,L,M} \psi_{l\lambda L}(p', q; q_0) Y_{l\lambda LM}(\hat{\mathbf{p}}', \hat{\mathbf{q}}) \bar{Y}_L^M(\hat{\mathbf{q}}_0) \, d\mathbf{p}' \\ &= \int \bar{\varphi}_{n_d,0}(p') \sum_{L,M} \psi_{0LL}(p', q; q_0) Y_L^M(\hat{\mathbf{q}}) \bar{Y}_L^M(\hat{\mathbf{q}}_0) p'^2 \, dp'. \end{aligned} \tag{F.45}$$

If now expand the elastic scattering amplitude $f(\mathbf{q}, \mathbf{q}_0)$ into spherical harmonics as

$$f(\mathbf{q}, \mathbf{q}_0) \equiv 4\pi \sum_{L,M} Y_L^M(\hat{\mathbf{q}}) \bar{Y}_L^M(\hat{\mathbf{q}}_0) f_L(q_0), \tag{F.46}$$

we obtain from Eqs. (F.44) and (F.45) the following expression for the partial-wave elastic scattering amplitude $f_L(q_0)$:

$$f_L(q_0) = -\lim_{q\to q_0} \frac{\pi}{2} \left(q_0^2 - q^2\right) \hbar \int \bar{\varphi}_{n_d,0}(p) \psi_{0LL}(p, q; q_0) p^2 \, dp. \tag{F.47}$$

Since we are taking the limit $q \to q_0$, we see that only one term in Eq. (F.35) contributes to $f_L(q_0)$, namely the term which contains the factor $\tau_{n_d,0}(Z_q)$. Since close to the singularity $\tau_{n_d,0}(Z_q)$ can be written as

$$\begin{aligned} \tau_{n_d,0}(Z_q) &= -\frac{1}{4\pi} \frac{X_{n_d,0}^2}{Z_q - E_{2b}} \\ &= -\frac{m}{3\pi} \frac{X_{n_d,0}^2}{q_0^2 - q^2}, \end{aligned} \tag{F.48}$$

we have

$$\lim_{q\to q_0} \left(q_0^2 - q^2\right) \tau_{n_d,0}(Z_q) = -\frac{m}{3\pi} X_{n_d,0}^2. \tag{F.49}$$

Furthermore, $X^2_{n_d,0}$ can be calculated from the normalization of the wave function $\varphi_{n_d,0}(p)$ which is given by Eq. (F.33), i.e.,

$$X^2_{nl} = \left( \int_0^\infty \left( \frac{g_{nl}(p, E_{2b,nl})}{E_{2b,nl} - \frac{p^2}{2\mu}} \right)^2 p^2 \, dp \right)^{-1} . \tag{F.50}$$

So we can now write Eq. (F.47) evaluated at $L = 0$ as

$$\begin{aligned} f_0(q_0) &= -\lim_{q \to q_0} 2\pi^2 \left(q_0^2 - q^2\right) \hbar \int X^2_{n_d,0} \frac{g_{n_d,0}(p, E_{2b,n_d,0})}{E_{2b,n_d,0} - \frac{p^2}{2\mu}} \frac{g_{n_d,0}(p, Z_q)}{Z_q - \frac{p^2}{2\mu}} \tau_{n_d,0}(Z_q) A_{n_d,0}(q, q_0) p^2 \, dp \\ &= \frac{2}{3} \pi m \hbar X^4_{n_d,0} A_{n_d,0}(q_0, q_0) \int_0^\infty \left( \frac{g_{n_d,0}(p, E_{2b,n_d,0})}{E_{2b,n_d,0} - \frac{p^2}{2\mu}} \right)^2 p^2 \, dp \\ &= \frac{2}{3} \pi m \hbar X^2_{n_d,0} A_{n_d,0}(q_0, q_0). \end{aligned} \tag{F.51}$$

The $s$-wave atom-dimer scattering length can be calculated from Eq. (C.26). It is simply given by

$$a_{ad} = -\frac{2}{3} \pi m \hbar X^2_{n_d,0} \lim_{q_0 \to 0} A_{n_d,0}(q_0, q_0). \tag{F.52}$$

# G. Hilbert-Schmidt theory

This Appendix deals with integral equations. Integral equations for which the kernel is real and symmetric, i.e. $K(s,t) = K(t,s)$, have some special properties which can also be applied to the three-body problem. The operator $K$ must also be nearly finite-dimensional [74] which means that the inequality

$$\iint K^2(s,t)\,ds\,dt < \infty \tag{G.1}$$

must hold. When these conditions apply, there exists a nonempty set of eigenfunctions $\varphi$, which satisfy

$$\int K(s,t)\varphi(t)\,dt = \lambda\varphi(s). \tag{G.2}$$

All eigenvalues of $\lambda$ are real for any real symmetric kernel [94]. The number of nonzero eigenvalues may be finite or infinite [74]. The number of eigenvalues whose value is zero can be zero, finite or infinite [74]. Another important property of this kernel is the existence of an orthonormal system of eigenfunctions which is complete [74]. The kernel can then be expanded in terms of the eigenfunctions as [74]

$$K(s,t) \doteq \sum_{n=1}^{\infty} \lambda_n \varphi_n(s)\varphi_n(t) \tag{G.3}$$

where the eigenfunctions and corresponding eigenvalues are labeled by the index $n$. The arrangement of the eigenvalues is such that the magnitude decreases as $n$ increases ($|\lambda_1| \geq |\lambda_2| \geq |\lambda_3| \geq ...$). Eq. (G.3) is called the spectral representation of the kernel. The $\doteq$ represents the approach of this series to the kernel, so that the spectral representation is at least approximately equal to the kernel.

With this expansion for the kernel we can analyze the double integral of Eq. (G.1). Using the orthonormality of the set $\{\varphi_n\}$, this double integral can be written as

$$\begin{aligned} \iint K^2(s,t)\,ds\,dt &= \iint \left(\sum_{n=1}^{\infty} \lambda_n \varphi_n(s)\varphi_n(t)\right)^2 ds\,dt \\ &= \sum_{n=1}^{\infty} \lambda_n^2, \end{aligned} \tag{G.4}$$

so that the condition of Eq. (G.1) can also be written as

$$\sum_{n=1}^{\infty} \lambda_n^2 < \infty. \tag{G.5}$$

The series in Eq. (G.3) need not to converge pointwise and when the series converges at some point in the domain, it may not converge to the kernel $K(s,t)$ [74]. Mercer's theorem is a statement about the convergence of the spectral representation. Mercer's theorem states that if the kernel $K(s,t)$ is definite, continuous and symmetric or if it has only a finite number of eigenvalues of one sign, the expansion of the kernel $K(s,t)$ in Eq. (G.3) is valid and converges absolutely and uniformly [94].

In order to apply Mercer's theorem we need to know when the kernel is definite. First, we introduce the quadratic integral form

$$J(f,f) = \iint K(s,t)f(s)f(t)dsdt, \tag{G.6}$$

where $f$ is any continuous or piecewise continuous function. The kernel $K(s,t)$ is called positive definite or negative definite when $J(f,f)$ can assume only positive or negative values respectively unless $f$ vanishes identically [94]. It can be proven that a kernel is positive definite if and only if all its eigenvalues are positive [94]. When all eigenvalues are negative, the kernel is negative definite.

The Hilbert-Schmidt theorem is a statement about a different series expansion. It states that

$$\int K(s,t)f(t)dt = \sum_{n=1}^{\infty} \lambda_n \varphi_n(s) \langle \varphi_n, f \rangle \tag{G.7}$$

for any function $f$ in Hilbert space [74]. The dot product $\langle \varphi_n, f \rangle$ is just the projection of $f$ on the eigenvector $\varphi_n$. Eq. (G.7) is absolutely convergent in all points $s$ for which $C^2(s) \equiv \int K^2(s,t)\,dt = \sum_{n=1}^{\infty} (\lambda_n \varphi_n(s))^2 < \infty$. When $C(s)$ has a finite upper bound for all $s$, the series of Eq. (G.7) converges uniformly. Furthermore, when $K(s,t)$ is continuous over the whole domain, the series of Eq. (G.7) converges and equals the left-hand-side for each value of $s$ [74].

## G.1 Real symmetric matrices

When it is not possible to calculate the eigenfunctions in Eq. (G.2) analytically, it is possible to solve it numerically by defining the variables $s$ and $t$ on a grid of size $N_k$ and solve the resulting matrix equation. In this case, the kernel $K$ is a real symmetric matrix. For real symmetric matrices there exists an orthonormal system of eigenvectors of this matrix which is complete [74]. Any real, symmetric matrix $K$ with an orthonormal system $\{\varphi_n\}$ of eigenvectors and corresponding eigenvalues $\{\lambda_n\}$ can be written as

$$K = \sum_{n=1}^{N_k} \lambda_n \varphi_n \varphi_n \tag{G.8}$$

which is called the spectral representation of the matrix $K$ [74]. So even if we cannot find an analytical form of the spectral representation of $K(s,t)$, we can find the spectral representation numerically.

# H. Additional figures

This Appendix contains some additional figures of the Efimov spectra corresponding to the potential resonances of the square well potential. Three different methods are used to approximate the two-body $T$-matrix.

## H.1 Method I

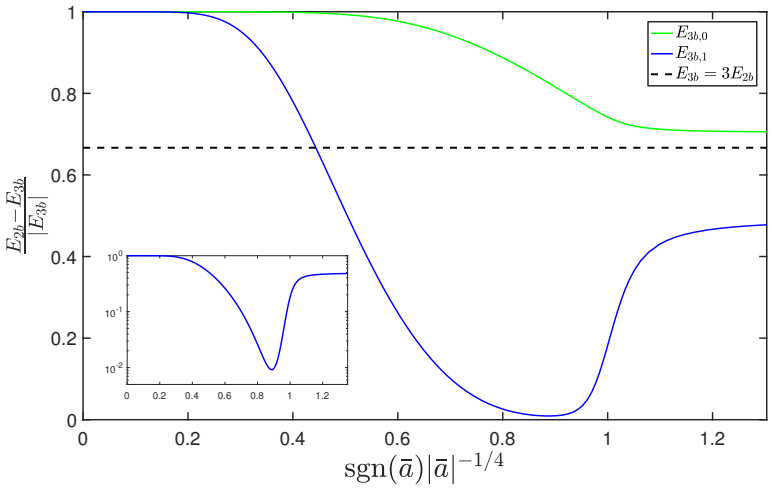


Figure H.1: Relative energy difference between the $s$-wave dimer state and the first two Efimov states corresponding to the first potential resonance of the square well potential. The dashed line corresponds to the limiting value $E_{3b,0} = 3E_{2b,0}$. The data corresponds to the three-body calculation with $N_s = 3$ and $N_d = 3$ as shown in Fig. 7.1.

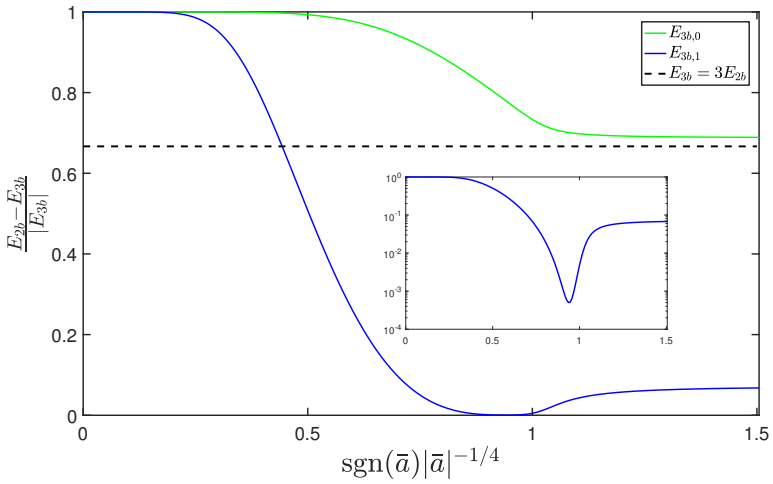


Figure H.2: Relative energy difference between the $s$-wave dimer state and the first two Efimov states corresponding to the first potential resonance of the square well potential. The dashed line corresponds to the limiting value $E_{3b,0} = 3E_{2b,0}$. The data corresponds to the three-body calculation with $N_s = 1$ and $N_d = 0$ as shown in Fig. 7.2.

## H.2 Method II

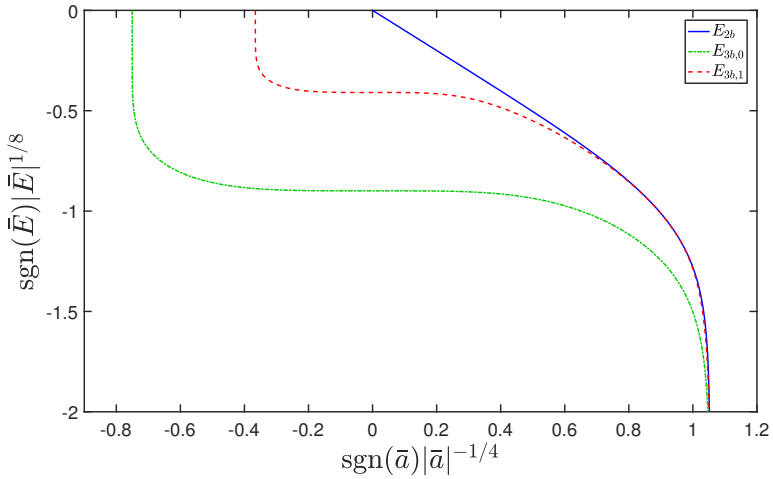


Figure H.3: Energy of the first two Efimov states calculated near the first potential resonance of the square well potential for $N_s = 1$ and $N_d = 0$ using the eigenfunctions of $VG_0$ as form factors. The blue line is the binding energy corresponding to the $s$-wave dimer state. The scattering length is calculated from Eqs. (5.20) and (5.21).

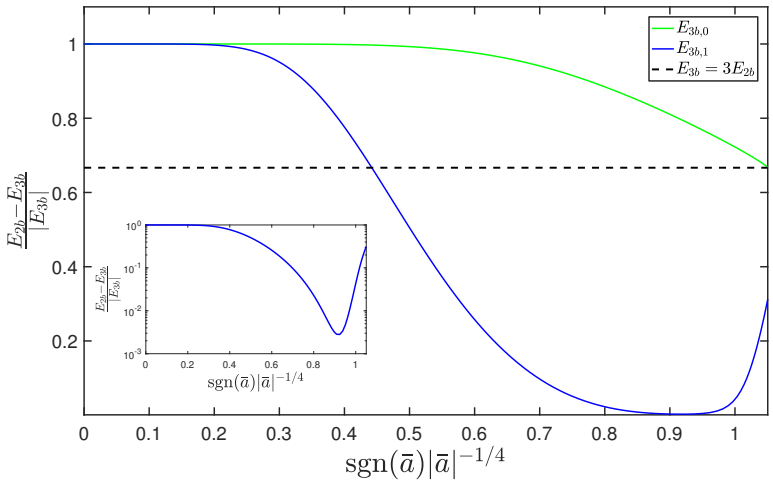


Figure H.4: Relative energy difference between the $s$-wave dimer state and the first two Efimov states corresponding to the first potential resonance of the square well potential. The dashed line corresponds to the limiting value $E_{3b,0} = 3E_{2b,0}$. The data corresponds to the calculation shown in Fig. H.3. The scattering length is calculated from Eqs. (5.20) and (5.21).

## H.3 Method III

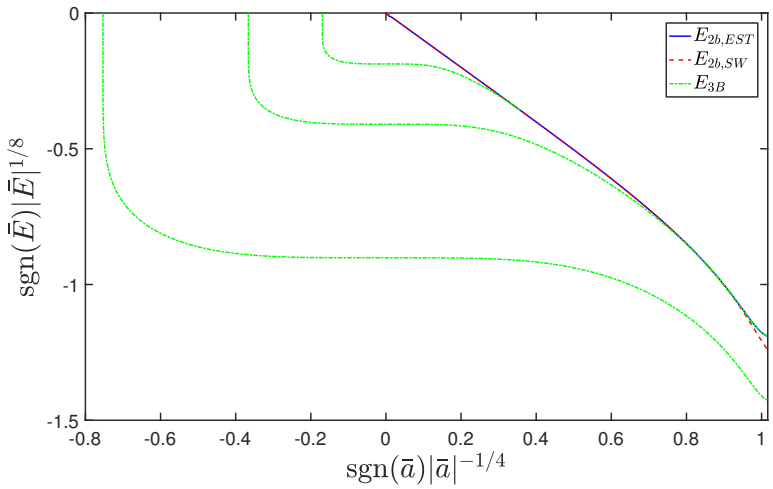


Figure H.5: Energy of the lowest three Efimov states calculated near the first potential resonance of the square well potential using the one-term EST approximation. The blue line is the binding energy corresponding to the $s$-wave dimer state of the separable potential and the red dashed line represents the binding energy of the $s$-wave dimer state of the square well potential.

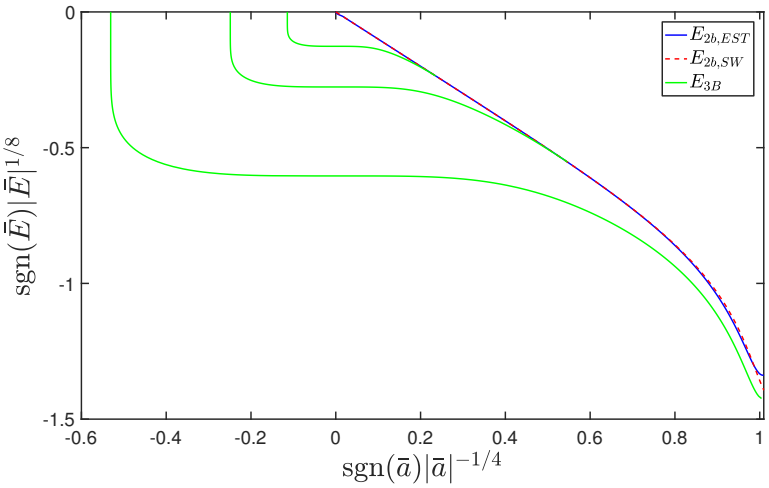


Figure H.6: Energy of the lowest three Efimov states calculated near the second potential resonance of the square well potential using the one-term EST approximation. The blue line is the binding energy corresponding to the $s$-wave dimer state of the separable potential and the red dashed line represents the binding energy of the $s$-wave dimer state of the square well potential.

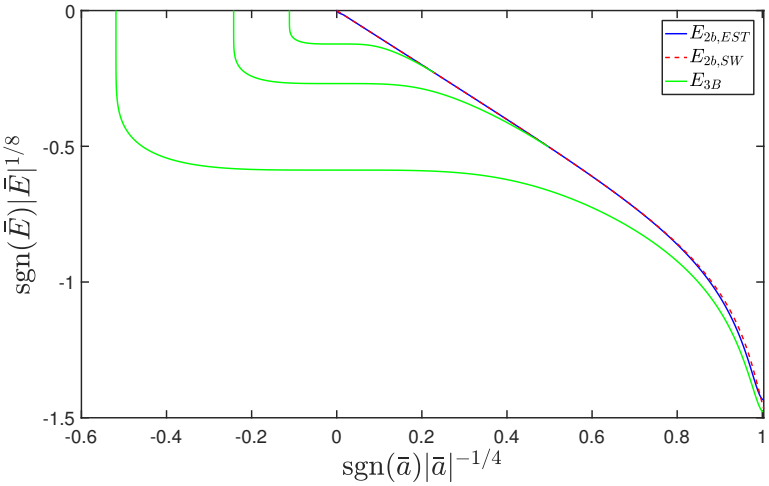


Figure H.7: Energy of the lowest three Efimov states calculated near the third potential resonance of the square well potential using the one-term EST approximation. The blue line is the binding energy corresponding to the $s$-wave dimer state of the separable potential and the red dashed line represents the binding energy of the $s$-wave dimer state of the square well potential.